Nonequilibrium phenomena in QCD and BEC: Boltzmann and beyond

Dissertation

zur Erlangung des Doktorgrades
an der Fakultät für Physik
der Universität Bielefeld

vorgelegt von
Tim Stockamp

22. Dezember 2006

„I wonder why. I wonder why.
I wonder why I wonder.
I wonder why I wonder why
I wonder why I wonder!“

R.P. Feynman

Contents

Chapter 1

Introduction

Various phenomena that we encounter in daily life are described by thermodynamics. Until the nineteenth century, however, thermodynamics itself was only understood empirically. The pioneering work of e.g. Clausius and Maxwell provided a much deeper understanding of this fundamental subject. They advocated the atomistic view of nature and thus tried to derive the empiric laws of thermodynamics from the underlying kinematics of atoms and molecules.
In 1872 Ludwig Boltzmann made an important contribution to the kinetic gas theory by introducing the famous transport equation named after him. The Boltzmann equation describes how collisions of the particles affect the time evolution of their distribution function. In particular, it provides insight into the equilibration process of a given system and can be used to compute transport coefficients such as viscosity. In this thesis we will repeatedly encounter the Boltzmann equation in the modern context of quantum field theory.

Nonequilibrium quantum field theory

The physical ideas behind Boltzmann's approach remain to some extend valid in quantum field theory. This is not at all obvious as a quantum mechanical definition of the phase space distribution function is nontrivial. Therefore, in a given situation one needs to find a suitable quasiparticle approximation to obtain a meaningful generalization of the transport equation. In cases where off-shell effects are important, however, such an approximation must fail.
There are modern methods in quantum field theory that can overcome the shortcomings of the Boltzmann equation. We focus on the so-called two particle irreducible (2PI) effective action techniques. They provide powerful tools - both perturbative and nonperturbative ones - to study quantum fields far from equilibrium. In particular, they can deal with typical problems in nonequilibrium field theory like secularity and nonuniversality. As the resulting 2PI equations of motion can in general be very efficiently solved numerically, these methods have been applied with increasing popularity in recent years.
Nonequilibrium phenomena play an important role in a variety of current research fields, ranging from particle physics to cosmology. Indeed, in this thesis we will investigate two seemingly very different topics, namely heavy ion collisions and Bose-Einstein condensates.

Heavy ion collisions

It is predicted by Quantum Chromodynamics (QCD) that the elementary constituents of hadrons - quarks and gluons - are liberated at high energies. The state of matter consisting

of deconfined quarks and gluons in thermal equilibrium is called a Quark Gluon Plasma, or QGP for short. According to the standard model of cosmology it existed about ten millionths of a second after the Big Bang. Nowadays one may find a QGP in the core of neutron stars or create it - on a smaller scale - in collisions of two heavy nuclei (e.g. Pb, Au) at sufficiently high energies. These collisions are intensively investigated at CERN (SPS and in near future LHC) and BNL (RHIC). In figure 1.1 we show the detector traces of a central Au-Au collision. It becomes obvious that a theoretical description of such a complex event represents a huge challenge to the QCD community.

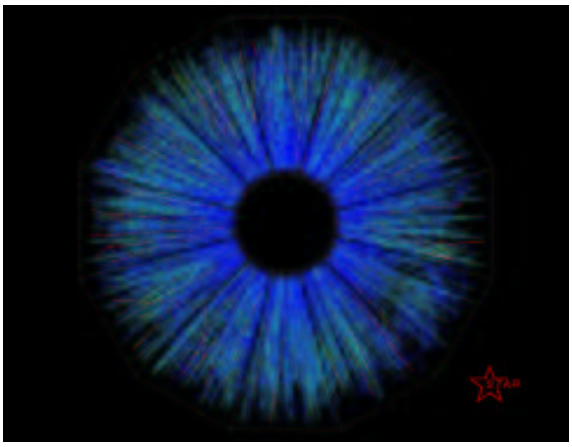

Figure 1.1: Gold beam-beam collision event at RHIC recorded by the STAR collaboration (taken from http://www.star.bnl.gov/STAR/imagelib/collisions/).

On the other hand, at high energies and densities some important simplifications apply. For instance, the gluons become the dominant degrees of freedom and the strong coupling constant becomes small. These are the assumptions of the so-called bottom-up scenario, which provides a framework for the time evolution of a heavy ion collision from the initial state to a thermal system. It consists of parametric estimates based on perturbation theory and implements a Boltzmann equation to describe the equilibration of gluons.

Bose-Einstein condensates

The second application of nonequilibrium quantum field theory in this thesis deals with systems that differ with respect to a QGP by about 10 orders of magnitude in length and 18 in temperature.

After the prediction of a novel phase transition in dilute gases at ultracold temperatures in 1925 it took experimentalists 70 years to achieve it. The quest for the so-called Bose-Einstein condensation (BEC) was rewarded with the 2001 Nobelprize for Cornell, Wiemann and Ketterle.
To prevent a transition into the liquid or solid state one confines a very dilute gas (typically $\simeq 10^4$ atoms per cm^3) in a magnetic trap and cools it with laser techniques into the μK regime. The crucial step to achieve BEC is evaporative cooling. The fastest atoms are released from the trap and the remaining gas thermalizes below the critical temperature.
Since the first experimental realization in the summer of 1995 the interset in this field increased immensly. To visualize this we show in figure 1.2 the results of a keyword search performed in the condensed matter online arXiv. The approximately constant number of

„quantum Hall effect“ papers indicates that the steep rise in the „Bose Einstein“ curve is not due to a growing popularity of online publication.

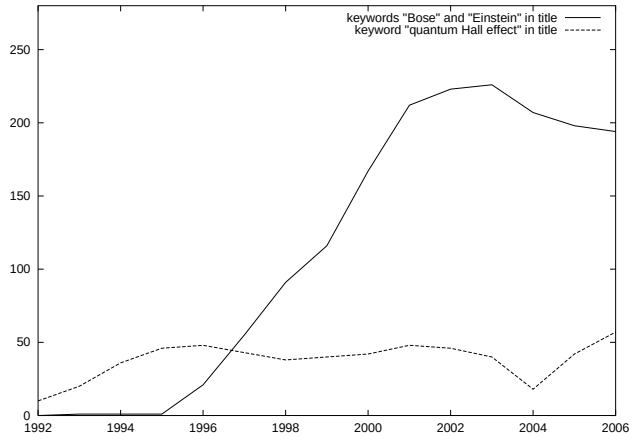

Figure 1.2: Papers on BEC found in the online arXiv (http://arxiv.org/find/cond-mat) since 1992.

In pure condensates a variety of fascinating phenomena like vortex lattices and interference of matter waves appear. But in recent years experimental effort was also dedicated to the study of the interactions between condensed and excited atoms. After the evaporative cooling procedure the gas clearly is out of equilibrium. Therefore, condensate growth - and the inverse process which we call condensate melting - provide a unique possibility to test nonequilibrium techniques in quantum field theory on a macroscopic level.

Outline of the thesis

In chapter 2 we chose the real time formalism to dicuss some basic principles in quantum field theory at finite temperature. This will enable us to derive the quantum Boltzmann equation from the Schwinger-Dyson series. We then shortly introduce the basic concepts of QCD which are needed to understand the physics of QGP formation. After a detailed account on the bottom-up scenario we show the consistency of this approach by a diagramatical analysis of the relevant Boltzmann collision integrals.

Chapter 3 deals with BEC dynamics out of equilibrium. After an introdution to the fundamental theoretical tool - namely the Gross-Pitaevskii equation - we focus on a generalization to finite temperature developed by Zaremba, Nikuni and Griffin (ZNG). These authors use a Boltzmann equation to describe the interactions between condensed and excited atoms and manage in this way to describe condensate growth.
We then turn to a discussion on the 2PI effective action and derive equations of motion for a relativistic scalar field theory. In the nonrelativistic limit these equations are shown to concide with the ZNG theory when a quasiparticle approximation is applied.
Finally, we perform a numerical analysis of the full 2PI equations. These remain valid even at strong coupling and far from equilibrium, and thus go far beyond Boltzmann's approach. For simplicity, we limit ourselves to a homogeneous system and present the first $3+1$ dimensional study of condensate melting.

Chapter 2

Thermalization to hot QCD matter

In this chapter we deal with thermalization as a central issue in heavy ion collisions (HIC). In the past two decades considerable experimental effort was dedicated to the production of a new state of matter, labelled Quark Gluon Plasma (QGP). Due to QCD's asymptotic freedom confined quarks in hadronic matter are liberated at high energies.
Indeed, lattice QCD simulations suggest that a phase transition takes place at a critical temperature around 192 MeV [1].

Accelerator	Projectile-Target	$\sqrt{s}$ [A·GeV]	T_{max}[MeV]
AGS (BNL)	*Si-Au*, *Au-Au*	4-5	150
SPS (CERN)	*S-U*, *Pb-Pb*	17-20	190
RHIC (BNL)	*Au-Au*	200	230
LHC (CERN)	*Pb-Pb*	5500	260

In the above table former, present and future experiments at BNL and CERN are listed where heavy nuclei are collided at ever increasing energies to study deconfined matter (from [2]). Also a rough estimate for the maximally attainable temperature is given. The fireball produced in these collisions is expected to thermalize and thus to form a QGP. But it turns out that the theoretical description of the fireballs time evolution towards equilibrium is quite involved. It requires appropriate initial conditions and nonequilibrium tools in quantum field theory, some of which we will review in the following.

2.1 Boltzmann equation

In 1872 Ludwig Eduard Boltzmann, then assistant professor in Graz/Austria, published a famous article including a discussion on the transport equation named after him [3].
The Boltzmann equation describes the statistical distribution of particles in a gas. It is widely used to study thermodynamic properties of a given system, e.g. its viscosity, thermal conductivity or other transport coefficients. Formally, it is an integro-differential equation for the particle distribution function f which is defined such that $f(\mathbf{x}, \mathbf{p}, t) d^3x d^3p$ is the number of particles in the phase-space volume $d^3x d^3p$ at time t. Consider f experiencing an external force $\mathbf{F}$. Then f must satisfy

$$f\left(\mathbf{x} + \frac{\mathbf{p}}{m}dt, \mathbf{p} + \mathbf{F}dt, t + dt\right) d^3x d^3p - f\left(\mathbf{x}, \mathbf{p}, t\right) d^3x d^3p = \left.\frac{\partial f(\mathbf{x}, \mathbf{p}, t)}{\partial t}\right|_{coll} d^3x d^3p dt. \quad (2.1)$$

The right hand side takes into account changes of the distribution induced by particle collisions.
Deviding the above equation by $d^3x d^3p dt$ one obtains the Boltzmann equation

$$\frac{\partial f}{\partial t} + \frac{\partial f}{\partial \mathbf{x}} \frac{\mathbf{p}}{m} + \frac{\partial f}{\partial \mathbf{p}} \mathbf{F} = \left. \frac{\partial f}{\partial t} \right|_{coll} . \tag{2.2}$$

In modern applications of transport theory quantum effects often play a crucial role. The Boltzmann equation therefore has to be combined with quantum mechanics. This, however, is not easily achieved as the very concept of a distribution function - depending simultaneously on $\mathbf{x}$ and $\mathbf{p}$ - is in contradiction to Heisenbergs uncertainty principle. It turns out that a quantum analogue of f can be defined that preserves many of its properties.
Proceeding in this direction, we now recall some basic features of thermal field theory (TFT).

2.2 Real time formalism

Quantum systems in and out of equilibrium are most suitably described within the real time formalism. We mainly follow the presentations of Das in [4, 5]. For more details we also refer to other textbooks, e.g. [6, 7].
First, we would like to compute the Greens functions of some general quantum system, i.e. the expectation value of a product of field operators. The system can be naturally described in terms of a density matrix which in the Schrödinger picture is defined as

$$\rho(t) = \sum_n p_n \, |\psi_n(t)\rangle\langle\psi_n(t)| \tag{2.3}$$

Here, p_n represents the probability for finding the quantum mechanical system in the state $|\psi_n(t)\rangle$ and, for simplicity, we have assumed the quantum mechanical states to form a discrete set. The expectation value of a general operator $\mathcal{O}$ can now be written in terms of the density matrix ρ like

$$\langle \mathcal{O} \rangle(t) = \sum_n p_n \, \langle \psi_n(t)|\mathcal{O}|\psi_n(t)\rangle = \mathrm{Tr}\, \rho(t)\, \mathcal{O}. \tag{2.4}$$

The dynamics of ρ is governed by Liouville's equation

$$i \, \frac{\partial \rho(t)}{\partial t} = [H, \rho(t)] \, , \tag{2.5}$$

which has the formal solution

$$\rho(t) = U(t,0)\rho(0)U^\dagger(t,0) = U(t,0)\rho(0)U(0,t). \tag{2.6}$$

The time evolution operator U is defined as

$$U(t,t') = T\left(e^{-i\int_{t'}^{t} dt'' \, H(t'')}\right). \tag{2.7}$$

Furthermore, it satisfies the following properties

$$\begin{aligned} U(t_1,t_2)U(t_2,t_1) &= 1 \\ U(t_1,t_2)U(t_2,t_3) &= U(t_1,t_3) \qquad \text{for } t_1 > t_2 > t_3. \end{aligned} \tag{2.8}$$

The underlying physical idea of the real time formalism consists of preparing the system in an equilibrium state at negative times, let it evolve and for positive times the true Hamiltonian is switched on. The latter may be time dependent and thus describe a nonequilibrium situation. To clarify this we introduce

$$H(t) = \begin{cases} H_i & \text{for} \quad \mathrm{Re}t \leq 0 \\ \mathcal{H}(t) & \text{for} \quad \mathrm{Re}t \geq 0 \end{cases} \quad . \tag{2.9}$$

For the initial configuration of the system we can then write

$$\begin{aligned} \rho(0) &= \frac{e^{-\beta H_i}}{\mathrm{Tr}\, e^{-\beta H_i}} \\ &= \frac{U(T - i\beta, T)}{\mathrm{Tr}\, U(T - i\beta, T)} \quad , \end{aligned} \tag{2.10}$$

where β denotes the inverse temperature and the time T must be negative. This finally leads to an important expression for the time dependent density matrix

$$\begin{aligned} \rho(t) &= U(t,0)\rho(0)U(0,t) \\ &= \frac{U(t,0)U(T - i\beta, T)U(0,t)}{\mathrm{Tr}\, U(T - i\beta, T)} \quad . \end{aligned} \tag{2.11}$$

Using this result together with (2.8) and the cylicity of the trace, one can compute the expectation value of a given Operator $\mathcal{O}$ in terms of the time evolution operator U

$$\begin{aligned} \langle \mathcal{O} \rangle &= \mathrm{Tr}\, \rho(t)\, \mathcal{O} \\ &= \frac{\mathrm{Tr}\, U(t,0)\, U(T - i\beta, T)\, U(0,t)\, \mathcal{O}}{\mathrm{Tr}\, U(T - i\beta, T)} \\ &= \frac{\mathrm{Tr}\, U(T - i\beta, T)\, U(0,t)\, \mathcal{O}\, U(t,0)\, U(0,T)\, U(T,0)}{\mathrm{Tr}\, U(T - i\beta, T)} \\ &= \frac{\mathrm{Tr}\, U(T - i\beta, T)\, U(T,0)\, U(0,t)\, \mathcal{O}\, U(t,0)\, U(0,T)}{\mathrm{Tr}\, U(T - i\beta, T)} \\ &= \frac{\mathrm{Tr}\, U(T - i\beta, T)\, U(T,t)\, \mathcal{O}\, U(t,T)}{\mathrm{Tr}\, U(T - i\beta, T)} \quad . \end{aligned} \tag{2.12}$$

Note that $U(T - i\beta, T)$ and $U(T, 0)$ commute for $T < 0$, as the Hamiltonian is then time independent. To bring the above expression into the standard form, we introduce a large positive time T'. Using again the property (2.8) we can write

$$\begin{aligned} \langle \mathcal{O} \rangle &= \frac{\mathrm{Tr}\, U(T - i\beta, T)\, U(T,T')\, U(T',T)\, U(T,t)\, \mathcal{O}\, U(t,T)}{\mathrm{Tr}\, U(T - i\beta, T)} \\ &= \frac{\mathrm{Tr}\, U(T - i\beta, T)\, U(T,T')\, U(T',t)\, \mathcal{O}\, U(t,T)}{\mathrm{Tr}\, U(T - i\beta, T)\, U(T,T')\, U(T',T)} \quad . \end{aligned} \tag{2.13}$$

The numerator of (2.13), read from right to left, has a simple physical interpretation. The system evolves from some negative time T to a time t when the operator $\mathcal{O}$ is acting. Then

it evolves to some large positive time T' before evolving backwards to T again and finally along the imaginary axis.
This complex time contour, consisting of three parts denoted $\mathcal{C}_+$, $\mathcal{C}_-$ and $\mathcal{C}_\beta$, is shown in figure 2.1. In the limit $T \to -\infty$ and $T' \to \infty$, it can be shown that the third branch, $\mathcal{C}_\beta$, gets decoupled from the other two (the factors in the propagators connecting such branches are asymptotically damped [4]). Consequently, in this limit, we are effectively dealing with two branches leading to the name "closed time path (CTP) formalism" [8, 9, 10, 11]. On this contour the time integration has to be thought of as

$$\int_c dt = \int_{-\infty}^{\infty} dt_+ - \int_{-\infty}^{\infty} dt_- \tag{2.14}$$

where the relative negative sign arises because time is decreasing in the second branch of the time contour.

2.2.1 Finite temperature Green functions

With the above discussion in mind, it is quite simple to generalize a vacuum field theory to finite temperature [4, 7]. It has become clear that the CTP formalism leads to a doubling of the degrees of freedom. To take this into account one may introduce a field ϕ_+ living on the upper branch and correspondingly a field ϕ_- on the lower one.
As an example, we study next the self-interacting scalar field theory in some detail. The Lagrangian density is given by

$$\mathcal{L}(\phi) = \frac{1}{2}\partial_\mu\phi\partial^\mu\phi - \frac{m^2}{2}\phi^2 - \frac{\lambda}{4!}\phi^4\,, \tag{2.15}$$

but following the above discussion, we should take the complete Lagrangian density for the system to be

$$\mathcal{L} = \mathcal{L}(\phi_+) - \mathcal{L}(\phi_-) \quad . \tag{2.16}$$

The ϕ_- fields must have a relative negative sign arising from the observation that time is decreasing along the second branch. The Feynman propagator is defined as $iG(x,y) = \langle T_c\phi(x)\phi(y)\rangle$, where T_c denotes time ordering along the contour. Equivalently, due to the doubling of the field degrees of freedom, one can introduce the 2×2 matrix

$$G = \begin{pmatrix} G_{++} & G_{+-} \\ G_{-+} & G_{--} \end{pmatrix}. \tag{2.17}$$

The matrix components are then given by

$$iG_{++}(x,y) = \langle T\phi(x)\phi(y)\rangle \quad \text{for } x^0,\, y^0 \text{ on } C_+\,,$$

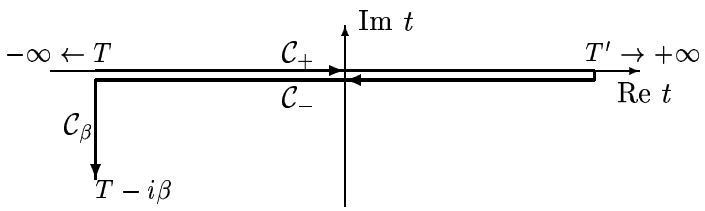

Figure 2.1: Complex time path in the real-time formalism

$$iG_{+-}(x,y) = \langle\phi(y)\phi(x)\rangle \quad \text{for } x^0 \text{ on } C_+,\ y^0 \text{ on } C_- \ ,$$
$$iG_{-+}(x,y) = \langle\phi(x)\phi(y)\rangle \quad \text{for } y^0 \text{ on } C_+,\ x^0 \text{ on } C_- \ ,$$
$$iG_{--}(x,y) = \langle T^*\phi(x)\phi(y)\rangle \quad \text{for } x^0,\ y^0 \text{ on } C_- \ ,$$

where $T(T^*)$ prescribes (anti-)chronological time ordering

$$T\phi(x)\phi(y) = \Theta(x^0-y^0)\phi(x)\phi(y) + \Theta(y^0-x^0)\phi(y)\phi(x) \ ,$$

$$T^*\phi(x)\phi(y) = \Theta(y^0-x^0)\phi(x)\phi(y) + \Theta(x^0-y^0)\phi(y)\phi(x) \ .$$

The contour theta function is naturally defined as

$$\Theta_c(x^0-y^0) = \begin{cases} \Theta(x^0-y^0) & \text{for } x^0,\ y^0 \text{ on } C_+ \\ \Theta(y^0-x^0) & \text{for } x^0,\ y^0 \text{ on } C_- \\ 0 \quad \text{for } x^0 \text{ on } C_+,\ y^0 \text{ on } C_- \\ 1 \quad \text{for } y^0 \text{ on } C_+,\ x^0 \text{ on } C_-. \end{cases} \tag{2.18}$$

As a result, we give the explicit form of the free propagators read in momentum space

$$\begin{aligned} G^0_{++}(k) &= \frac{1}{k^2-m^2+i\epsilon} - 2i\pi n_B(|k^0|)\delta(k^2-m^2), \\ G^0_{+-}(k) &= -2i\pi\left(\theta(k^0)+n_B(|k^0|)\right)\delta(k^2-m^2), \\ G^0_{-+}(k) &= -2i\pi\left(\theta(-k^0)+n_B(|k^0|)\right)\delta(k^2-m^2), \\ G^0_{--}(k) &= -\frac{1}{k^2-m^2-i\epsilon} - 2i\pi n_B(|k^0|)\delta(k^2-m^2), \end{aligned} \tag{2.19}$$

with the Bose distribution $n_B = \frac{1}{e^{\beta\omega}-1}$, involving $\omega = \sqrt{\mathbf{p}^2+m^2}$.
These functions are known as the causal propagators of the theory and are useful in diagrammatic evaluation.

For later purposes we also introduce the retarded and advanced Green functions

$$G^R(x,y) = \Theta(x^0-y^0)\big(G^>(x,y) - G^<(x,y)\big) \ , \tag{2.20}$$

$$G^A(x,y) = \Theta(y^0-x^0)\big(G^<(x,y) - G^>(x,y)\big) \ , \tag{2.21}$$

with $G^>(x,y) = \langle\phi(x)\phi(y)\rangle$ and $G^<(x,y) = \langle\phi(y)\phi(x)\rangle$. The advantage of these propagators is that the positions of their time arguments on the contour branches need not to be specified. This is useful, for example, when x^0 or y^0 is an integration variable.

2.3 From field theory to kinetic theory

The previous discussion only dealt with free Green functions. Now let us take into account the interaction term in the Lagrangian (2.15). Like in the vacuum case, the dynamics of the full propagator is given by the Schwinger-Dyson equation

$$G(x,y) = G_0(x,y) + \int_c d^4z \int_c d^4z' G_0(x,z)\Sigma(z,z')G(z',y) \ , \tag{2.22}$$

where $\Sigma(x,y)$ is the self-energy. Again, the difference to vacuum fields is encoded in the time integrations which are performed along the CTP. In the rest of this section we will show how a quantum analogue of Boltzmann's equation can be obtained from the above exact evolution equation. Our discussion closely follows the presentations given by Mrowczynski and Carrington in [12, 13].
First we observe that (2.22) can be rewritten as two equations

$$\left[\partial_x^2 + m^2\right] G(x,y) = \delta_c^{(4)}(x,y) + \int_c d^4z \Sigma(x,z) G(z,y) \ , \tag{2.23}$$

$$\left[\partial_y^2 + m^2\right] G(x,y) = \delta_c^{(4)}(x,y) + \int_c d^4z G(x,z) \Sigma(z,y) \ . \tag{2.24}$$

The integration over z_0 is performed on the CTP and the contour delta function is defined as $\delta_c(t-t') = \frac{d}{dt}\Theta_c(t-t')$, leading to

$$\delta_c^{(4)}(x,y) = \begin{cases} \delta^{(4)}(x-y) & \text{for} \quad x^0 \ , \ y^0 \ \text{on C}_+, \\ 0 & \text{for} \quad x^0 \ , \ y^0 \ \text{on different branches}, \\ -\delta^{(4)}(x-y) & \text{for} \quad x^0 \ , \ y^0 \ \text{on C}_-. \end{cases}$$

In the ϕ^4-model it is convenient to split the self energy into the local tadpole contribution and non-local parts

$$\Sigma(x,y) = \Sigma^\delta(x)\delta_c^{(4)}(x-y) + \Sigma^>(x,y)\Theta_c(x^0-y^0) + \Sigma^<(x,y)\Theta_c(y^0-x^0) \ .$$

As we shall see later, Σ^δ provides a dominant contribution to the mean-field while $\Sigma^{\gtrless}$ determine the collision terms of the transport equations.

With the help of the retarded and advanced Green functions (2.20) and (2.21), and the retarded and advanced self-energies defined in an analogous way, the equations (2.23) and (2.24) can be rewritten as

$$\begin{aligned} \left[\partial_x^2 + m^2 \right. &- \left. \Sigma^\delta(x)\right] G^{\gtrless}(x,y) \\ &= \int d^4z \left[\Sigma^{\gtrless}(x,z) G^A(z,y) + \Sigma^R(x,z) G^{\gtrless}(z,y)\right] \ , \end{aligned} \tag{2.25}$$

$$\begin{aligned} \left[\partial_y^2 + m^2 \right. &- \left. \Sigma^\delta(y)\right] G^{\gtrless}(x,y) \\ &= \int d^4z \left[G^{\gtrless}(x,z) \Sigma^A(z,y) + G^R(x,z) \Sigma^{\gtrless}(z,y)\right] \ , \end{aligned} \tag{2.26}$$

where all time integrations run from $-\infty$ to $+\infty$.
These equations of motion are referred to as Kadanoff-Baym equations. Originally, they were developed for nonrelativistic systems [14] and later generalized to the relativistic case [15].

Similarly, one can derive the corresponding equations for G^A and G^R. Choosing x^0 and y^0 to be on the upper branch and using the relation $G^{A/R}(x,y) = G_{++} - G^{\gtrless}$ one obtains

$$\left[\partial_x^2 + m^2 - \Sigma_\delta(x)\right] G^{A/R}(x,y) = \delta^{(4)}(x-y) + \int d^4z \Sigma^{A/R}(x,z) G^{A/R}(z,y) \ , \tag{2.27}$$

$$\left[\partial_y^2 + m^2 - \Sigma_\delta(y)\right] G^{A/R}(x,y) = \delta^{(4)}(x-y) + \int d^4z G^{A/R}(x,z)\Sigma^{A/R}(z,y) \ . \tag{2.28}$$

So the equations for the retarded and advanced propagators are decoupled from each other.

2.3.1 Transport equations

We will now convert the Kadanoff-Baym equations (2.25, 2.26) into transport equations under the assumption that the system is weakly inhomogeneous with a short correlation length. Speaking in terms of relative and center of mass coordinates $s = x - y$, $X = \frac{x+y}{2}$ this means that the Green functions and self-energies vary slowly with X and are strongly peaked near $s = 0$.
Implementing the above approximation via a gradient expansion (i.e. neglecting higher than linear terms in ∂_X) and performing a Wigner transformation

$$f(k,X) = \int d^4s e^{is\cdot k} f(\frac{1}{2}s + X, -\frac{1}{2}s + X)$$

for all Green functions and self-energies is equivalent to the following set of translation rules [12]

$$\begin{aligned}
\int d^4x' f(x,x')g(x',y) \quad &\longrightarrow \quad f(X,p)g(X,p) \\
&+ \quad \frac{i}{2}\left[\frac{\partial f(X,p)}{\partial p_\mu}\frac{\partial g(X,p)}{\partial X^\mu} - \frac{\partial f(X,p)}{\partial X^\mu}\frac{\partial g(X,p)}{\partial p_\mu}\right] , \\
h(x)g(x,y) \quad &\longrightarrow \quad h(X)g(X,p) - \frac{i}{2}\frac{\partial h(X)}{\partial X^\mu}\frac{\partial g(X,p)}{\partial p_\mu} , \\
h(y)g(x,y) \quad &\longrightarrow \quad h(X)g(X,p) + \frac{i}{2}\frac{\partial h(X)}{\partial X^\mu}\frac{\partial g(X,p)}{\partial p_\mu} , \\
\partial_x^\mu f(x,y) \quad &\longrightarrow \quad (-ip^\mu + \frac{1}{2}\partial^\mu) f(X,p) , \\
\partial_y^\mu f(x,y) \quad &\longrightarrow \quad (ip^\mu + \frac{1}{2}\partial^\mu) f(X,p) .
\end{aligned} \tag{2.29}$$

Here $\partial^\mu \equiv \frac{\partial}{\partial X_\mu}$ and the functions $f(x,y)$ and $g(x,y)$ satisfy the assumptions discussed above. The function $h(x)$ is assumed to be weakly dependent on x.
Applying the translation rules to (2.25, 2.26) and taking the difference and sum of the resulting equations, we obtain

$$\begin{aligned}
\left[p^\mu\partial_\mu - \frac{1}{2}\partial_\mu\Sigma^\delta(X)\partial_p^\mu\right] G^{\gtrless}(X,p) \quad &= \quad \frac{i}{2}\Big(\Sigma^>(X,p)G^<(X,p) - \Sigma^<(X,p)G^>(X,p)\Big) \\
&- \quad \frac{1}{4}\Big\{\Sigma^{\gtrless}(X,p), G^A(X,p) + G^R(X,p)\Big\} \\
&- \quad \frac{1}{4}\Big\{\Sigma^A(X,p) + \Sigma^R(X,p),\ G^{\gtrless}(X,p)\Big\} ,
\end{aligned} \tag{2.30}$$

$$\begin{aligned}\Big[-p^2+m^2 \;-\; \Sigma^\delta(X)\Big]G^{\gtrless}(X,p) \\ = \;& \frac{1}{2}\Big(\Sigma^{\gtrless}(X,p)\big(G^A(X,p)+G^R(X,p)\big)+\big(\Sigma^A(X,p)+\Sigma^R(X,p)\big)G^{\gtrless}(X,p)\Big) \\ + \;& \frac{i}{4}\Big\{\Sigma^{>}(X,p),\,G^{<}(X,p)\Big\}-\frac{i}{4}\Big\{\Sigma^{<}(X,p),\,G^{>}(X,p)\Big\}\,, \qquad (2.31)\end{aligned}$$

where we have applied the identity $G^R(x,y)-G^A(x,y)=G^{>}(x,y)-G^{<}(x,y)$ to the Green functions and self-energies. The Poisson-like bracket is defined as

$$\Big\{C(X,p),\,D(X,p)\Big\}\equiv\frac{\partial C(X,p)}{\partial p_\mu}\frac{\partial D(X,p)}{\partial X^\mu}-\frac{\partial C(X,p)}{\partial X^\mu}\frac{\partial D(X,p)}{\partial p_\mu}\,.$$

Equations (2.30, 2.31) can be rewritten in a more compact way

$$\begin{aligned}\Big\{p^2-m^2+\Sigma^\delta(X)+\mathrm{Re}\Sigma^R(X,p),\,G^{\gtrless}(X,p)\Big\} \;&=\; i\Big(\Sigma^{>}(X,p)G^{<}(X,p)-\Sigma^{<}(X,p)G^{>}(X,p)\Big) \\ &-\; \Big\{\Sigma^{\gtrless}(X,p),\,\mathrm{Re}G^R(X,p)\Big\}\,, \qquad (2.32)\end{aligned}$$

$$\begin{aligned}\Big[p^2-m^2+\Sigma_\delta(X)+\mathrm{Re}\Sigma^R(X,p)\Big]G^{\gtrless}(X,p) \;&=\; -\Sigma^{\gtrless}(X,p)\mathrm{Re}G^R(X,p) \\ &-\; \frac{i}{4}\Big\{\Sigma^{>}(X,p),\,G^{<}(X,p)\Big\} \\ &+\; \frac{i}{4}\Big\{\Sigma^{<}(X,p),\,G^{>}(X,p)\Big\}\,, \qquad (2.33)\end{aligned}$$

where we introduced

$$\mathrm{Re}G^{A/R}(X,p)=\frac{G^A(X,p)+G^R(X,p)}{2}\,, \qquad (2.34)$$

$$\mathrm{Im}G^{A/R}(X,p)=\pm\frac{1}{2i}\Big(G^A(X,p)-G^R(X,p)\Big)\,. \qquad (2.35)$$

The gradient terms in the right-hand-sides of both above equations are usually neglected, which is the last approximation on the way towards the quantum Boltzmann equation [16, 17]. To justify the dropping of these terms we introduce some small parameter ϵ that characterizes the gradient expansion. In addition, for any analytical calculation one has to assume the coupling constant λ to be small. It can be shown by expanding the self energy pertubatively that the leading order contributions to $\Sigma^\delta(X)+\mathrm{Re}\Sigma^R(X,p)$ and $\Sigma^{\gtrless}(X,p)$ are of order λ and λ^2, respectively.

Now, we compute the order of each term in equation (2.32). We can split the Poisson-like bracket on the left hand side into two pieces. The first piece does not contain the self-energy and is of order ϵ. The second piece is of order $\lambda\epsilon$. The first term on the right hand side (without the Poisson-like bracket) is of order λ^2, while the gradient term is of order $\lambda^2\epsilon$. Thus, we find that the gradient term on the right hand side of equation (2.32) is of higher order than the remaining terms and can be dropped. The same arguments apply to the gradient terms on the right hand side of equation (2.33).

Curiously, the argument presented above breaks down near equilibrium. First one observes that at full equilibrium the non-gradient term on the right hand side of equation (2.32) is identically zero, and thus cannot be considered to be bigger than the gradient term. In this case the gradient term can be combined with the interaction term on the left hand side to produce the usual Vlasov term [12]. However, this shows that somewhere in the transition from very close to full equilibrium the dropping of gradient terms becomes invalid.

2.3.2 Spectral function

As our ultimate goal is the derivation of the quantum Boltzmann equation we have to find a suitable field theoretical analogue of the distribution function f, which in the classical case is the particle density in phase space. Thus, one needs a phenomenological bridge connecting the field and particle languages. The gradient expansion now reveals its usefulness as it indeed coincides with a quasiparticle description. To see this it is helpful to consider the spectral function ρ defined as

$$\rho(x,y) = \langle[\phi(x),\phi(y)]\rangle = iG^{>}(x,y) - iG^{<}(x,y) = -2\mathrm{Im}G^{R}(x,y)\ , \tag{2.36}$$

where $[\phi(x),\phi(y)]$ denotes the field commutator. From the transport and mass-shell equations (2.32, 2.33), one derives the equations satisfied by $\rho(X,p)$, which are

$$\Big\{p^2 - m^2 + \Sigma^{\delta}(X) + \mathrm{Re}\Sigma^{R}(X,p),\ \rho(X,p)\Big\} = 2\Big\{\mathrm{Im}\Sigma^{R}(X,p),\ \mathrm{Re}G^{R}(X,p)\Big\}\ , \tag{2.37}$$

$$\Big[p^2 - m^2 + \Sigma^{\delta}(X) + \mathrm{Re}\Sigma^{R}(X,p)\Big]\rho(X,p) = 2\,\mathrm{Im}\Sigma^{R}(X,p)\,\mathrm{Re}G^{R}(X,p)\ . \tag{2.38}$$

where $\mathrm{Re}\Sigma^{A/R}$ and $\mathrm{Im}\Sigma^{A/R}$ are defined analogously to (2.34, 2.35).

In order to understand the physical meaning of the spectral function one needs to specify $\mathrm{Im}G^{R}(X,p)$. This is achieved using the equations of motion for the physical propagators. Applying the transformation rules (2.29) to equations (2.27, 2.28) and taking the sum leads to

$$\Big[p^2 - m^2 + \Sigma^{\delta}(X) + \Sigma^{A/R}(X,p)\Big]G^{A/R}(X,p) = 1\ . \tag{2.39}$$

As the gradient terms drop out entirely in (2.39) one immediately finds the solution

$$G^{A/R}(X,p) = \frac{1}{p^2 - m^2 + \Sigma^{\delta}(X) + \Sigma^{A/R}(X,p)}\ . \tag{2.40}$$

Thus, for $\mathrm{Im}G^{R}(X,p)$ one obtains

$$\mathrm{Im}G^{R}(X,p) = -\frac{\mathrm{Im}\Sigma^{R}(X,p)}{\big(p^2 - m^2 + \Sigma^{\delta}(X) + \mathrm{Re}\Sigma^{R}(X,p)\big)^2 + \big(\mathrm{Im}\Sigma^{R}(X,p)\big)^2}\ . \tag{2.41}$$

Plugging this expression into (2.36) directly gives

$$\rho(X,p) = \frac{2\mathrm{Im}\Sigma^{R}(X,p)}{\big(p^2 - m^2 + \Sigma^{\delta}(X) + \mathrm{Re}\Sigma^{R}(X,p)\big)^2 + \big(\mathrm{Im}\Sigma^{R}(X,p)\big)^2}\ . \tag{2.42}$$

Since $\mathrm{Re}\Sigma^R$ determines the quasiparticle effective mass and $\mathrm{Im}\Sigma^R$ its width, the spectral function characterizes the quasiparticle properties. This will be helpful to find a suitable definition for the distribution function. The quasiparticle dispersion relation is found as a solution of the equation

$$p^2 - m^2 + \Sigma^\delta(X) + \mathrm{Re}\Sigma^R(X,p) = 0 \; . \tag{2.43}$$

2.3.3 Distribution function and quantum Boltzmann equation

To motivate a convenient definition of a quantum distribution function we briefly discuss the physical meaning of the Wigner transformed propagator $G^<(X,p)$. The free-field energy-momentum tensor can be expressed as [13]

$$T_0^{\mu\nu}(X) = \int \frac{d^4p}{(2\pi)^4} p^\mu p^\nu \, iG^<(X,p) \; .$$

This is the standard form of the energy-momentum tensor in the kinetic theory with the function $iG^<(X,p)$ giving the density of particles with four-momentum p in a space-time point X. Therefore, the function $iG^<(X,p)$ is closely related to the classical distribution function. However it is not positively definite and can be nonzero for the off-mass-shell four-momenta, in contrast to classical distributions.
The distribution function $f(X,p)$ is now defined as

$$\Theta(p^0) iG^<(X,p) = \Theta(p^0) \; \rho(X,p) \; f(X,p) \; ,$$

where the theta function selects quasiparticles with positive energy. An immediate consequence of this definition is $\Theta(p^0) iG^>(X,p) = \Theta(p^0) \; \rho(X,p)[1 + f(X,p)]$.

The transport equation satisfied by the distribution function f can be obtained from equation (2.32) for $G^>$ or $G^<$. After using (2.37) and the following property of the Poisson-like brackets

$$\{A, \, BC\} = \{A, \, B\} \, C + \{A, \, C\} \, B$$

one finally ends up with the quantum Boltzmann equation [13]

$$\begin{aligned} \rho(X,p) \Big\{ p^2 - m^2 \; &+ \; \Sigma^\delta(X) + \mathrm{Re}\Sigma^R(X,p), \, f(X,p) \Big\} \\ &= \; i\rho(X,p) \Big(\Sigma^>(X,p) \, f(X,p) - \Sigma^<(X,p) \big(f(X,p) + 1 \big) \Big) \\ &+ \; if(X,p) \Big\{ \Sigma^>(X,p), \, \mathrm{Re}G^R(X,p) \Big\} \\ &- \; i\big(f(X,p) + 1 \big) \Big\{ \Sigma^<(X,p), \, \mathrm{Re}G^R(X,p) \Big\} \; , \end{aligned} \tag{2.44}$$

where $p^0 > 0$. It appears here in a rather obscure form, but one can easily show the similarities to the classical case. Computing the Poisson-like bracket of equation (2.44) and imposing the mass-shell constraint (thereby losing the dependence on p^0) one finds for the left hand side the familiar structure

$$\Big\{p^2 - m^2 \;+\; \Sigma^\delta(X) + \mathrm{Re}\Sigma^R(X,p),\; f(X,p)\Big\}$$
$$= \; 2E_p\Big(\frac{\partial}{\partial t} + \mathbf{v}\partial_{\mathbf{X}}\Big) f(X,\mathbf{p}) + \partial_{\mathbf{X}}\Big(\Sigma^\delta(X) + \mathrm{Re}\Sigma^R(X,\mathbf{p})\Big)\cdot\partial_{\mathbf{p}} f(X,\mathbf{p}) \quad (2.45)$$

where the velocity $\mathbf{v}$ equals $\partial E_p/\partial\mathbf{p}$ with the energy E_p being the (positive) solution of the dispersion equation (2.43).
On the right-hand-side of equation (2.44) the gradient terms can be neglected, as discussed above. The remaining term takes into account the collisions of quasiparticles. This becomes evident when the self energies are expanded perturbatively to second order in λ. As a result one then obtains [18]

$$i\Big(\Sigma^>(X,p)\, f(X,p) \;-\; \Sigma^<(X,p)\,\big(f(X,p)+1\big)\Big)$$
$$= \; \frac{\lambda^2}{2}\int \frac{d^3k}{(2\pi)^3 2E_k}\,\frac{d^3q}{(2\pi)^3 2E_q}\,\frac{d^3r}{(2\pi)^3 2E_r}\,(2\pi)^4\delta^{(4)}(p+q-k-r)$$
$$\times \; \Bigg(\underbrace{(f^p+1)\,(f^q+1)\,f^k\,f^r}_{\text{gain}} - \underbrace{f^p\,f^q\,(f^k+1)\,(f^r+1)}_{\text{loss}}\Bigg), \quad (2.46)$$

where $f^k = f(X,\mathbf{k})$. The collision term is composed into a gain and a loss term, describing the scattering of quasiparticles into and out of the momentum state under consideration.
For a more detailed analysis of the Boltzmann equation in scalar and gauge field theories we refer to [19, 20] and the references already given in this section. An interesting numerical analysis of its range of validity is presented in [21, 22].

2.4 Basics of QCD

From the discussion of kinetic theory in the scalar case we now turn to applications in heavy ion collisions. Here the relevant theory, however, is Quantum Chromodynamics (QCD). We thus begin with a brief introduction of its basic properties.

The force that binds quarks and gluons inside hadrons is called for good reasons the strong interaction. Calculated for two quarks at a distance of order 1 fm it is about 100 times stronger than the electromagnetic force, a factor of 10^{14} stronger than the weak interaction, and a factor of 10^{40} stronger than the gravitational force [32]. In spite of these differences, it is the gravitational and the electromagnetic forces which seem to play the dominating role in the universe which we experience in the macroscopic world. The restriction of the strong force to subatomic distances is a consequence of two characteristic features which are called confinement and asymptotic freedom.

Gell-Mann and Zweig realized independently in 1964 that the whole spectroscopy of hadrons could be explained by a small number of elementary particles with -1/3 or +2/3 of electrical charge units and a newly introduced quantum number called color. In their model baryons contain three of these so-called quarks while mesons consist of one quark pand its antiquark [24]. Confinement is a necessary requirement to explain the experimentel fact that no isolated quarks have ever been observed (e.g. as fractional charges on a Millikan oil drop). So at low

momentum or energy transfer in elementary particle reactions, the strong force prevents the existence of free quarks. Trying to separate two quarks from each other apparently results in an increase of the force field energy, such that new quarks are created out of the vacuum - the initial quarks dress up with other quarks to build hadrons. These hadrons exhibit no net colour charge to the outside, such that they appear as elementary constituents rather than the quarks themselves.

Asymptotic freedom, on the other hand, describes the behaviour of quarks at high energy or momentum transfers. This feature is based on experimental observations, as well. In high energy scattering processes between leptons (e.g. electrons or neutrinos) with protons or neutrons, the scattering occurs at pointlike partons, the quarks, rather than at a homogenuous object. Apparently, at sufficiently high momentum transfers, quarks behave like free or weakly bound particles. The fact that the strong interaction becomes weak at high energy scales, and ultimately vanishes at asymptotically high energies, led to the term asymptotic freedom.

So any theory describing and predicting the dynamics of quarks inside hadrons and in high energy reactions has to incorporate these two basic features. A theoretical description of the strong interaction in terms of a consistent quantum field theory, called Quantum Chromodynamics (QCD), was presented in 1972 by Fritzsch and Gell-Mann [25], which was formally published later in [26]. We give in the following a short review of its basic conceptions (see, e.g. [27, 28, 29]) and then concentrate on the running coupling in QCD as the key to the understanding of both confinement and asymptotic freedom.

2.4.1 General formalism

Quantum Chromodynamics was originally developed from the naive quark model, combining it with local SU(3) gauge invariance. The crucial difference to QED is that gluons - which appear as the force mediators - carry color charge and thus are themselves subject to the strong interaction.
The Lagrangian of the theory reads

$$\mathcal{L}_{\mathrm{QCD}} = \sum_q \bar{q}(x)\left(i\gamma_\mu D^\mu - m_q\right) q(x) - \frac{1}{4g^2}\mathrm{tr}\; G^{\mu\nu}(x) G_{\mu\nu}(x). \tag{2.47}$$

The sum and trace are taken over color states, g is the strong coupling constant and

$$\partial^\mu q^j(x) \quad \rightarrow \quad D^\mu_{kj} q^j(x) \equiv \left\{\delta_{kj}\partial^\mu - iA^\mu_{kj}(x)\right\} q^j(x) \tag{2.48}$$

is the covariant derivative acting on the quark field $q^j(x)$. The gluon field strength tensor G is given in terms of the gauge field A by

$$G^{\mu\nu}(x) = [D^\mu, D^\nu] = \partial^\mu A^\nu(x) - \partial^\nu A^\mu(x) - i\left[A^\mu(x), A^\nu(x)\right]. \tag{2.49}$$

Provided that A and q transform under local SU(3) gauge transformations like

$$U: \qquad A^\mu(x) \rightarrow U(x)A^\mu(x)U^\dagger(x) + iU(x)\partial^\mu U^\dagger(x), \tag{2.50}$$

$$U: \qquad q^j(x) \quad \rightarrow \quad U_{jk}(x)q^k(x), \tag{2.51}$$

the above Lagrangian stays indeed invariant. The unitary transformation matrix

$$U(x) = \exp\left(-i\phi_a(x)T^a\right) \tag{2.52}$$

involves eight Hermitian and traceless generators of the gauge group SU(3). They do not commute and obey

$$\left[T^a, T^b\right] = if_{abc}T^c. \tag{2.53}$$

The values of the structure constants f^{abc} may be looked up in textbooks (e.g. [30]).
The fundamental processes in QCD, as can be deduced from the Lagrangian (2.47), are shown in figure 2.2. When quantizing the theory it is convenient to add ghost fields which cancel contributions from unphysical gluon polarizations. This procedure is merely a mathematical trick that allows for a simple covariant quantization. Therefore, vertices involving ghosts have no physical meaning and are missing in figure 2.2.

2.4.2 Running coupling

We emphasized above that the key to the understanding of confinement and asymptotic freedom in QCD is the energy dependence of the interaction strength. This dependence is encoded in Symanzik's β function [31] which is nowadays standard material in many textbooks, e.g. [30]. We also rely in our presentation on the review articles [27, 28, 29, 32].
The QCD Lagrangian - describing all the physics of strong interactions - is remarkably simple. Especially, neglecting quark masses it does not contain any energy scale. Thus, for a given process one cannot decide whether its energy is large or small as a reference scale is missing. But experimentally, nuclear physics heavily depends on energy or, equivalently, spatial resolution. So if QCD is the right theory for strong interactions it should contain some dynamically generated energy scale. This is indeed the case as can be seen by taking a closer look on the strong coupling parameter $\alpha = \frac{g^2}{4\pi}$.
In quantum field theories like QCD physical quantities like cross sections or decay rates can be expressed by a perturbation series in powers of α. If the coupling is small the series may provide a reliable prediction of $\mathcal{O}$ even if only a limited number of perturbative orders can be computed. As an example we consider some dimensionless observable $\mathcal{O}$ which depends on α and on a single energy scale Q. This scale shall be larger than any other relevant parameter like quark masses so that we can neglect these masses in the following.
Calculating $\mathcal{O}$ as a perturbation series in α leads to ultraviolet divergencies which have to be removed by the renormalization of a small set of physical parameters. This means that one absorbs the ultraviolet divergencies by fixing these parameters at some artificial energy scale μ. Consequently, $\mathcal{O}$ and α become functions of this renormalization scale. Since $\mathcal{O}$ is dimensionless it can only depend on the ratio Q^2/μ^2 and on the renormalized coupling $\alpha(\mu^2)$. As the choice of μ is arbitrary the actual value of the experimental observable $\mathcal{O}(Q^2/\mu^2, \alpha)$ cannot depend on it. This can be put in formula like

$$\mu^2 \frac{\mathrm{d}}{\mathrm{d}\mu^2}\mathcal{O}(Q^2/\mu^2, \alpha) = \left(\mu^2\frac{\partial}{\partial\mu^2} + \mu^2\frac{\partial\alpha}{\partial\mu^2}\frac{\partial}{\partial\alpha}\right)\mathcal{O} = 0\ , \tag{2.54}$$

where the multiplication by μ^2 keeps the expression dimensionless. Equation (2.54) implies the important fact that any explicit dependence of $\mathcal{O}$ on μ must be cancelled by an appropriate dependence on μ of α to all orders. In order to get rid of artificial scale one may identify it with the physical energy scale of the process under consideration and set $\mu^2 = Q^2$. In this case, one refers to α as the running coupling constant $\alpha(Q^2)$ with its energy dependence given by the β function [31]

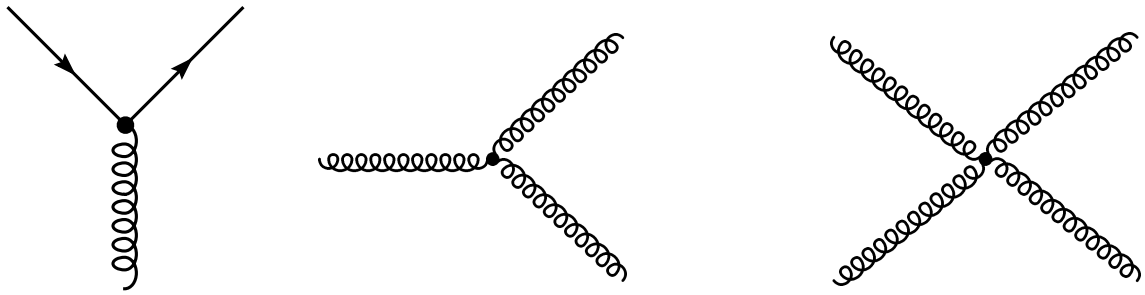

Figure 2.2: Fundamental processes in QCD. Quarks and gluons are represented by straight and wiggly lines, respectively.

$$Q^2 \frac{\partial \alpha(Q^2)}{\partial Q^2} = \beta\left(\alpha(Q^2)\right) \ . \tag{2.55}$$

The β function can be expanded perturbatively

$$\beta(\alpha) = -\beta_0 \alpha^2(Q^2) - \beta_1 \alpha^3(Q^2) - \beta_2 \alpha^4(Q^2) - \beta_3 \alpha^5(Q^2) + \mathcal{O}(\alpha^6) \ , \tag{2.56}$$

and a detailed calculation gives [33, 34, 35, 36, 37]

$$\begin{aligned} \beta_0 &= \frac{33 - 2N_f}{12\pi} \ , \\ \beta_1 &= \frac{153 - 19N_f}{24\pi^2} \ , \end{aligned} \tag{2.57}$$

where N_f is the number of active quark flavours at the energy scale Q and the number of colors is taken to $N_c = 3$. The coefficients beyond two loop accuracy dependend on the renormalization scheme (see [38] for details on a four loop calculation).

For simplicity, let us neglect β_1 and higher order terms in equation (2.55). A simple solution is then given by

$$\alpha(Q^2) = \frac{\alpha(\kappa^2)}{1 + \alpha(\kappa^2)\beta_0 \ln \frac{Q^2}{\kappa^2}} \ , \tag{2.58}$$

introducing some reference scale κ. This expression finally reveals QCD's property of asymptotic freedom. For large Q^2 and postive β_0, i.e. for $N_f < 17$, the coupling parameter α indeed decreases logarithmically to zero.
Similarly, equation (2.58) also indicates that α becomes large and, in this perturbative form, actually diverges to infinity at small Q^2. To be specific let us take the recent experimental value $\alpha(\mu^2 = M_{Z^0}^2) = 0.1198 \pm 0.0010$ [32]. For realistic values of $N_f = 2 \ldots 5$, $\alpha(Q^2)$ exceeds unity for $Q^2 \leq \mathcal{O}(100 \text{ MeV} \ldots 1 \text{ GeV})$. Thus, at energy scales below the order of 1 GeV the nonperturbative region begins where perturbation theory fails and confinement sets in.
The theoretical predictions on the running coupling in QCD are in excellent agreement with experimental data, as can be seen in figure 2.3.

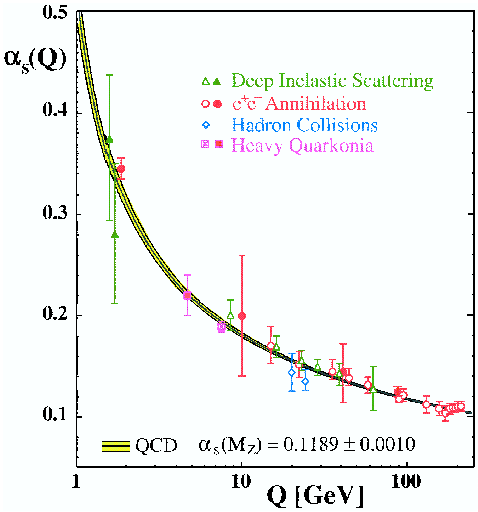

Figure 2.3: The running coupling in QCD [32]

2.5 Approaches to QGP formation

As we have already discussed, quarks and gluons are at low temperatures confined into hadrons. This already suggests that at some critical temperature T_c a phase transition to the deconfined state should occur. This new state of matter (in fact, it is only new in human experiments) is called Quark Gluon Plasma (QGP). Following Hands [39], some basic features of this phase transition can be understood by very simple considerations. If we assume a vanishing net baryon number the hadronic phase may be treated as a simple pion gas as these hadrons are easiest pair produced. Neglecting their mass the pressure in this medium is deduced from the blackbody formula

$$P_\pi = 3 \times \left(\frac{\pi^2}{90}\right) T^4, \tag{2.59}$$

where the factor three counts the different charge states π^+,π^-,π^0.
The deconfined phase of quasi free gluons and $q\bar{q}$-pairs is a state with a larger number of degrees of freedom, i.e. of higher entropy. One has to take into account prefactors for helicity-, flavor- and color states and, in addition, one needs the right quantum statistics. All in all, the corresponding expressions for the pressure in the deconfined phase reads [39]

$$P_{q\bar{q}} = 2 \times 2 \times 3 \times \frac{7}{4} \times \left(\frac{\pi^2}{90}\right) T^4 \quad , \quad P_g = 2 \times 8 \times \left(\frac{\pi^2}{90}\right) T^4. \tag{2.60}$$

Both phases are in thermal equilibrium when their pressures coincide. Taking confinement into account as negative pressure $-\Lambda_B$ (following the MIT bag model) this leads to

$$\frac{1}{30}\pi^2 T_c^4 = \frac{37}{90}\pi^2 T_c^4 - \Lambda_B^4. \tag{2.61}$$

From this equation one estimates the critical temperature T_c to be around 144 MeV [39]. Much more sophisticated calculations in lattice gauge theory basically confirm this simple picture, see figure 2.4. For T_c, the latest lattice results suggest a value around 192 MeV [1].

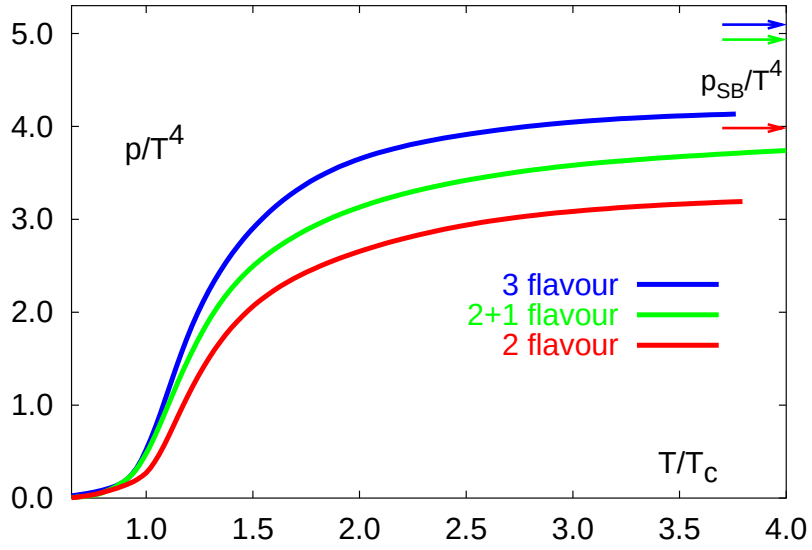

Figure 2.4: QCD's equation of state from lattice simulations [40].

The main goal of experiments involving collisions of heavy nuclei at high energies is to observe this predicted phase transition and to study the properties of deconfined matter. A simple picture of the time evolution of a heavy ion collision is shown in figure 2.5. When the Lorentz contracted 'pancakes' penetrate each other a large number of partons is liberated in elastic collisions between individual nucleons. If the system thermalizes fast enough a QGP forms and expands around the mid-rapidity region. Eventually, the temperature drops below the critical one and quarks are again confined into hadrons (chemical freeze-out). This hadronic medium continues to expand and cool until collision rates become insufficient to maintain thermal equilibrium (thermal freeze-out).
Thus, concerning the possible formation of a QGP in heavy ion collisions the single most important question is thermalization. To tackle this problem theoretically a consistent dynamical framework starting from realistic initial conditions is required. A variety of different approaches has been developed in the past, both perturbative and non-pertubative ones. We will focus in the following on the McLerran-Venugopalan (MV) model [41] - providing us with classical initial conditions - and subsequently the bottom-up scenario where Boltzmann's equation is employed to describe thermalization. We mainly follow the lecture provided by Mueller [52] as well as the original presentation of the bottom-up scenario in [42].

2.5.1 McLerran-Venugopalan model

In relativistic heavy ion collisions it is believed that - besides the QGP - a new region of QCD can be explored. Due to the huge center of mass energies perturbative methods are expected to be applicable. At the same time, we are dealing with a high density system, so the involved fields should be large. This means that the theory cannot be linearized and QCD's rich nonlinear structure reveals entirely.
McLerran and Venugopalan proposed a classical effective theory for this regime [41]. It is based on the phenomenon of parton saturation in the nuclear wave function [43, 44, 45]. The parton density inside the nucleus reaches a limit when the occupation number of gluon

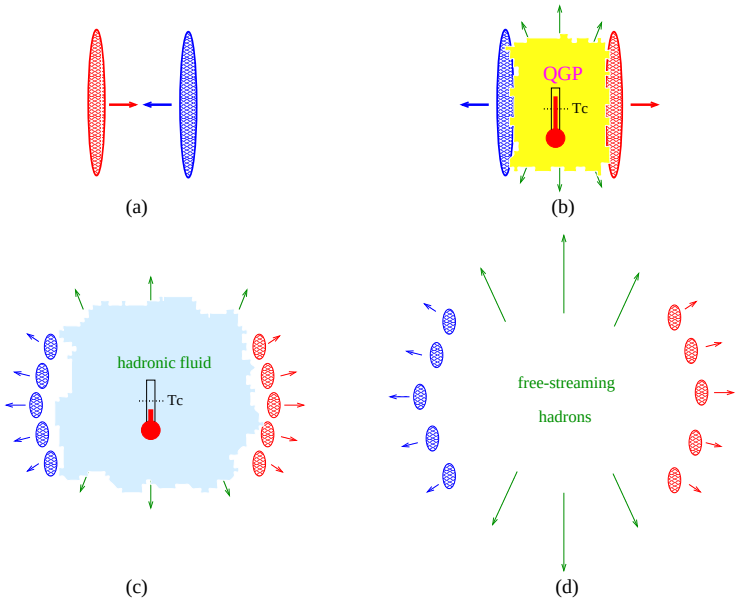

Figure 2.5: Qualitative picture of HIC [39].

modes with transverse momenta $p_T < Q_s$ become of the order α^{-1}. Note that occupation numbers of size α^{-1} are characteristic of classical field theory solutions. The saturation momentum Q_s is estimated to about 1 GeV at RHIC and 2-3 GeV at LHC energies. Using the MV wavefunction as initial condition one may numerically solve the classical Yang-Mills equations to describe the earliest stage of a heavy ion collision.
As a result, the distribution of gluons liberated in the collision is well fitted by the empirical formula

$$f_g^{in} \simeq \frac{1}{\alpha N_c} \frac{0.11}{e^{p_\perp/1.1Q_s} - 1}, \tag{2.62}$$

as long as $p_\perp/1.1Q_s$ is not too small [46].
So at higher energies more gluons are produced that collide more frequently with each other. This advocates the formation of a plasma as thermalization is obtained via collisions. On the other hand, α decreases with energy, making thermalization harder to achieve. Whether the system has enough time to equilibrate before falling apart is thus a delicate question requiring detailed consideration of different physical processes.

2.5.2 Bottom-up picture

So we have to describe the time evolution of the created fireball - as already shown qualitatively in figure 2.5 - in a more accurate way.
In the bottom-up scenario the focus is on central rapidity gluons as the dominant degrees of freedom [42]. Assuming boost invariance in this region and infinitely large nuclei in the transverse directions, one is left with the proper time $\tau = \sqrt{t^2 - z^2}$ (where z is the beam direction) as the single coordinate that physical quantities depend on.
When $Q_s\tau$ grows larger than 1, the classical gluon field becomes almost linear and one can start to describe the gluons as particles on mass shell with well-defined distributions. The MV model suggests, as we have seen, that gluons are freed with large occupation numbers of

the order α^{-1}. These gluons are called hard as their momenta are around Q_s, much larger than those of the susequently produced soft gluons.
From parametrical estimates, which we discuss below, one obtains a sequence of different evolution stages shown in figure 2.6.

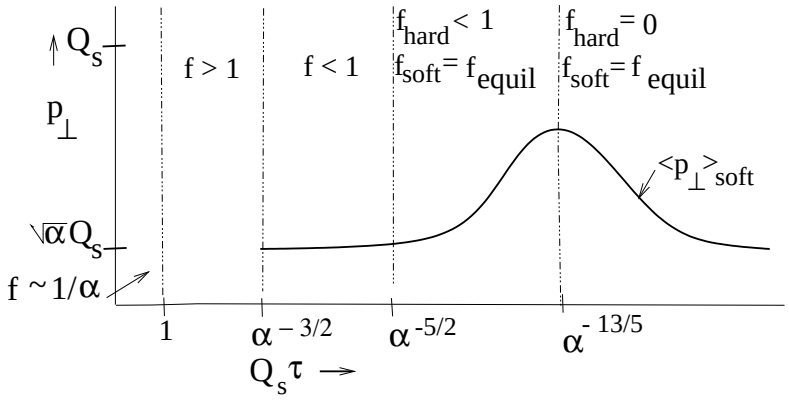

Figure 2.6: Bottom-up scenario of HIC [52].

Early time, $1 \ll Q_s\tau \ll \alpha^{-3/2}$

Let us try to give a parametrical estimate of the typical occupation number f_h for hard gluons, which can be written as

$$f_h = \frac{N_h}{Q_s^2 p_z}. \tag{2.63}$$

Here, N_h and p_z are the density and the typical longitudinal momentum of hard gluons. The density decreases with time due to the one-dimensional expansion of the system and is given parametrically by

$$N_h \sim \frac{Q_s^2}{\alpha\tau}. \tag{2.64}$$

The longitudinal momentum p_z is determined by elastic scatterings. Most of these scatterings are small angle, i.e. with exchange momentum $q \ll Q_s$. The lowest possible momentum exchange is the Debye mass m_D. Introducing N_{col} as the number of collisions that a typical particle encounters one can thus write

$$p_z^2 \sim N_{col} m_D^2 \,. \tag{2.65}$$

The Debye mass is given by [47, 48, 49]

$$m_D^2 \sim \alpha \int d^3p \, \frac{f_h(p)}{p} \sim \frac{\alpha N_h}{Q_s} \sim \frac{Q_s^2}{Q_s\tau}\,, \tag{2.66}$$

while N_{col} can be estimated as

$$\frac{N_{col}}{\tau} \sim \sigma N_h (1 + f_h)\,, \tag{2.67}$$

where we took care of Bose enhancement. For the cross section σ one has approximately

$$\sigma \sim \frac{\alpha^2}{m_D^2}\,. \tag{2.68}$$

Assuming $f_h \gg 1$ and putting everything together directly leads to the desired parametrical estimate

$$f_h \sim \alpha^{-1}(Q_s\tau)^{-2/3}. \tag{2.69}$$

From this one sees that the assumption $f_h \gg 1$ is indeed valid as long as $Q_s\tau \ll \alpha^{-3/2}$.

In this stage the most important physical processes are inelastic scatterings, i.e. the production of soft gluons. The momentum of these gluons is of order p_z and their number can be estimated to [42, 50]

$$N_s \sim \tau\frac{\alpha^3}{m_D^2}N_h^2(1+f_h)^2 \sim \frac{Q_s^3}{\alpha(Q_s\tau)^{4/3}}\,. \tag{2.70}$$

It is interesting to note that, although $N_s \ll N_h$, one has $N_s/p_z \sim N_h/Q_s$. So the soft gluons already contribute equally to the Debye mass

$$m_D^2 \sim \frac{\alpha N_h}{Q_s} + \frac{\alpha N_s}{p_z}\,. \tag{2.71}$$

The estimate of equation (2.66) is still valid parametrically in this regime, but it seems reasonable to assume $m_D^2 \sim \frac{\alpha N_s}{p_z}$ when $Q_s\tau \gg \alpha^{-3/2}$.

Intermediate time, $\alpha^{-3/2} \ll Q_s\tau \ll \alpha^{-5/2}$

As we have seen f_h decreases to the order of 1 when $Q_s\tau \sim \alpha^{-3/2}$. So in the present stage we have $f_h \ll 1$ and the previous results have to be revised. Assuming $m_D^2 \sim \frac{\alpha N_s}{p_z}$, as we motivated before, the longitudinal or soft momentum becomes

$$p_z^2 \sim N_{col}m_D^2 \sim \tau\sigma N_h m_D^2 \sim \alpha Q_s^2\,. \tag{2.72}$$

The number of soft gluons that have been produced at time τ now reads

$$N_s \sim \tau\frac{\alpha^3}{m_D^2}N_h^2 \sim \frac{\alpha Q_s^4}{m_D^2\tau} \sim \frac{\alpha^{1/4}Q_s^3}{(Q_s\tau)^{1/2}}\,. \tag{2.73}$$

The latter expression, in turn, can be used to give an estimate for the Debye mass

$$m_D \sim \frac{\alpha^{3/8}Q_s}{(Q_s\tau)^{1/4}}\,. \tag{2.74}$$

As a check of consistency, one easily confirms that the assumption of this section, $N_s/p_z \gg N_h/Q_s$, requires $Q_s\tau \gg \alpha^{-3/2}$.

Similarly, one recognizes that the number of soft gluons becomes comparable to that of hard ones at $Q_s\tau \sim \alpha^{-5/2}$. This indicates that the system enters a new regime. The soft sector thermalizes quickly and hard gluons lose their energy to this heat bath. We will justify below that a relaxation time approximation for the soft gluons indeed becomes applicable when $Q_s\tau \gg \alpha^{-5/2}$.

Late time, $\alpha^{-5/2} \ll Q_s\tau \ll \alpha^{-13/5}$

The soft gluons are now nearly equilibrated and characterized by the temperature T, which is a function of time. The system as a whole is still not in thermal equilibrium, since most of the energy is carried by a small number of hard gluons. These few gluons constantly lose energy by hard branching. They emit a particle with a softer momentum p_{br}, which subsequently splits into two gluons with comparable momenta. The products of this branching quickly cascade further, giving all their energy to the thermal bath.
The typical momentum of such a process is parametrically given by [42]

$$p_{br} \sim \alpha^4 T^3 \tau^2 \,, \tag{2.75}$$

and for the temperature one finds the time dependence

$$T \sim \alpha^3 Q_s^2 \tau \,. \tag{2.76}$$

So the temperature of the soft thermal bath increases linearly with time, despite the expansion of the system. This is due to the hard gluons which serve as an energy source. Clearly, this linear growth stops when no more branching processes can take place. This happens when $p_{br} \sim Q_s$, or $Q_s\tau \sim \alpha^{-13/5}$. Subsequently, the system cools down like $\tau^{-1/3}$ due to its expansion [51].
In order to justify a posteriori the treatment of the soft sector as a thermal bath, we consider the relaxation time for soft gluons which is approximately

$$\tau_{rel} \sim \frac{1}{\alpha^2 T} \sim \frac{1}{\alpha^5 Q_s^2 \tau} \,. \tag{2.77}$$

So when $Q_s\tau \gg \alpha^{-5/2}$ the necessary condition for the relaxation time approximation, $\tau_{rel} \ll \tau$, is indeed fulfilled.

The estimates of this evolution stage can be made quantitative by using a Boltzmann equation to describe the kinetics of the branching processes. A suitable form of the Boltzmann equation reads

$$\left(\frac{\partial}{\partial\tau} - \frac{p_z}{\tau}\frac{\partial}{\partial p_z}\right) f(\mathbf{p}) = C_{el} + C_{prod} \,. \tag{2.78}$$

The elastic collision integral C_{el} is responsible for the thermalization of the soft gluons. The inelastic term C_{prod} contains $2 \to 3$ and $3 \to 2$ processes and describes the energy flow from the hard to the soft sector.
As a result, one obtains for the temperature [42]

$$T = c_T \alpha^3 Q_s^2 \tau \,, \tag{2.79}$$

where the coefficient c_T can be determined to logarithmic accuracy. Thus, the qualitative estimate of equation (2.76) is confirmed in a more rigorous way.

An important remark on the MV model and the bottom-up scenario is in order. As we have seen, the various stages of a heavy ion collision are described theoretically by quite different tools. For very early times (i.e. $f \gg 1$) quantum fluctuations are negligible and classical nonlinear field theory is expected to work. On the other hand, when the system is nearly equilibrated ($f \ll \alpha^{-1}$) quantum effects become important and can adequately be taken into

account by the Boltzmann equation. However, it is a priori not clear whether these two frameworks give consistent results in the intermediate region where $1 \ll f \ll \alpha^{-1}$. This is necessary in order to end up with a smooth continuous description of the complete evolution, see figure 2.7.
To answer this question one needs to find a classical approximation of the quantum Boltzmann equation and compare these two equations at moderately large occupation numbers. The rest of this chapter deals with this problem, starting with a scalar field theory for simplicity and then generalizing the result to high energy QCD [53].

2.6 Classical field theory vs. Boltzmann equation

2.6.1 Scalar field theory

We briefly review here the main results of Mueller and Son [54] who showed the equivalence between classical field theory and the Boltzmann equation in a scalar field theory. It turns out that their arguments and computations can be largely simplified using some topological and diagramatical considerations. Similar methods can be found, e.g., in [55].

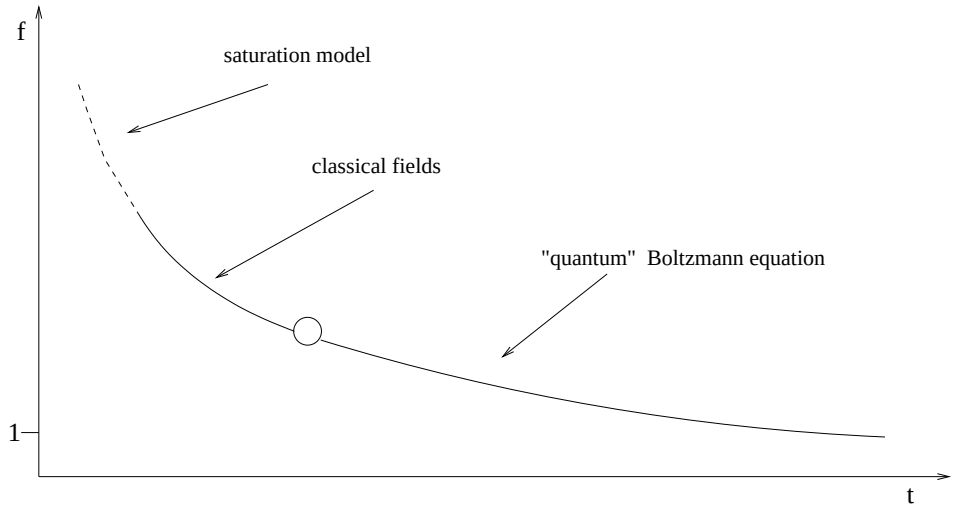

Figure 2.7: time evolution of the gluon occupation number.

2.6.2 Separation of classical and quantum contributions

Our starting point is the scalar field theory with $\lambda\phi^4$ interaction given by the Lagrangian

$$\mathcal{L} = \frac{1}{2}\partial_\mu\phi\partial^\mu\phi - \frac{1}{2}m^2\phi^2 - \frac{\lambda}{4!}\phi^4 \quad . \tag{2.80}$$

Throughout this section we assume coupling constants to be small and perform the relevant computations in first order perturbation theory.
As our ultimate interest will be to gain deeper insight into the time evolution of heavy ion collisions we have to generalize our theory to finite temperature. We apply the formerly introduced CTP formalism which leads to a doubling of the field variables [8, 9]: $\phi \to \Phi_-,\Phi_+$. The Lagrangian then reads

$$\begin{aligned}\mathcal{L}_{CTP} &= \frac{1}{2}\partial_\mu\Phi_-\partial^\mu\Phi_- - \frac{1}{2}m^2\Phi_-^2 - \frac{\lambda}{4!}\Phi_-^4 \\ &- (\frac{1}{2}\partial_\mu\Phi_+\partial^\mu\Phi_+ - \frac{1}{2}m^2\Phi_+^2 - \frac{\lambda}{4!}\Phi_+^4) \quad . \end{aligned} \tag{2.81}$$

We now perform a change of the field variables in order to distinguish the classical field (denoted Φ) and quantum fluctuations (denoted Π)

$$\Phi = \frac{1}{2}(\Phi_- + \Phi_+)\,, \tag{2.82}$$

$$\Pi = \Phi_- - \Phi_+\,. \tag{2.83}$$

As we are interested in systems where both Φ_+ and Φ_- are large, the above interpretations of Φ and Π are already at least qualitatively justified.
In terms of these new fields the Lagrangian becomes

$$\mathcal{L}_{\Phi\Pi} = \partial_\mu\Phi\partial^\mu\Pi - m^2\Phi\Pi - \frac{\lambda}{3!}(\Phi^3\Pi + \frac{1}{4}\Phi\Pi^3) \quad . \tag{2.84}$$

The classical Lagrangian is then obtained by neglecting the cubic term in Π, giving

$$\mathcal{L}_{\Phi\Pi} = \partial_\mu\Phi\partial^\mu\Pi - m^2\Phi\Pi - \frac{\lambda}{3!}\Phi^3\Pi \quad . \tag{2.85}$$

Indeed, using (2.85) it can be easily shown now that Φ fulfills the classical equation of motion

$$(\Box + m^2)\Phi + \frac{\lambda}{3!}\Phi = 0 \quad . \tag{2.86}$$

From the Lagrangian (2.84) one can identify the vertices of the theory (fig. 2.8).

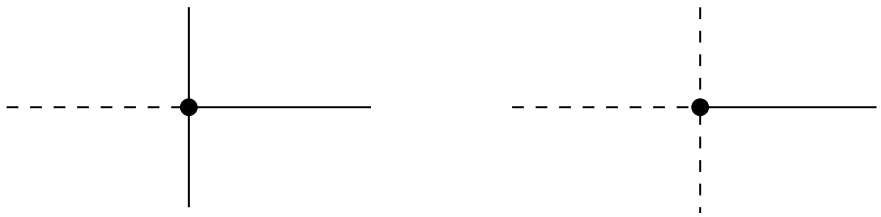

Figure 2.8: vertices of the scalar theory.

The full lines correspond to the classical field Φ and the dashed lines to the quantum fluctuations Π. The diagram on the left will be called classical vertex, the right one quantum vertex.
The most important quantities for our argumentations will be the free propagators for the Φ and Π fields, respectively. In a more rigorous discussion one should adopt the full propagators, but mass corrections are negligible as long as the coupling constant is small enough, i.e. $f\lambda \ll 1$. (For details on this point see [54].)
Note that there are also mixed propagators describing the change from Φ to Π and vice versa. Mueller and Son use the definition $G_{\Phi\Phi}(x,y) = \langle\Phi(x)\Phi(y)\rangle$ and similarly for $G_{\Pi\Phi}$, $G_{\Phi\Pi}$ and $G_{\Pi\Pi}$. Taking the relations (2.83) and remembering the previous discussion on free

propagators in the real time formalism, especially equation (2.19), one easily obtains the momentum-space expression

$$G_{\Phi\Phi} = 2\pi\delta(p^2 - m^2)(f + \frac{1}{2}) \quad . \tag{2.87}$$

As was pointed out by Jeon [56] this propagator looks slightly different when derived more carefully via a classical path integral. But it turns out that the final result in [54] is essentially correct for $f \gg 1$ with an adjustment of $f + \frac{1}{2} \to f$. The other propagators read

$$G_{\Pi\Phi} = \frac{i}{p^2 - m^2 - i\varepsilon p_0} \quad , \tag{2.88}$$

$$G_{\Phi\Pi} = \frac{i}{p^2 - m^2 + i\varepsilon p_0} \quad , \tag{2.89}$$

$$G_{\Pi\Pi} = 0 \quad . \tag{2.90}$$

The crucial observation here is that only $G_{\Phi\Phi}$ depends on the occupation number f. Thus, it is easy to give the parametrical dependence on f of a given diagram.
Mueller and Son now derive a Boltzmann-like equation starting from the Schwinger-Dyson series and applying a gradient expansion [54]. Their result is

$$\frac{d}{dt}f = \frac{-i}{2\omega(p)}\left(\Sigma_{\Pi\Phi} - \Sigma_{\Phi\Pi}\right)\left(f + \frac{1}{2}\right) + \frac{i}{2\omega(p)}\Sigma_{\Pi\Pi} \quad , \tag{2.91}$$

where $\omega(p) = \sqrt{\mathbf{p}^2 + m^2}$. The Σ's are the different self-energies in this basis, which are defined such that each $-i\Sigma$ is a sum of one-particle irreducible graphs [54].

2.6.3 Boltzmann equation

As we have already discussed, the Boltzmann equation describes the time evolution of the occupation number f of a given state as the difference between the scattering of particles into and out of this state (gain and loss terms). These scatterings are included in the collision term $C(p)$. Considering the scalar field theory (2.80) one may express the collision term to lowest order diagrammatically (fig. 2.9).

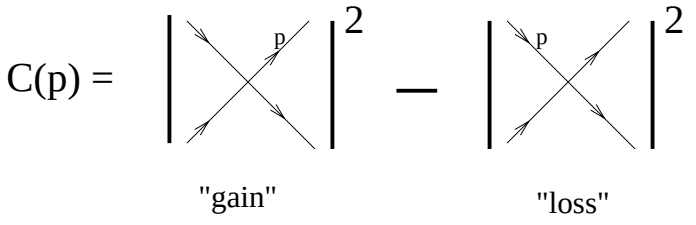

Figure 2.9: collision term to lowest order.

Mueller and Son show now by an explicit calculation that in lowest order perturbation theory the collision term $C(p)$ agrees with the right hand side of (2.91) in the leading (cubic and quadratic) terms in f when the classical Lagrangian (2.85) is used to compute the Σ's [54]. The full Lagrangian (2.84) has to be incorporated in (2.91) to exactly reproduce the Boltzmann equation.
These useful conclusions can be understood more easily in looking at the topology of the

involved diagrams in $C(p)$. It is easy to see that these are effectively sunset graphs (fig. 2.10), just like the lowest order contributions to the Σ's in (2.91).

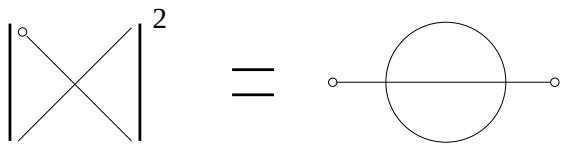

Figure 2.10: collision term topology.

Speaking again in terms of Φ and Π fields we now adopt the corresponding vertices in these diagrams. The classical field approximation then consists in retaining only collision term diagrams without quantum vertices.

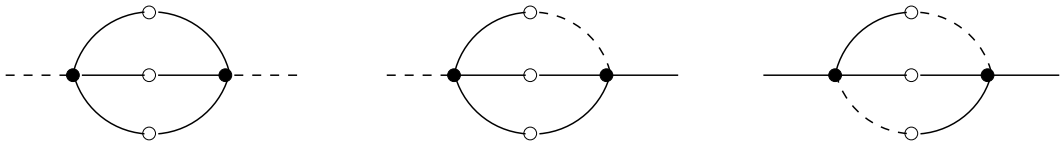

Figure 2.11: classical contribution to $C(p)$.

In figure 2.11 the three different classical diagrams are shown. The left one is proportional to $(f+\frac{1}{2})^3$ as three propagators $G_{\Phi\Phi}$ appear. Here and in the following empty circles appear in propagators while full circles stand for vertices. Similarly, the other graphs are proportional to $(f+\frac{1}{2})^2$ and $(f+\frac{1}{2})^1$, respectively. (To be precise, we should remark that the right diagram is in fact zero, as $\Sigma_{\Phi\Phi}$ vanishes to any order in perturbation theory [55].)
In the Boltzmann equation one has to include additionally the diagrams with one quantum vertex (fig. 2.12).

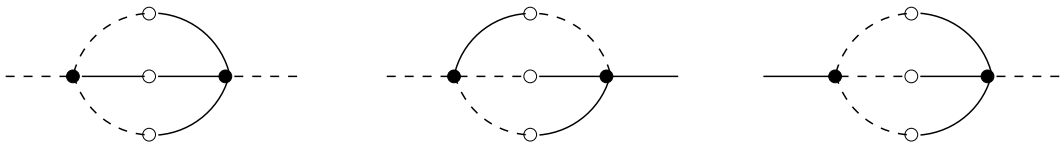

Figure 2.12: quantum contribution to $C(p)$.

In figure 2.12 the left diagram is proportional to $(f+\frac{1}{2})^1$ while the others are independent of f. There are no lowest order diagrams with two quantum vertices as at least one propagator $G_{\Pi\Pi}=0$ would appear.
Thus one may conclude without any computation that classical field theory and the Boltzmann equation are equivalent in orders f^3 and f^2. So we obtain the same result as Mueller and Son in [54] but in a considerably simpler way. This method also enables us to treat the more interesting case of hot QCD [53], as we will show in the next section.

2.7 High energy QCD

2.7.1 Separation of classical and quantum contributions

The results of the previous section may be generalized to QCD by making two approximations which are frequently used in the context of heavy ion collisions.
First, we will work within the gluon saturation scenario [41, 43, 44, 45]. This means that we may neglect the fermionic degrees of freedom in our system. So the QCD Lagrangian simplifies considerably and reads in the CTP formalism

$$\mathcal{L}_{CTP} = -\frac{1}{4}F_a^{\mu\nu}F_{a\mu\nu}[A^-_{a\mu}] + \frac{1}{4}F_a^{\mu\nu}F_{a\mu\nu}[A^+_{a\mu}] \quad . \tag{2.92}$$

In analogy to the field transformation in the scalar case we now define

$$\Phi_{a\mu} = \frac{1}{2}(A^-_{a\mu} + A^+_{a\mu}) \,, \tag{2.93}$$

$$\Pi_{a\mu} = A^-_{a\mu} - A^+_{a\mu} \,, \tag{2.94}$$

This leads to the following expression for $F^{a+}_{\mu\nu}$

$$\begin{aligned} F^{a+}_{\mu\nu} &= \partial_\mu A^{a+}_\nu - \partial_\nu A^{a+}_\mu + g f^{abc} A^{b+}_\mu A^{c+}_\nu \\ &= \partial_\mu \Phi^a_\nu - \partial_\nu \Phi^a_\mu + g f^{abc} \Phi^b_\mu \Phi^c_\nu \\ &- \frac{1}{2}(\partial_\mu \Pi^a_\nu - \partial_\nu \Pi^a_\mu - \frac{1}{2} g f^{abc} \Pi^b_\mu \Pi^c_\nu) \\ &- \frac{1}{2} g f^{abc} (\Phi^b_\mu \Pi^c_\nu + \Pi^b_\mu \Phi^c_\nu) \quad , \end{aligned} \tag{2.95}$$

and similarly for $F^{a-}_{\mu\nu}$.
Although there is no explicit mass term in (2.95) gluons will acquire a thermal mass in the medium created. Thus we can ignore in the following specific difficulties coming from the masslessness of the gauge fields. A discussion on these problems can be found in [12].
Next we express the Lagrangian (2.92) in terms of the fields Φ_μ and Π_μ. Neglecting higher than linear terms in the quantum fluctuations Π_μ one obtains

$$\mathcal{L}_{\text{linear}} = (D^{ab}_\mu F^{\mu\nu}_b[\Phi])\Pi^a_\nu \tag{2.96}$$

with

$$D^{ab}_\mu = \partial_\mu \delta^{ab} - g f^{abc} \Phi^c_\mu \quad , \tag{2.97}$$

$$F^{\mu\nu}_b[\Phi] = \partial^\mu \Phi^\nu_b - \partial^\nu \Phi^\mu_b + g f^{bcd} \Phi^\mu_c \Phi^\nu_d \quad . \tag{2.98}$$

Thus, Φ_μ fulfills the classical equation of motion

$$D^{ab}_\mu F^{\mu\nu}_b[\Phi] = 0 \quad . \tag{2.99}$$

So our interpretation of Φ_μ as classical field is justified in complete analogy to the scalar case. From the equations (2.96) to (2.98) one also sees that there is only one classically allowed vertex in first order in the coupling constant g (fig. 2.13).

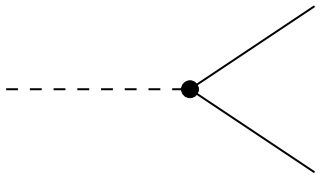

Figure 2.13: classical vertex in QCD.

Here full lines denote classical fields and dashed lines quantum corrections like in the previous section.
In order to obtain the quantum couplings one has to take into account the terms nonlinear in Π_μ. The corresponding Lagrangian may easily be computed and reads

$$\mathcal{L}_{nonlin} = -\frac{1}{4} g f_{abc} \Pi^{b\mu} \Pi^{c\nu} \{ \frac{1}{2} (\partial_\mu \Pi^a_\nu - \partial_\nu \Pi^a_\mu) + g f^{ade} \Phi^d_\mu \Pi^e_\nu \} \quad . \tag{2.100}$$

So we have one first order quantum coupling (fig. 2.14).

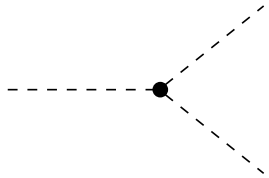

Figure 2.14: quantum vertex in QCD.

2.7.2 The collision term

Our second approximation leads to a simple topology of the collision term C. As fermions are neglected the only contributions to C come from gluon scattering. We now assume that the t-channel dominates, where t is the Mandelstam variable (see, e.g., [57]). (In fact, our only assumption is to work in the high energy limit where both approximations are valid.)
The t-channel gluon scattering is shown diagramatically in figure 2.15.

Figure 2.15: t-channel gluon scattering.

This makes the relevant collision term topology quite simple as can be seen in figure 2.16 (in contrast to the previous section only three-field vertices are present).

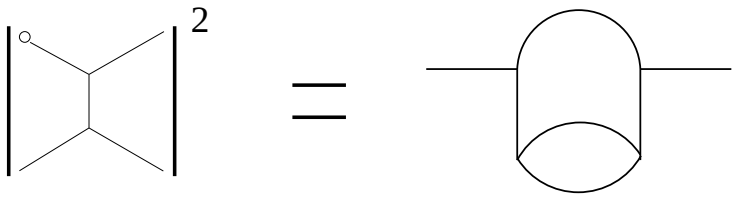

Figure 2.16: collision term topology in QCD.

As the main features of the propagators do not change, especially $G_{\Phi\Phi} \propto (f+\frac{1}{2})$ and $G_{\Pi\Pi} = 0$, we are now again ready to compare classical field theory with the Boltzmann equation. As before the classical approximation consists in neglecting diagrams with quantum vertices which are only taken into account in the full collision term.
Let us consider for example the diagram in figure 2.17 that clearly has the required topology.

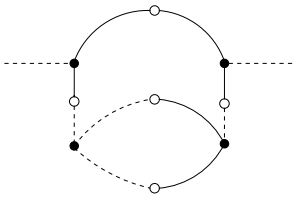

Figure 2.17: quantum contribution to $C(p)$.

It contains one quantum vertex so it is not included in the classical approximation. The contribution from this graph to the collision term is proportional to $(f+\frac{1}{2})$ as one propagator $G_{\Phi\Phi}$ appears. Similarly, the diagram in figure 2.18 is classical and proportional to $(f+\frac{1}{2})^3$.

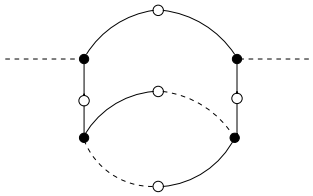

Figure 2.18: classical contribution to $C(p)$.

It is easy to check that these examples give already the highest order contributions to the classical approximation and the quantum corrections, respectively.
In summary, we re-examined the equivalence of classical field theory and the Boltzmann equation at large occupation numbers. Using a simple and elegant graphical method we are able to show that the main conclusions in the scalar case remain valid in high energy QCD: The classical field approximation and the quantum Boltzmann equation match in orders f^3 and f^2, i.e. in all but linear orders of the gluon occupation number.

2.8 Puzzles and perspectives

We end this chapter with a short discussion on some open questions related to thermalization in HIC.
We showed that the framework presented here - the MV model followed by the bottom-up scenario - is in itself consistent. But one may worry if at currently available collider energies perturbative QCD gives reliable results. At least, it is probably too optimistic to believe that the separate bottom-up regimes are sharply distinct at RHIC energies.

Indeed, the community was quite puzzled by some features of recent experimental data. First, the MV model, based on leading order pQCD calculations, predicts a saturation scale Q_s of at most 2 GeV for RHIC. This is insufficient to describe mid-rapidity data and one has to artificially enhance Q_s due too (poorly understood) non-perturbative effects [58].
In addition, RHIC data provides strong indications for collective phenomena in the created medium. The measured elliptic flow appears to be successfully described by hydrodynamical models. The success of hydro led to the notion sQGP for the produced matter at RHIC [59]. The letter s stands for strong coupling, which in the literature normally means that $\alpha \gtrsim 1$ but may also refer to the plasma coupling parameter [60]. Note that hydrodynamics becomes applicable when the mean free path of partons is much smaller than the size of the system, i.e. when the system is sufficiently thermalized. To reproduce data correctly, however, one has to assume a very short thermalization time $\tau_{th} \lesssim 0.6$ fm. This rapid thermalization remains somewhat mysterious. The traditional bottom-up approach gives parametrically $Q_s \tau_{th} \approx \alpha^{-13/5}$ which corresponds to $\tau_{th} \approx 2 - 3$ fm for RHIC energies [61].

In recent years, several new ideas have been discussed to explain this apparent discrepancy. For instance, Kharzeev and Tuchin proposed a new thermalization scenario ('black hole thermalization') which is based on the Hawking-Unruh effect in heavy ion collisions [62]. Kovchegov advocates that thermalization in QCD cannot be described by Feynman diagrams and tries to mimic non-perturbative effects by an instanton ensemble [63, 64].
Others argue that the onset of hydrodynamics does not necessarily require thermalization but only isotropization. The use of hydrodynamics is based on conservation laws which involve the different components of the energy-momentum tensor. In ideal hydro (i.e. dissipative terms are neglected) these equations can be closed if an isotropic pressure can be expressed as a function of the energy density by an equation of state. Indeed, it could be demonstrated in a scalar model that isotropization happens much faster than the approach to thermal equilibrium [65].
Finally, in gauge theories like QCD it was discovered that plasma instabilities may strongly affect the relevant time scales [66, 67, 68, 69]. In [70] the modifications of these instabilities on the Bottom-up scales are discussed. As it seems, the thermalization time is hardly changed but isotropization may be reached at a rate which is parametrically faster compared to perturbative scattering rates [71, 72]. Therefore, the early onset of hydrodynamic behaviour at RHIC is not necessarily in conflict with theoretical expectations based on pQCD.

To summarize, the mechanism of thermalization in HIC still lacks a complete and satisfactory understanding. More work is needed to deepen our insight in this fundamental issue. Hopefully, some of the remaining puzzles can be solved with the help of the upcoming experiments at the LHC.

Chapter 3

BEC and the 2PI effective action

In 1925 Einstein used statistical methods (inspired by work of Bose) to examine the ideal bosonic quantum gas [73]. He predicted that below a critical temperature a large fraction of the particles in the gas suddenly start to populate the energy ground state. Indeed, this phase transition, referred to as Bose-Einstein condensation (BEC), was observed experimentally in 1995 by three independent groups using alkali atoms [74, 75, 76]. The same phenomenon also plays a crucial role in the context of superfluidity and supraconductivity. A detailed description of the dynamics of the phase transition clearly requires nonequilibrium methods. In this chapter we use 2PI effective action techniques to deal with this problem. These powerful tools were applied to a variety of situations in recent years, e.g. [77, 78, 79, 80, 81, 82] (see also the review articles [83, 84, 85, 86]).

We start this chapter with a discussion on the Gross-Pitaevskii (GP) equation, representing the standard approach to BEC, and its generalization to finite temperature. Then we switch to the main concepts of 2PI techniques in scalar theories. Finally, we use 2PI equations of motion to reproduce former results on BEC dynamics and to numerically go beyond Boltzmann's approximation.

3.1 Gross-Pitaevskii approach to BEC

In 1924 Bose gave a novel derivation of the Planck distribution for photons [87] using statistical considerations. This work led Einstein to the prediction that a gas of bosonic atoms exhibits a phase transition at low temperatures, when a macroscopic number of atoms occupy the lowest energy level [73]. Nowadays, the basic physics of this phase transition is dicussed in every textbook on statistical mechanics (e.g. [88]).
Following Griffin [90] we estimate the critical temperature T_c in a simple manner by considering the thermal de Broglie wavelength λ_T and the interparticle distance $d \sim \frac{1}{n^{1/3}}$, where n is the particle density. The transition occurs when λ_T becomes comparable or bigger to $d \sim \frac{1}{n^{1/3}}$. All the atoms then become correlated and the gas exhibits new collective behaviour even in absence of interactions. This simple picture leads to the criterion $n\lambda_T^3 \gtrsim 1$, while a more careful analysis [88] gives for the case of a uniform ideal Bose gas $n\lambda_T^3 = \zeta(3/2) = 2.612$. In a gas of atoms at temperature T the thermal de Broglie wavelength is given by

$$\lambda_T = \left(\frac{2\pi\hbar^2}{m k_B T} \right)^{\frac{1}{2}} . \tag{3.1}$$

Thus, writing $n = N/V$, we obtain for the critical temperature

$$T_c = \frac{2\pi\hbar^2}{mk_B}\left(\frac{N}{2.612V}\right)^{2/3}. \tag{3.2}$$

For a temperature T below T_c equation (3.2) no longer involves the total number of atoms N but only the number of excited atoms N_{exc}. Thus, for the condensate atoms N_c one has the well-known formula

$$N_c = N - N_{exc} = N \cdot \left[1 - \left(\frac{T}{T_c}\right)^{3/2}\right]. \tag{3.3}$$

At $T = 0$, all the atoms in an ideal gas are in this $\mathbf{p} = \mathbf{0}$ state.
This result was used by Fritz London in 1938 [91] - many years after Einstein's prediction - to explain superfluidity in liquid ^{4}He, a composite Boson ($S = 0$). Indeed, the formula in (3.2) gives $T_c \sim 3K$ for liquid ^{4}He, which agrees quite well with the observed transition temperature $T_\lambda \sim 2.17K$.

As we emphasized above, equation (3.3) is only valid for a uniform gas. For dilute gases in a harmonic trap, as it is used in most experiments today, the corresponding result is [92]

$$\frac{N_c(T)}{N} = \left[1 - \left(\frac{T}{T_c}\right)^3\right]. \tag{3.4}$$

The comparison of equation (3.4) with experimental data is shown in figure 3.1.

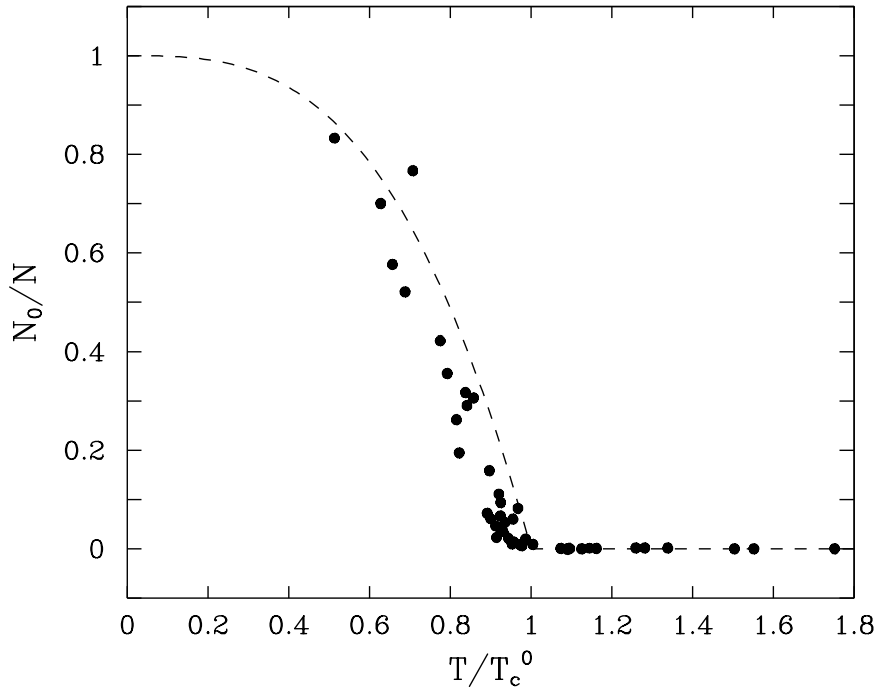

Figure 3.1: Condensate fraction as a function of T/T_c^0 (from [92]). Circles are the experimental results of Ensher et al.[89], while the dashed line is the law (3.4).

Since the 1970's, there has been increasing interest by experimentalists to find a pure form of BEC, namely in a dilute low temperature gas. The two early candidates for Bosons were excitons (electron-hole pairs) in semiconductors and spin-polarized hydrogen atoms.
Since the early 1990's, attention has focussed on the bosonic alkali atoms Li, Na, K, Rb, Cs. They have a magnetic moment and can therefore be trapped by magnetic fields. In the summer of 1995, BEC was announced by three groups led by C. Wieman and E. Cornell (JILA), using ^{87}Rb atoms [74] (see fig. 3.2), W. Ketterle (MIT), using ^{23}Na atoms [75] and R. Hulet (Rice University), using ^{7}Li atoms [76]. The strategy of each group was to use laser-cooling to get to very low temperatures. Then, one selectively flips the spin of higher energy trapped atoms. These atoms are ejected from the magnetic trap and the remaining atoms quickly thermalize to a lower temperature. This very efficient technique is called evaporative cooling.

Early reports on atomic condensates discussed the system as an ideal Bose gas. It was soon realized that even in these very dilute gases the interactions play a crucial role, for instance after evaporative cooling. After fast atoms are removed by induced spin-flips, it is important that remaining atoms can quickly rethermalize through collisions. In this section we will give a short account on the standard approach to the theory of dilute Bose condensed gases, namely the Gross-Pitaevskii equation. First, we discuss the simple case of a pure condensate at $T = 0$ including its description in terms of hydrodynamic variables. Our presentation of this material heavily relies on review articles by Griffin [90, 93]. We then show how interactions with the cloud of non-condensed atoms can be taken into account by a Boltzmann equation.

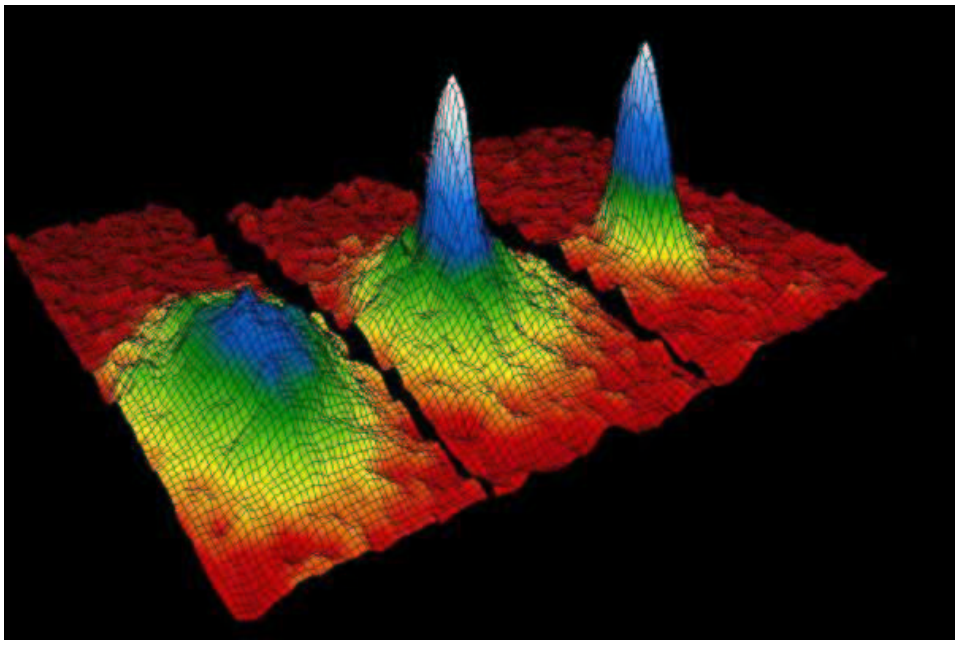

Figure 3.2: Images of the velocity distribution of rubidium atoms. The left frame corresponds to a gas at a temperature just above condensation; the center frame, just after the appearance of the condensate; the right frame, after further evaporation leaves a sample of nearly pure condensate [92].

3.1.1 Dynamics of the pure condensate

Bose condensed gases are normally discussed using quantum field operators. Pioneering work on this subject was done by Landau, Beliaev, Bogoliubov and others [94, 95, 96, 97, 98]. More recent reviews on the theory of dilute weakly interacting quantum gases can be found in [92, 99, 100, 101].
We begin by introducing

$$\begin{aligned} \psi^\dagger(\mathbf{r}) &\longmapsto \text{ creates atom at } \mathbf{r} \\ \psi(\mathbf{r}) &\longmapsto \text{ destroys atom at } \mathbf{r}. \end{aligned} \tag{3.5}$$

These field operators satisfy the usual equal time commutation relations, such as

$$\left[\psi(\mathbf{r}), \psi^\dagger(\mathbf{r}')\right] = \delta(\mathbf{r} - \mathbf{r}'). \tag{3.6}$$

All observables can be expressed in terms of ψ and $\psi^\dagger$. As an example, the interaction energy reads

$$\begin{aligned} V_{int} &= \frac{1}{2}\int d\mathbf{r} \int d\mathbf{r}' \psi^\dagger(\mathbf{r}')\psi^+(\mathbf{r})v(\mathbf{r}-\mathbf{r}')\psi(\mathbf{r}')\psi(\mathbf{r}) \\ &= \frac{1}{2}g\int d\mathbf{r}\psi^\dagger(\mathbf{r})\psi^\dagger(\mathbf{r})\psi(\mathbf{r})\psi(\mathbf{r}). \end{aligned} \tag{3.7}$$

Here we used the fact that we deal with a dilute gas, so only binary collisions have to be taken care of. Thus, we can approximate the real interatomic potential $v(\mathbf{r})$ by a pseudopotential using the s-wave scattering length a [92]

$$v(\mathbf{r}) \simeq \frac{4\pi\hbar^2}{m} a\delta(\mathbf{r}) = g\delta(\mathbf{r}). \tag{3.8}$$

This replacement is valid if a is much smaller than the average distance between atoms, or $na^3 \ll 1$. In current experiments with about 10^6 atoms at temperatures around 100 nK typical values are $a = 58 \cdot 10^{-10} m$ for ^{87}Rb and $n \simeq \frac{10^{13}-10^{14}}{cm^3}$, so the approximation (3.8) is well justified [102].

As an aside, we give here a short account on a recent experimental technique allowing to study Bose condensed systems in the strong coupling regime.
When one considers a gas of bosonic atoms the underlying fermionic degrees of freedom do not play any role, as the energy needed to split an atom into two fermions is orders of magnitude larger than the condensation energy. In recent years, however, experimentalists become very interested in exploring Bose Einstein condensation with fermionic atoms [102, 103, 104]. Starting with e.g. ^{40}Ka one can tune the interatomic interaction by an external magnetic field. At a so-called Feshbach resonance a new diatomic bound state appears, allowing for the formation of weakly bound bosonic molecules (with a binding energy of only some kHz) which can condense into the energy ground state. Around this resonance the scattering length diverges and changes its sign, going from effectively attractive ($a > 0$) to repulsive ($a < 0$) interaction (see fig. 3.3).
In these experiments one can also explore the close connection between fermionic superconductivity (on the BCS side of the resonance) and Bose-Einstein condensation. Thus,

the BEC-BCS crossover region provides an important example of strongly coupled quantum gases, which will be interesting for our contribution to this field.

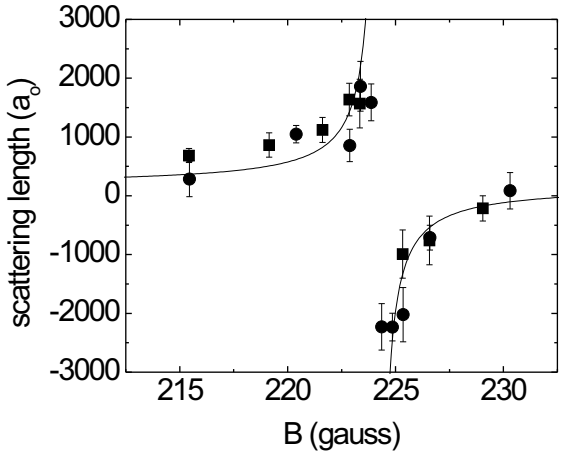

Figure 3.3: Experimental data confirming the characteristic divergence of the scattering length at a Feshbach resonance. On the left (BEC) side one has weakly bound diatomic molecules while on the right (BCS) side of the resonance the fermionic nature of ^{40}Ka atoms prevails (from [104]).

Returning to the discussion on quantum field operators, the important next step is to separate out the condensate part

$$\begin{aligned} \psi(\mathbf{r}) &= \langle\psi(\mathbf{r})\rangle + \widetilde{\psi}(\mathbf{r}) \\ &= \Phi(\mathbf{r}) + \widetilde{\psi}(\mathbf{r})\,. \end{aligned} \tag{3.9}$$

The macroscopic wavefunction $\Phi(\mathbf{r})$ plays the role of the order parameter for the phase transition

$$\begin{aligned} \Phi(\mathbf{r}) &= 0 \quad \text{for } T > T_c \\ &\neq 0 \quad \text{for } T < T_c\,. \end{aligned} \tag{3.10}$$

Taking the second-quantized Hamiltonian for an interacting gas in an external potential V_{ex},

$$H = \int d\mathbf{r}\psi^\dagger(\mathbf{r})\left(-\frac{\hbar^2\nabla^2}{2m} + V_{ex}(\mathbf{r})\right)\psi(\mathbf{r}) + \frac{1}{2}g\int d\mathbf{r}\psi^\dagger(\mathbf{r})\psi^\dagger(\mathbf{r})\psi(\mathbf{r})\psi(\mathbf{r})\,, \tag{3.11}$$

one obtains the exact Heisenberg equation of motion for the field operator

$$\begin{aligned} i\hbar\frac{\partial\psi(\mathbf{r},t)}{\partial t} &= [\psi(\mathbf{r},t), H] \\ &= \left(-\frac{\hbar^2\nabla^2}{2m} + V_{ex}(\mathbf{r})\right)\psi(\mathbf{r},t) + g\psi^\dagger(\mathbf{r},t)\psi(\mathbf{r},t)\psi(\mathbf{r},t)\,. \end{aligned} \tag{3.12}$$

This gives an exact equation of motion for the macroscopic field

$$i\hbar\frac{\partial\Phi(\mathbf{r},t)}{\partial t} = \left[-\frac{\hbar^2\nabla^2}{2m} + V_{ex}(\mathbf{r})\right]\Phi(\mathbf{r},t) + g\langle\psi^\dagger(\mathbf{r},t)\psi(\mathbf{r},t)\psi(\mathbf{r},t)\rangle, \tag{3.13}$$

with

$$\psi^\dagger\psi\psi = |\Phi|^2\Phi + 2|\Phi|^2\widetilde{\psi} + \Phi^2\widetilde{\psi}^\dagger + \Phi^\dagger\widetilde{\psi}\widetilde{\psi} + 2\Phi\widetilde{\psi}^\dagger\widetilde{\psi} + \widetilde{\psi}^\dagger\widetilde{\psi}\widetilde{\psi}. \tag{3.14}$$

Taking the expectation value of equation (3.14), one finds

$$\langle\psi^\dagger\psi\psi\rangle = n_c\Phi + \widetilde{m}\Phi^\dagger + 2\widetilde{n}\Phi + \langle\widetilde{\psi}^\dagger\widetilde{\psi}\widetilde{\psi}\rangle, \tag{3.15}$$

where we introduced

$$\begin{aligned} n_c(\mathbf{r},t) &= |\Phi(\mathbf{r},t)|^2, \\ \widetilde{n}(\mathbf{r},t) &= \langle\widetilde{\psi}^\dagger(\mathbf{r},t)\widetilde{\psi}(\mathbf{r},t)\rangle, \\ \widetilde{m}(\mathbf{r},t) &= \langle\widetilde{\psi}(\mathbf{r},t)\widetilde{\psi}(\mathbf{r},t)\rangle. \end{aligned}$$

The condensate equation (3.13) is formally exact, but not closed since it involves the three-field correlation function $\langle\widetilde{\psi}^\dagger\widetilde{\psi}\widetilde{\psi}\rangle$, the noncondensate density $\widetilde{n}$ and the off-diagonal (anomalous) density $\widetilde{m}$. In this section we limit ourselves to $T \ll T_c$, where we can assume that these noncondensate variables are negligible, leaving

$$i\hbar\frac{\partial\Phi(\mathbf{r},t)}{\partial t} = \left[-\frac{\hbar^2\nabla_r^2}{2m} + V_{ex}(\mathbf{r}) + g|\Phi(\mathbf{r},t)|^2\right]\Phi(\mathbf{r},t). \tag{3.16}$$

This is the well-known time-dependent Gross-Pitaevskii equation for the condensate macroscopic wavefunction [105, 106]. It gives a complete description of the dynamics of a coherent matter wave at $T = 0$. A condensate described by $\Phi(\mathbf{r},t)$ may be viewed as a classical matter wave, as emphasized by Pitaevskii and Stringari [107]. This is quite different from ordinary quantum de Broglie waves, since one can ignore quantum fluctuations due to the large number of condensate atoms N_c. It is also quite different than ordinary classical macroscopic objects and electromagnetic waves, since $\Phi(\mathbf{r},t)$ is described by the GP equation (3.16) which involves Planck's constant $\hbar$. Thus $\Phi(\mathbf{r},t)$ is a classical object which is described by a quantum equation [90].

3.1.2 Quantum hydrodynamic formulation

In order to further understand the physical meaning of the condensate wavefunction Φ we rewrite the GP equation in terms of the amplitude and phase variables [92]

$$\Phi(\mathbf{r},t) = \sqrt{n_c}e^{i\theta}. \tag{3.17}$$

Inserting this into (3.16) and separating out the real and imaginary parts of the equation gives

$$\frac{\partial n_c(\mathbf{r},t)}{\partial t} + \boldsymbol{\nabla}\cdot n_c(\mathbf{r},t)\mathbf{v}_c(\mathbf{r},t) = 0, \tag{3.18}$$

$$\hbar\frac{\partial\theta(\mathbf{r},t)}{\partial t} = -\left[\mu_c(\mathbf{r},t) + \frac{1}{2}mv_c^2(\mathbf{r},t)\right]. \tag{3.19}$$

Here we introduced the superfluid velocity $\mathbf{v}_c$, which is related to the condensate phase θ by

$$m\mathbf{v}_c(\mathbf{r},t) = \hbar\boldsymbol{\nabla}\theta(\mathbf{r},t)\,, \tag{3.20}$$

and the condensate chemical potential is

$$\mu_c(\mathbf{r},t) = -\frac{\hbar^2\nabla^2\sqrt{n_c}}{2m\sqrt{n_c}} + V_{ex}(\mathbf{r}) + gn_c(\mathbf{r},t). \tag{3.21}$$

Taking the gradient of (3.19) gives

$$m\left(\frac{\partial\mathbf{v}_c}{\partial t} + \frac{1}{2}\boldsymbol{\nabla}\mathbf{v}_c^2\right) = -\boldsymbol{\nabla}\mu_c. \tag{3.22}$$

Equations (3.18) and (3.22) describe the system in a notation familiar from hydrodynamics and can be identified with the continuity and Euler equations, respectively.

3.1.3 Generalized GP equation at finite temperature

Let us recall from (3.13) and (3.14) the exact equation of motion for Φ

$$\begin{aligned} i\hbar\frac{\partial\Phi}{\partial t} &= \left[-\frac{\nabla^2}{2m} + V_{ex} + gn_c(\mathbf{r},t) + 2g\widetilde{n}(\mathbf{r},t)\right]\Phi \\ &+ g\widetilde{m}(\mathbf{r},t)\Phi^\dagger + g\langle\widetilde{\psi}^\dagger(\mathbf{r},t)\widetilde{\psi}(\mathbf{r},t)\widetilde{\psi}(\mathbf{r},t)\rangle. \end{aligned} \tag{3.23}$$

In the last section we neglected the effect of the thermal cloud on the condensate atoms. There are, however, interesting topics like the study of condensate growth where an analysis at $T = 0$ is obviously not sufficient. Thus we have to take into account the non-condensed variables $\langle\widetilde{\psi}^\dagger\widetilde{\psi}\widetilde{\psi}\rangle$, $\widetilde{n}$ and $\widetilde{m}$. There exist various approximations in the literature to deal with this problem, e.g.

- The Hartree-Fock-Bogoliubov (HFB) approximation for Φ corresponds to neglecting the three-field correlation function $\langle\widetilde{\psi}^\dagger\widetilde{\psi}\psi\rangle$ but keeping the $n_c, \widetilde{n}$ and $\widetilde{m}$ fluctuations [108, 109, 110, 111].
- The dynamic Popov approximation corresponds to ignoring both $\langle\widetilde{\psi}^\dagger\widetilde{\psi}\widetilde{\psi}\rangle$ and $\widetilde{m}$ in (3.23), leading to coupled equations for Φ and $\widetilde{n}$ [112].
- The static Popov approximation [92, 108, 113] additionally ignores fluctuations in the density $\widetilde{n}(\mathbf{r},t)$ of the thermal cloud in setting $\widetilde{n}(\mathbf{r},t) \simeq \widetilde{n}_0(\mathbf{r})$.

All the above approximations neglect the three-field correlation function. But as we will see shortly, $\langle\widetilde{\psi}^\dagger\widetilde{\psi}\psi\rangle$ plays an important role for collisions between condensed and excited atoms. Thus, it must appear in any approximation to (3.23) that is able to capture condensate growth.

In [114] Zaremba, Nikuni and Griffin (ZNG) show how $\langle\widetilde{\psi}^\dagger\widetilde{\psi}\psi\rangle$ can be approximated within a quasiparticle picture. In the following, we give a dense review of their work and refer to [114] for a more detailed presentation (see also [115, 116, 117, 118] for related work). They start with the exact equation of motion for $\widetilde{\psi}$, which can be derived from (3.12) and (3.23) together with (3.9), giving

$$i\hbar\frac{\partial\widetilde{\psi}}{\partial t} = \left(-\frac{\hbar^2\nabla^2}{2m} + U_{ext} + 2gn \right)\widetilde{\psi} - 2g\widetilde{n}\widetilde{\psi} + g\Phi^2\widetilde{\psi}^\dagger$$
$$+ g\Phi^\dagger(\widetilde{\psi}\widetilde{\psi} - \widetilde{m}) + 2g\Phi(\widetilde{\psi}^\dagger\widetilde{\psi} - \widetilde{n}) + g(\widetilde{\psi}^\dagger\widetilde{\psi}\widetilde{\psi} - \langle\widetilde{\psi}^\dagger\widetilde{\psi}\widetilde{\psi}\rangle)\,, \quad (3.24)$$

where $n = n_c + \widetilde{n}$ is the total density.
It is useful for the following reasoning to describe the time evolution of $\widetilde{\psi}$ alternatively by

$$\widetilde{\psi}(\mathbf{r},t) = U^\dagger(t,t_0)\widetilde{\psi}(\mathbf{r},t_0)U(t,t_0)\,, \quad (3.25)$$

The unitary time evolution operator $U(t,t_0)$ evolves according to the equation of motion

$$i\hbar\frac{dU(t,t_0)}{dt} = H_{\rm eff}(t)U(t,t_0)\,, \quad (3.26)$$

with $U(t_0,t_0) = 1$. Here, t_0 is the time at which the initial nonequilibrium density matrix $\rho(t_0)$ is specified. The effective Hamiltonian in (3.26) can be defined such that equations (3.25) and (3.26), together with the equal time commutatatin relations (3.6), reproduce the equation of motion for $\widetilde{\psi}$ in (3.24) [114].

Let us now turn to the problem of evaluating the expectation value of some arbitrary operator $\mathcal{O}(t)$ which is made up of some combination of noncondensate field operators $\widetilde{\psi}(\mathbf{r},t)$ and $\widetilde{\psi}^\dagger(\mathbf{r},t)$. Following the discussion in section 2.2 we introduce the initial density matrix $\rho(t_0)$. The expectation value $\langle\mathcal{O}(t)\rangle$ can now be expressed as

$$\begin{aligned}\langle\mathcal{O}(t)\rangle &= {\rm Tr}\rho(t_0)\mathcal{O}(t) \\ &= {\rm Tr}\widetilde{\rho}(t,t_0)\mathcal{O}(t_0)\,, \end{aligned} \quad (3.27)$$

where $\widetilde{\rho}(t,t_0) = U(t,t_0)\rho(t_0)U^\dagger(t,t_0)$ satisfies the following equation

$$i\hbar\frac{d\widetilde{\rho}(t,t_0)}{dt} = [H_{\rm eff}(t),\widetilde{\rho}(t,t_0)]\,. \quad (3.28)$$

Using the formalism given by equations (3.25) - (3.28), ZNG manage to compute in a lengthy excercise the three-field correlation function $\langle\widetilde{\psi}^\dagger\widetilde{\psi}\psi\rangle$ (see especially Appendix A in [114]). Their result is

$$\begin{aligned}\langle\widetilde{\psi}^\dagger\widetilde{\psi}\widetilde{\psi}\rangle &= -\frac{ig\Phi}{(2\pi)^5\hbar^6}\int d\mathbf{p}_1\int d\mathbf{p}_2\int d\mathbf{p}_3\,\delta(m\mathbf{v}_c + \mathbf{p}_1 - \mathbf{p}_2 - \mathbf{p}_3) \\ &\quad\times\delta(\varepsilon_c + \widetilde{\varepsilon}_{p_1} - \widetilde{\varepsilon}_{p_2} - \widetilde{\varepsilon}_{p_3})[f_1(1+f_2)(1+f_3) - (1+f_1)f_2f_3]\,, \end{aligned} \quad (3.29)$$

where the distribution function of excited atoms $f_i = f(\mathbf{p}_i,\mathbf{r},t)$ appears, which is defined below. The condensate and excited atom energy are given by $\epsilon_c = \mu_c(\mathbf{r},t) + \frac{1}{2}m\mathbf{v}_c^2(\mathbf{r},t)$ and $\widetilde{\varepsilon}_p(\mathbf{r},t) = \frac{p^2}{2m} + V_{ex}(\mathbf{r}) + 2g\,[n_c(\mathbf{r},t) + \widetilde{n}(\mathbf{r},t)]$, respectively, while $\mathbf{p}_c = m\mathbf{v}_c$ is the condensate atom momentum.
Obviously, equation (3.29) involves several approximations that deserve some discussion. First, it is a perturbative result, only linear terms in the coupling g are kept. Furthermore, ZNG claim that the anomalous density $\widetilde{m}$ can be consistently neglected. The appearance of

$f(\mathbf{p},\mathbf{r},t)$ and the single-particle spectrum used for $\widetilde{\varepsilon}_p(\mathbf{r},t)$ are appropriate in the semi-classical limit. More specifically, the conditions of validity for a gas in a harmonic trap are

$$k_B T \gg g n_c \ , \ k_B T \gg \hbar\omega_0, \tag{3.30}$$

where $\hbar\omega_0$ is the spacing of the energy levels of the trap.

The distribution function $f(\mathbf{p},\mathbf{r},t)$ is in this formalism conveniently defined as

$$f(\mathbf{p},\mathbf{r},t) = \mathrm{Tr}\widetilde{\rho}(t,t_0)\hat{f}(\mathbf{p},\mathbf{r},t_0)\,, \tag{3.31}$$

with the Wigner operator

$$\hat{f}(\mathbf{p},\mathbf{r},t_0) = \int d\mathbf{r}'\, e^{i\mathbf{p}\cdot\mathbf{r}'/\hbar}\widetilde{\psi}^{\dagger}(\mathbf{r}+\frac{\mathbf{r}'}{2},t_0)\widetilde{\psi}(\mathbf{r}-\frac{\mathbf{r}'}{2},t_0)\,. \tag{3.32}$$

It is easy to see that this definition of $f(\mathbf{p},\mathbf{r},t)$ preserves the desired properties. It allows one to calculate various nonequilibrium quantities, such as the noncondensate density

$$\widetilde{n}(\mathbf{r},t) = \int \frac{d\mathbf{p}}{(2\pi\hbar)^3} f(\mathbf{p},\mathbf{r},t)\,. \tag{3.33}$$

All in all, ZNG obtain the follwing approximated finite temperature GP equation

$$\begin{aligned} i\hbar\frac{\partial\Phi}{\partial t} &= \left[-\frac{\nabla^2}{2m} + V_{ex} + g n_c(\mathbf{r},t) + 2g\widetilde{n}(\mathbf{r},t)\right]\Phi \\ &- \frac{ig^2\Phi}{(2\pi)^5\hbar^6}\int d\mathbf{p}_1\int d\mathbf{p}_2\int d\mathbf{p}_3\delta(m\mathbf{v}_c+\mathbf{p}_1-\mathbf{p}_2-\mathbf{p}_3) \\ &\times\delta(\varepsilon_c+\widetilde{\varepsilon}_{p_1}-\widetilde{\varepsilon}_{p_2}-\widetilde{\varepsilon}_{p_3})[f_1(1+f_2)(1+f_3)-(1+f_1)f_2f_3]. \end{aligned} \tag{3.34}$$

This equation, however, is not closed. In order to have a complete set of equations, we need to derive a quantum Boltzmann equation that determines the distribution function $f(\mathbf{p},\mathbf{r},t)$. This can equally well be achieved within the ZNG formalism, as we will discuss now.

3.1.4 Boltzmann dynamics for excited atoms

The Boltzmann equation is obtained by manipulating the equation of motion for $f(\mathbf{p},\mathbf{r},t)$. Using (3.31) in (3.28), one obtains

$$\frac{\partial f(\mathbf{p},\mathbf{r},t)}{\partial t} = \frac{1}{i\hbar}\mathrm{Tr}\widetilde{\rho}(t,t_0)[\hat{f}(\mathbf{p},\mathbf{r},t_0),H_{\mathrm{eff}}(t)]\,. \tag{3.35}$$

Using the same approximations as before one may convert (3.35) into [114]

$$\frac{\partial f(\mathbf{p},\mathbf{r},t)}{\partial t} + \frac{\mathbf{p}}{m}\cdot\nabla f(\mathbf{p},\mathbf{r},t) - \nabla V\cdot\nabla_{\mathbf{p}} f(\mathbf{p},\mathbf{r},t) = \left.\frac{\partial f}{\partial t}\right|_{coll}, \tag{3.36}$$

where $V(\mathbf{r},t) = V_{ex}(\mathbf{r}) + 2g[\widetilde{n}(\mathbf{r},t)+n_c(\mathbf{r},t)]$ is assumed to vary slowly in space.
The right hand side of this Boltzmann equation represents the effect of collisions between the atoms. Within the applied approximations this term has the form of a binary collision integral. The detailed computation is quite involved (we refer again to Appendix A of [114] for details). However, the final result has a physically transparent form. The collision term is the sum of two contributions

$$\left.\frac{\partial f}{\partial t}\right|_{coll} = C_{12}[f] + C_{22}[f]\,, \tag{3.37}$$

with C_{12} and C_{22} given by

$$\begin{aligned} C_{12}[f] &= \frac{2g^2 n_c}{(2\pi)^2\hbar^4}\int d\mathbf{p}_1 \int d\mathbf{p}_2 \int d\mathbf{p}_3 \delta(m\mathbf{v}_c + \mathbf{p}_1 - \mathbf{p}_2 - \mathbf{p}_3) \\ &\quad \times\delta(\varepsilon_c + \widetilde{\varepsilon}_{p_1} - \widetilde{\varepsilon}_{p_2} - \widetilde{\varepsilon}_{p_3})[\delta(\mathbf{p}-\mathbf{p}_1) - \delta(\mathbf{p}-\mathbf{p}_2) - \delta(\mathbf{p}-\mathbf{p}_3)] \\ &\quad \times[(1+f_1)f_2 f_3 - f_1(1+f_2)(1+f_3)]\,, \end{aligned} \tag{3.38}$$

$$\begin{aligned} C_{22}[f] &= \frac{2g^2}{(2\pi)^5\hbar^7}\int d\mathbf{p}_2 \int d\mathbf{p}_3 \int d\mathbf{p}_4 \delta(\mathbf{p} + \mathbf{p}_2 - \mathbf{p}_3 - \mathbf{p}_4) \\ &\quad \times\delta(\widetilde{\varepsilon}_p + \widetilde{\varepsilon}_{p_2} - \widetilde{\varepsilon}_{p_3} - \widetilde{\varepsilon}_{p_4})\,[(1+f)(1+f_2)f_3 f_4 - f f_2(1+f_3)(1+f_4)]\,. \end{aligned} \tag{3.39}$$

Clearly C_{22} describes two-body collisions between excited atom while collisions involving one condensate atom are encoded in C_{12}. The latter collisions include scatterings of two noncondensate atoms into a noncondensate and a condensate state as well as the inverse process leading to a loss of condensate states. This is shown pictorially in figure 3.4. Dashed lines correspond to the condensate atoms and full ones to the excited quasi particles. The delta functions guarantee conservation of momentum and energy in the different processes. As a result of Bose statistics, the creation of an atom in a state i is associated with the statistical factor $(1 + f_i)$.

Figure 3.4: Scattering processes included in C_{12}

We argued earlier that the three-field correlation function $\langle\widetilde{\psi}^\dagger\widetilde{\psi}\psi\rangle$ must not be neglected as it is closely related to collisions between condensed and excited atoms. This makes sense, since the C_{12} collisions modify the condensate described by $\Phi(\mathbf{r}, t)$. Indeed, comparing (3.29) and (3.38) one easily verifies

$$\int \frac{d\mathbf{p}}{(2\pi)^3} C_{12}[f] = 2g\sqrt{n_c}\ \mathrm{Im}\langle\widetilde{\psi}^\dagger\widetilde{\psi}\widetilde{\psi}\rangle\,. \tag{3.40}$$

In summary, equations (3.34) and (3.36), together with (3.37) - (3.39), form a closed set of equations. The same results have been obtained by Stoof [119]. The approach builds in enough physics to describe nonequilibrium phenomena such as condensate growth and have has studied numerically using N-body simulations (see fig. 3.5). The range of validity, however, is quite restricted as a consequence of the various approximations used in the derivations. Most importantly, (3.34) and (3.36) are not applicable in strong coupling situations like in recent experiments that explore the BEC-BCS crossover region. Even to second order

in g these equations are not complete, as the anomalous density $\widetilde{m}$ is neglected.
In the next sections we provide a systematic non-perturbative approximation scheme for the nonequilibrium evolution of a Bose-Einstein condensate based on the 2PI effective action. After a general introduction to this powerful tool we derive nonequilibrium evolution equations in the NLO 1/N-expansion. These will enable us to reproduce the ZNG results as a nontrivial test of our approach. Then we solve numerically the full non-perturbative equations of motion and simulate BEC dynamics far from equilibrium.

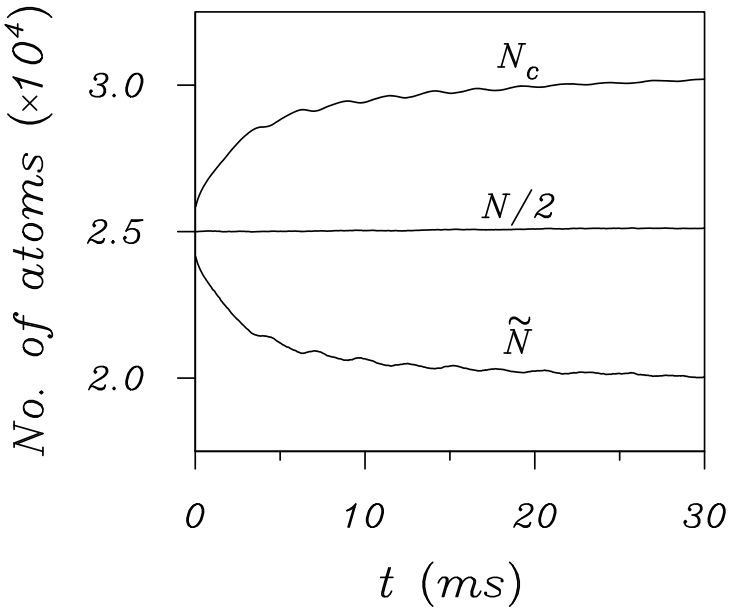

Figure 3.5: The condensate (N_c), noncondensate ($\widetilde{N}$) and total (N) number of ^{87}Rb atoms as a function of time resulting from many-body simulations of the ZNG theory (from [115]).

3.2 2PI effective action techniques

In a variety of different fields, ranging from high energy particle physics to cosmology, many interesting topics involve dynamics of quantum fields out of thermal equilibrium. In the last chapter we dealt with heavy ion collisions as a specific example of such a situation. We showed the consistency of two different approaches connecting the early and late stages of the time evolution. In far from equilibrium situations, however, standard approaches like kinetic descriptions are not applicable. In addition, it would certainly be more convenient and reliable to describe the evolution within a single framework only. But for several reasons it is quite challenging to describe the approach to equilibrium from first principles.

There are two typical complications in nonequilibrium situations, namely secularity and nonuniversality, which do not appear in vacuum or thermal equilibrium [86]. Secularity means that the perturbative evolution may contain so-called secular terms. These grow with some positive power of time and invalidate the expansion at late times even in the presence of a weak coupling.
Nonuniversality means that the late-time behavior is still sensitive to the details of the initial

conditions. But if thermal equilibrium is reached, then the system becomes uniquely determined by conserved charges like the energy density. A successful description of quantum fields away from equilibrium is thus tightly related to the basic problem of how macroscopic irreversible behavior arises from time-reversal invariant dynamics. It is clear that during the nonequilibrium time evolution there is no loss of information in a strict sense. Therefore, equilibrium cannot be reached on a fundamental level but only effectively. Stated differently, solving the problem of nonuniversal behaviour requires an effective loss of information about the initial conditions during the evolution.

Both requirements of a nonsecular and universal behavior can be fulfilled using an efficient functional integral technique based on the so-called 2PI (two particle irreducible) effective action. In this section we give a short introduction to these methods, focussing on a scalar theory. Our presentation closely follows the in-depth review of Berges [86] to which we refer for more details.

3.2.1 Constructing the 2PI effective action

We limit our disussion to a real N-component scalar quantum field theory given by the classical action

$$S[\varphi] = \int_x \left(\frac{1}{2} \partial^\mu \varphi_a(x) \partial_\mu \varphi_a(x) - \frac{m^2}{2} \varphi_a(x) \varphi_a(x) - \frac{\lambda}{4!N} \left(\varphi_a(x) \varphi_a(x) \right)^2 \right) . \tag{3.41}$$

Here we use the shorthand notation $\int_x = \int_c \mathrm{d}x^0 \int \mathrm{d}^3 x$, reminding that the time integration is performed along the CTP.
In the following we construct the 2PI effective action for this theory and point out the differences to the 1PI case. Then we derive exact evolution equations and discuss two possible approximation schemes. Concentrating on the nonperturbative $1/N$ expansion, we derive the corresponding equations of motion and also express them in terms of spectral and statistical components.

The generating functional $W[J]$ for connected Green's functions in the presence of a source term $J_a(x)$, as discussed in standard field theory textbooks (e.g. [120]), is given by

$$\begin{aligned} Z[J] &= \exp\left(iW[J]\right) \\ &= \int \mathcal{D}\varphi \, \exp\left(i \left[S[\varphi] + \int_x J_a(x) \varphi_a(x) \right] \right) . \end{aligned} \tag{3.42}$$

Applying the same procedure for two source terms $J_a(x)$ and $R_{ab}(x,y)$ analogously leads to

$$Z[J,R] = \int \mathcal{D}\varphi \, \exp\left(i \left[S[\varphi] + \int_x J_a(x) \varphi_a(x) + \frac{1}{2} \int_{xy} R_{ab}(x,y) \varphi_a(x) \varphi_b(y) \right] \right) . \tag{3.43}$$

The latter expression has the advantage to allow for a description of the theory in terms of the full connected two-point function G_{ab} . To clarify this, we recall the usual definitions of G_{ab} and the macroscopic field ϕ_a by variation of W in the presence of the source terms

$$\frac{\delta W[J,R]}{\delta J_a(x)} = \phi_a(x)\,, \tag{3.44}$$

$$\frac{\delta W[J,R]}{\delta R_{ab}(x,y)} = \frac{1}{2}\Big(\phi_a(x)\phi_b(y) + G_{ab}(x,y)\Big)\,, \tag{3.45}$$

with $G_{ab} = \langle T\varphi_a(x)\varphi_b(y)\rangle - \phi_a(x)\phi_b(y)$. In order to obtain a functional of the physical variables ϕ and G we perform a Legendre transform of $W[J,R]$ with respect to both source terms, leading to the 2PI effective action

$$\begin{aligned}\Gamma[\phi,G] &= W[J,R] - \int_x \frac{\delta W[J,R]}{\delta J_a(x)} J_a(x) - \int_{xy} \frac{\delta W[J,R]}{\delta R_{ab}(x,y)} R_{ab}(x,y) \\ &= W[J,R] - \int_x \phi_a(x) J_a(x) - \frac{1}{2}\int_{xy} R_{ab}(x,y)\phi_a(x)\phi_b(y) - \frac{1}{2}\,\mathrm{Tr}\,GR\,. \end{aligned} \tag{3.46}$$

All the information of the quantum theory is encoded in $\Gamma[\phi,G]$. For $R=0$ this expression is the standard 1PI effective action. One directly obtains the stationarity conditions

$$\frac{\delta\Gamma[\phi,G]}{\delta\phi_a(x)} = -J_a(x) - \int_y R_{ab}(x,y)\phi_b(y)\,, \tag{3.47}$$

$$\frac{\delta\Gamma[\phi,G]}{\delta G_{ab}(x,y)} = -\frac{1}{2}R_{ab}(x,y)\,. \tag{3.48}$$

These give the equations of motion for ϕ and G in the absence of the sources, i.e. for $J=0$ and $R=0$.

It is convenient to write the exact 2PI effective action as [121]

$$\Gamma[\phi,G] = S[\phi] + \frac{i}{2}\,\mathrm{Tr}\ln G^{-1} + \frac{i}{2}\,\mathrm{Tr}\,G_0^{-1}(\phi)\,G \;+\; \Gamma_2[\phi,G] + \text{const}\,. \tag{3.49}$$

Here we added an irrelevant constant which can be adjusted for normalization. The classical inverse propagator $iG^{-1}_{0,ab}(x,y;\phi) = \delta^2 S[\phi]/\delta\phi_a(x)\delta\phi_b(y)$ reads

$$\begin{aligned} iG^{-1}_{0,ab}(x,y;\phi) &= -\left(\Box_x + m^2 + \frac{\lambda}{6N}\,\phi_c(x)\phi_c(x)\right)\delta_{ab}\delta(x-y) \\ &\quad -\frac{\lambda}{3N}\,\phi_a(x)\phi_b(x)\delta(x-y)\,. \end{aligned} \tag{3.50}$$

The only unknown term in the decomposition (3.49) is $\Gamma_2[\phi,G]$. To get an understanding of this term it is useful to vary (3.49) with respect to G. Using equation (3.48) this leads to

$$G^{-1}_{ab}(x,y) = G^{-1}_{0,ab}(x,y;\phi) - iR_{ab}(x,y) - \Sigma_{ab}(x,y;\phi,G)\,, \tag{3.51}$$

where we have written

$$\Sigma_{ab}(x,y;\phi,G) = 2i\,\frac{\delta\Gamma_2[\phi,G]}{\delta G_{ab}(x,y)}\,. \tag{3.52}$$

Here, $\Sigma_{ab}(x,y)$ is the proper self-energy, to which only one-particle irreducible Feynman diagrams contribute, i.e. diagrams which cannot be separated by opening one line.
From the fact that to $\Sigma(\phi,G)$ only 1PI diagrams contribute one can conclude that $\Gamma_2[\phi,G]$ only contains contributions from two-particle irreducible (2PI) diagrams. To see this, note that the graphs contributing to $\Sigma(\phi,G)$ are obtained by opening one propagator line in graphs contributing to $\Gamma_2[\phi,G]$. This is exemplified for a two- and a three-loop graph for Γ_2 and the corresponding self-energy graphs in figure 3.6.

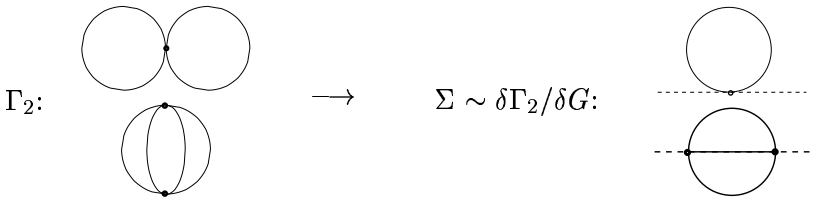

Figure 3.6: Diagramatical connection between Γ_2 and the self energy Σ (from [86]).

Now suppose $\Gamma_2[\phi,G]$ had a two particle reducible (2PR) contribution. The latter could schematically be written as $\widetilde{\Gamma}GG\widetilde{\Gamma}'$, where GG denotes two propagator lines connecting two parts $\widetilde{\Gamma}$ and $\widetilde{\Gamma}'$ of a diagram. Then $\Sigma(\phi,G)$ would contain a contribution of the form $\widetilde{\Gamma}G\widetilde{\Gamma}'$ since it is given by a derivative of Γ_2 with respect to G. Such a structure is 1PR and cannot occur for the self energy. Therefore 2PR contributions to $\Gamma_2[\phi,G]$ are absent [86].

Furthermore, equation (3.51) can be used to express the full propagator G as an infinite series in terms of the classical propagator G_0 and Σ

$$\begin{aligned} G &= (G_0^{-1} - iR)^{-1} + (G_0^{-1} - iR)^{-1}\,\Sigma\,(G_0^{-1} - iR)^{-1} \\ &\quad + (G_0^{-1} - iR)^{-1}\,\Sigma\,(G_0^{-1} - iR)^{-1}\,\Sigma\,(G_0^{-1} - iR)^{-1} + \dots\,. \end{aligned} \tag{3.53}$$

As a consequence, a given 2PI diagram with propagator lines associated to G corresponds to an infinite set of 1PI diagrams with propagator lines associated to the free propagator G_0. To give an example, we consider the 2PI two- and three-loop diagrams shown on the left side in figure 3.6. In terms of G_0 they contain e.g. the full resummation of so-called daisies and ladder diagrams, see figure 3.7.

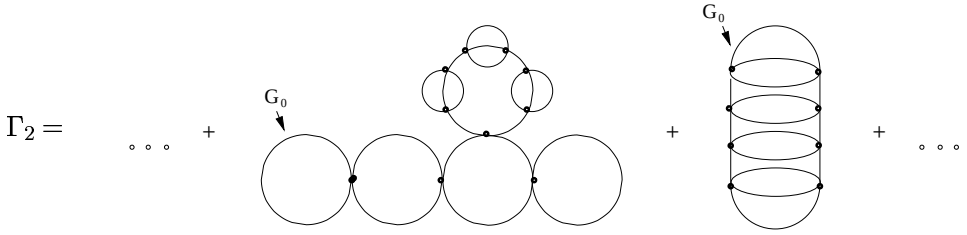

Figure 3.7: Contributions to Γ_2 in terms of G_0 [86].

3.2.2 Exact evolution equations

Dynamical equations for ϕ_a and G_{ab} can be found from the stationarity conditions (3.47) and (3.48). In the absence of external sources physical solutions require

$$\frac{\delta\Gamma[\phi,G]}{\delta\phi_a(x)} = 0, \tag{3.54}$$

which leads to the evolution equation for the field expectation value

$$\begin{aligned} -\left(\Box_x + m^2 + \frac{\lambda}{6N}\left[\phi^2(x) + G_{bb}(x,x)\right]\right)\phi_a(x) &= \frac{\lambda}{3N}\phi_b(x)G_{ba}(x,x) \\ &\quad -\frac{\delta\Gamma_2[\phi,G]}{\delta\phi_a(x)}\,. \end{aligned} \tag{3.55}$$

Similarly, the stationarity condition for the propagator is

$$\frac{\delta\Gamma[\phi,G]}{\delta G_{ab}(x,y)} = 0\,. \tag{3.56}$$

Remembering (3.51) this directly leads to

$$G^{-1}_{ab}(x,y) = G^{-1}_{0,ab}(x,y) - \Sigma_{ab}(x,y;\phi,G)\,. \tag{3.57}$$

For later purposes, it is useful to rewrite (3.57) as a partial differential equation suitable for initial value problems. Convolution with G gives

$$\int_z G^{-1}_{0,ab}(x,z)G_{bc}(z,y) = \int_z \Sigma_{ac}(x,z)G_{cb}(z,y) + \delta_{ab}\delta_{\mathcal{C}}(x-y)\,, \tag{3.58}$$

and with equation (3.50) for the classical inverse propagator this differential equation reads explicitly

$$\begin{aligned} -\left[\Box_x + m^2 + \frac{\lambda}{6N}\phi^2(x)\right]G_{ab}(x,y) &= \frac{\lambda}{3N}\phi_a(x)\phi_c(x)G_{cb}(x,y) \\ &\quad + i\int_z \Sigma_{ac}(x,z;\phi,G)G_{cb}(z,y) + i\delta_{ab}\delta_{\mathcal{C}}(x-y). \end{aligned} \tag{3.59}$$

For the sake of a compact notation we finally combine all local contributions in an effective mass parameter

$$M^2_{ab}(x) = \left[m^2 + \frac{\lambda}{6N}\left(\phi^2(x) + G_{cc}(x,x)\right)\right]\delta_{ab} + \frac{\lambda}{3N}\left[\phi_a(x)\phi_b(x) + G_{ab}(x,x)\right]\,, \tag{3.60}$$

leading to

$$-\left[\Box_x\delta_{ac} + M^2_{ac}(x)\right]G_{cb}(x,y) = i\delta_{ab}\delta_{\mathcal{C}}(x-y) + i\int_z \Sigma_{ac}(x,z)G_{cb}(z,y)\,. \tag{3.61}$$

The evolution of ϕ_a and G_{ab} is determined by (3.55) and (3.57/3.61), once $\Gamma_2[\phi,G]$ and hence Σ_{ab} is specified. Thus, in order to end up with tractable equations of motion, one first needs to find a suitably approximated expression for $\Gamma_2[\phi,G]$. We present in the following two possibilities, based on expansions in the coupling λ and the inverse number of field components $1/N$, respectively.

3.2.3 Perturbative expansion of the 2PI effective action

Perturbative approximation schemes are most commonly used in quantum field theory. Following Berges [86], we give here a short account on the loop expansion of the 2PI effective action. It proceeds along the same lines as the corresponding expansion for the standard 1PI effective action, with the important difference that the full propagator G is associated to propagator lines of a diagram. For the N-component scalar field theory, which we consider here, the diagrams are constructed from an effective interaction. This latter is obtained from the classical action (3.41) by shifting $\varphi_a(x) \to \phi_a(x) + \varphi_a(x)$. Collecting all terms cubic and quartic in the fluctuating field $\varphi_a(x)$ one finds [86]

$$S_{\rm int}[\phi,\varphi] = -\int_x \frac{\lambda}{6N}\phi_a(x)\varphi_a(x)\varphi_b(x)\varphi_b(x) - \int_x \frac{\lambda}{4!N}\Big(\varphi_a(x)\varphi_a(x)\Big)^2 . \tag{3.62}$$

As for the 1PI effective action, there is besides the quartic term an effective cubic interaction for non-vanishing field expectation value, i.e. for $\phi_a(x) \neq 0$.
Since $\Gamma[\phi, G]$ is a functional, which associates a number to the fields ϕ and G, only closed loop diagrams can appear. As in our later applications of 2PI techniques we use a nonpertubative approximation scheme, we consider here for simplicity the special case $N = 1$. To lowest order one clearly has $\Gamma_2[\phi, G] = 0$, while at two-loop order there are two diagrams shown in figure 3.8.

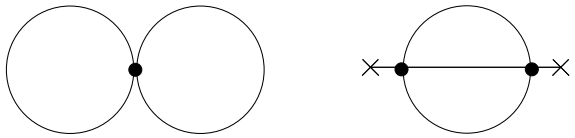

Figure 3.8: 2-loop diagrams contributing to Γ_2. Crosses denote insertions of the field expectation value.

Put in formula, these contributions read

$$\begin{aligned}\Gamma_2^{(2\text{loop})}[\phi,G] \;=\; & -i\,3\Big(-i\frac{\lambda}{4!}\Big)\int_x G^2(x,x) \\ & -i\,6\,\frac{1}{2}\int_{xy}\Big(-i\frac{\lambda}{6}\phi(x)\Big)\Big(-i\frac{\lambda}{6}\phi(y)\Big)G^3(x,y)\,,\end{aligned} \tag{3.63}$$

where the different factors come from the combinatorics, the vertices and the overall $-i$ in the defining functional integral for $\Gamma[\phi, G]$, respectively (see equation (3.43)).

It is insightful to count the number of topologically distinct diagrams in the 2PI loop expansion, which is of course much smaller than the respective number in the 1PI case. As an example, in the symmetric phase ($\phi = 0$) there is only a single diagram at each order up to four loops. At fifth order there are two distinct diagrams which are shown along with the lower-loop graphs in figure 3.9.

3.2.4 $1/N$ expansion

Now we turn to the discussion of a systematic non-perturbative approximation scheme for the 2PI effective action [122, 123]. It classifies the contributions to the 2PI effective action

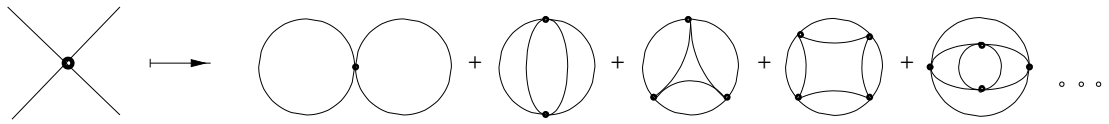

Figure 3.9: Topologically distinct diagrams in the 2PI loop expansion up to five-loop order for $\phi = 0$ [86].

according to their scaling with inverse powers the number of field components N like

$$\begin{aligned} \Gamma_2[\phi, G] \;=\; & \Gamma_2^{\mathrm{LO}}[\phi, G] + \Gamma_2^{\mathrm{NLO}}[\phi, G] + \Gamma_2^{\mathrm{NNLO}}[\phi, G] + \dots \\ & \sim N^1 \qquad\quad \sim N^0 \qquad\quad \sim N^{-1} \end{aligned}$$

Each subsequent contribution Γ_2^{LO}, Γ_2^{NLO}, Γ_2^{NNLO} etc. is suppressed by an additional factor of $1/N$. The method can be applied to any theory with a suitable field number parameter. Here, we are interested in the case of the real N-component scalar field theory given by the classical action (3.41).

Classification scheme

We will now discuss how one can specify the contributions to $\Gamma_2[\phi, G]$ at a given order in the 1/N-expansion. As we have seen, only 2PI diagrams contribute to $\Gamma_2[\phi, G]$, so our task essentially consists in identifying the order of these diagrams.
There are two sources of scaling properties for a given diagram. First, let us note that $\Gamma_2[\phi, G]$ is invariant under $O(N)$ rotations which is equally true for each included diagram. This has some immediate consequences, for instance that the number of field insertions must be even. The fields and propagators are combined such that no index structure is left, so each diagram involves a certain number of traces over these indices. This number is important for the order of the diagram as each trace scales like N. Note that the maximum number of traces is given by the number of loops.
The second origin of scaling properties stems from our definition of the classical action in equation (3.41). It is written such that $S[\phi]$ scales proportional to N, so each vertex provides a factor of $1/N$.
Let us now consider an arbitrary 2PI diagram with its highest contribution scaling like $N^{a_{max}}$. From the above reasoning we can write

$$a_{max} = l - v\,, \tag{3.64}$$

where l and v denote the number of loops and vertices, respectively. Two examples are shown in figure 3.10.
As two fields connected by a propagator always involve a trace, these parts of a diagram must be counted as a closed loop. This is emphasized by the dotted lines. In both cases we obtain $a_{max} = l - v = 4 - 5 = -1$, so the highest contributions of these diagrams are NNLO.
With the above rules in mind we are now ready to compute the LO and NLO contributions to $\Gamma_2[\phi, G]$. It is convenient to consider first the case of a vanishing field expectation value and subsequently add the $\phi \neq 0$ terms.

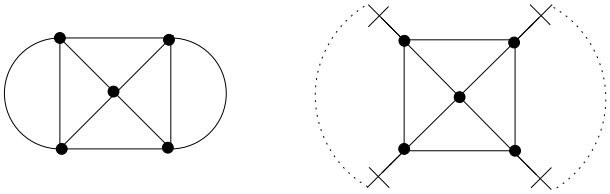

Figure 3.10: Some NNLO contributions to Γ_2.

Symmetric phase

The LO contribution to $\Gamma_2[G]$ consists of only one two-loop graph (called double-bubble, see figure 3.11) with indices such that two traces are involved, and one directly obtains

$$\Gamma_2^{\mathrm{LO}}[G] = -\frac{\lambda}{4!N}\int_x G_{aa}(x,x)G_{bb}(x,x)\,. \tag{3.65}$$

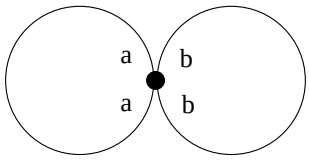

Figure 3.11: LO contribution to Γ_2 for $\phi = 0$.

At NLO there is an infinite series of contributions shown in figure 3.12. This series can be analytically summed like [122]

$$\Gamma_2^{\mathrm{NLO}}[G] = \frac{i}{2}\,\mathrm{Tr}\ln[\,\mathbf{B}(G)\,]\,, \tag{3.66}$$

with

$$\mathbf{B}(x,y;G) = \delta(x-y) + i\frac{\lambda}{6N}\,G_{ab}(x,y)G_{ab}(x,y)\,. \tag{3.67}$$

In order to see that (3.66) with (3.67) indeed corresponds to the infinite series in figure 3.12 one can perform the expansion

$$\begin{aligned}\mathrm{Tr}\ln[\,\mathbf{B}(G)\,] \;&=\; \int_x \left(i\frac{\lambda}{6N}G_{ab}(x,x)G_{ab}(x,x)\right)\\ &-\; \frac{1}{2}\int_{xy}\left(i\frac{\lambda}{6N}G_{ab}(x,y)G_{ab}(x,y)\right)\left(i\frac{\lambda}{6N}\,G_{a'b'}(y,x)G_{a'b'}(y,x)\right)\\ &+\; \ldots\end{aligned} \tag{3.68}$$

The first two terms on the right hand side in (3.68) correspond to the first two diagrams in figure 3.12 with the index structure such that only one trace is involved at a vertex. As the contribution to a given order in λ consists of a product of terms $\sim \frac{1}{N}G_{ab}G_{ab}$ which scale like $\mathrm{tr}G^2/N \sim N^0$, all contributions are indeed NLO.

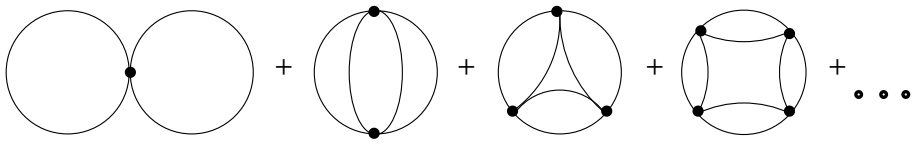

Figure 3.12: NLO contributions to Γ_2 for $\phi = 0$ [86].

Non-vanishing field expectation value

For $\phi \neq 0$ the action (3.62) contains an effective cubic interaction, leading to additional contributions to $\Gamma_2[G]$. At LO there is no ϕ-dependent graph and one can simply write

$$\Gamma_2^{\mathrm{LO}}[\phi, G] = \Gamma_2^{\mathrm{LO}}[G]\,. \tag{3.69}$$

The NLO contribution again consists of an infinite series of diagrams which are shown in figure 3.13. Also in this case the series can be summed by an analytical expression. The complete Γ_2^{NLO} then reads [123]

$$\Gamma_2^{\mathrm{NLO}}[\phi, G] = \Gamma_2^{\mathrm{NLO}}[\phi = 0, G] + \frac{i\lambda}{6N} \int_{xy} \mathbf{I}(x, y; G)\, \phi_a(x)\, G_{ab}(x, y)\, \phi_b(y)\,, \tag{3.70}$$

with

$$\mathbf{I}(x, y; G) = \frac{\lambda}{6N}\, G_{ab}(x, y) G_{ab}(x, y) - i\, \frac{\lambda}{6N} \int_z \mathbf{I}(x, z; G) G_{ab}(z, y) G_{ab}(z, y)\,. \tag{3.71}$$

For later purposes it is useful to note that the functions $\mathbf{I}(x, y; G)$ and the inverse of $\mathbf{B}(x, y; G)$ are closely related by

$$\mathbf{B}^{-1}(x, y; G) = \delta(x - y) - i\mathbf{I}(x, y; G)\,, \tag{3.72}$$

which follows from convoluting (3.67) with $\mathbf{B}^{-1}$ and using (3.71). Note that $\mathbf{B}$ and $\mathbf{I}$ do not depend on ϕ and thus $\Gamma_2[\phi, G]$ is only quadratic in ϕ at NLO.

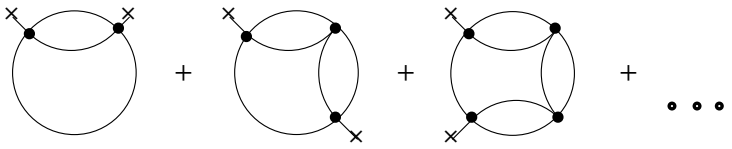

Figure 3.13: NLO contributions to Γ_2 for $\phi \neq 0$ [86].

3.2.5 Equations of motion in the $1/N$ expansion

The 2PI equations of motion in the $1/N$ expansion were derived and discussed by Aarts et al. in [123]. Following them, the results (3.65), (3.66) and (3.70) for Γ_2 lead via equation (3.52) to the corresponding expressions for the self energy at LO and NLO

$$\Sigma^{\rm LO}_{ab}(x,y) = -i\frac{\lambda}{6N}G_{cc}(x,x)\delta_{ab}\delta_{\mathcal{C}}(x-y)\,, \tag{3.73}$$

$$\Sigma^{\rm NLO}_{ab}(x,y) = -\frac{\lambda}{3N}\left\{\mathbf{I}(x,y)\left[\phi_a(x)\phi_b(y)+G_{ab}(x,y)\right]+\mathbf{P}(x,y)G_{ab}(x,y)\right\}\,. \tag{3.74}$$

Here we defined

$$\mathbf{P}(x,y) = -\frac{\lambda}{3N}\int_{uv}\mathbf{B}^{-1}(x,u)\Delta(u,v)\mathbf{B}^{-1}(v,y), \tag{3.75}$$

$$\Delta(x,y) = -\phi_a(x)G_{ab}(x,y)\phi_b(y)\,. \tag{3.76}$$

Now we have all the ingredients to write down the equations of motion for the macroscopic field ϕ and the propagator G in this approximation. The equation for the field expectation value (3.55) reads at NLO

$$-\left(\Box_x+m^2+\frac{\lambda}{6N}\left[\phi^2(x)+G_{cc}(x,x)\right]\right)\phi_a(x)=\mathbf{K}_a(x,x). \tag{3.77}$$

The left hand side of this evolution equation is LO while we combined the NLO contribution as

$$\mathbf{K}_a(x,y)=\mathbf{K}_a(x,y;\phi,G)=\frac{\lambda}{3N}\int_z\mathbf{B}^{-1}(x,z;G)G_{ab}(y,z)\phi_b(z), \tag{3.78}$$

evaluated at $x=y$. We have written $\mathbf{K}_a(x,y)$ as a function of x and y for later purposes. Next we derive a convenient form of the propagator equation. We start with equation (3.57) for the inverse propagator which after some manipulations can be written as

$$\begin{aligned} iG^{-1}_{ab}(x,y) = &-\left(\Box_x+m^2+\frac{\lambda}{6N}\left[\phi^2(x)+G_{cc}(x,x)\right]\right)\delta_{ab}\delta_{\mathcal{C}}(x-y) \\ &-\frac{\lambda}{3N}\mathbf{B}^{-1}(x,y;G)\phi_a(x)\phi_b(y)+i\mathbf{D}(x,y)G_{ab}(x,y), \end{aligned} \tag{3.79}$$

with the definition

$$\begin{aligned} \mathbf{D}(x,y)=\mathbf{D}(x,y;\phi,G) = &\,i\frac{\lambda}{3N}\mathbf{B}^{-1}(x,y;G) \\ &+\left(\frac{\lambda}{3N}\right)^2\int_{uv}\mathbf{B}^{-1}(x,u;G)\phi_a(u)G_{ab}(u,v)\phi_b(v)\mathbf{B}^{-1}(v,y;G). \end{aligned} \tag{3.80}$$

Using the function $\mathbf{K}_a$ defined in (3.78), it turns out that the double integration over the closed time path contained in equation (3.80) can be disentangled. Convoluting the functions $\mathbf{B}, \mathit{givenby}(3.67)$, and $\mathbf{D}$ leads to

$$\begin{aligned} \mathbf{D}(x,y) = &\,i\frac{\lambda}{3N}\delta_{\mathcal{C}}(x-y)+\frac{\lambda}{3N}\mathbf{K}_a(y,x)\phi_a(x) \\ &+i\frac{\lambda}{3N}\int_z\Pi(x,z)\mathbf{D}(z,y). \end{aligned} \tag{3.81}$$

with the short-hand notation

$$\Pi(x,y) = -\frac{1}{2} G_{ab}(x,y) G_{ab}(x,y)\,. \tag{3.82}$$

So the unconvenient nested integrals have disappeared in equation (3.81). It is also useful to rewrite equation (3.78) for $\mathbf{K}_a$ such that $\mathbf{B}$ does not appear. By convoluting $\mathbf{B}$ and $\mathbf{K}_a$, one obtains

$$\mathbf{K}_a(x,y) = \frac{\lambda}{3N}\phi_b(x) G_{ba}(x,y) + i\frac{\lambda}{3N}\int_z \Pi(x,z)\mathbf{K}_a(z,y). \tag{3.83}$$

So $\mathbf{B}$ and $\mathbf{B}^{-1}$ are eliminated completely from the coupled equations.
The above results can be used to simplify the equation for the inverse propagator (3.79). The equation of motion for G then takes the form

$$\begin{aligned} -\left(\Box_x + m^2 + \frac{\lambda}{6N}\left[\phi^2(x) + G_{cc}(x,x)\right]\right) G_{ab}(x,y) &= i\delta_{ab}\delta_{\mathcal{C}}(x-y) \\ &+\phi_a(x)\mathbf{K}_b(x,y) - i\int_z \mathbf{D}(x,z) G_{ac}(x,z) G_{cb}(z,y). \end{aligned} \tag{3.84}$$

In summary, equations (3.77, 3.84) together with (3.81, 3.83) form the closed set of equations which have to be solved. We stress that the 1/N expansion is done on the level of the effective action. There are no further approximations involved on the level of the evolution equations. In a later section we shall study the nonrelativistic limit of these equations for N=2. In particular, we will show how the previously discussed ZNG theory emerges in a quasiparticle approximation.

3.2.6 NLO evolution equations for spectral and statistical functions

In the following we introduce a decomposition of the two-point function G into spectral and statistical components. The corresponding evolution equations for these components are very convenient in numerical studies and we shall need them for these purposes in a later section. Let us first recall the definition of the propagator G_{ab} in terms of the field φ_a

$$\begin{aligned} G_{ab}(x,y) &= \langle T\varphi_a(x)\varphi_b(y)\rangle - \phi_a(x)\phi_b(y) \\ &= \langle T\widetilde{\varphi}_a(x)\widetilde{\varphi}_b(y)\rangle\,, \end{aligned} \tag{3.85}$$

with $\varphi_a(x) = \phi_a(x) + \widetilde{\varphi}_a(x)$ and $\langle\widetilde{\varphi}_a(x)\rangle = 0$.
For the real scalar field theory the spectral and statistical functions $\rho_{ab}(x,y)$ and $F_{ab}(x,y)$ are defined via the expectation value of the commutator and the anti-commutator of two fields

$$\rho_{ab}(x,y) = i\langle[\widetilde{\varphi}_a(x), \widetilde{\varphi}_b(y)]\rangle\,, \tag{3.86}$$

$$F_{ab}(x,y) = \frac{1}{2}\langle\{\widetilde{\varphi}_a(x), \widetilde{\varphi}_b(y)\}\rangle\,. \tag{3.87}$$

This definition implies the (anti)-symetry properties $F(x,y) = F(y,x)$ and $\rho(x,y) = -\rho(y,x)$. Mote that the convention used here for ρ differs from the one in section 2.3.2 by a factor i.

F and ρ have a simple physical interpretation [86]. While the spectral function contains information about the spectrum of the theory (i.e. what states are available), the statistical propagator encodes occupation numbers (i.e. how often these states are occupied).
For the decomposition of the propagator into spectral and statistical components one obtains

$$\begin{aligned} G_{ab}(x,y) &= \langle\widetilde{\varphi}_a(x)\widetilde{\varphi}_b(y)\rangle\Theta_{\mathcal{C}}(x^0-y^0) + \langle\widetilde{\varphi}_b(y)\widetilde{\varphi}_a(x)\rangle\Theta_{\mathcal{C}}(y^0-x^0) \\ &= \frac{1}{2}\langle\{\widetilde{\varphi}_a(x),\widetilde{\varphi}_b(y)\}\rangle \underbrace{\left(\Theta_{\mathcal{C}}(x^0-y^0)+\Theta_{\mathcal{C}}(y^0-x^0)\right)}_{=1} \\ &- \frac{i}{2}\,i\langle[\widetilde{\varphi}_a(x),\widetilde{\varphi}_b(y)]\rangle \underbrace{\left(\Theta_{\mathcal{C}}(x^0-y^0)-\Theta_{\mathcal{C}}(y^0-x^0)\right)}_{=\mathrm{sign}_{\mathcal{C}}(x^0-y^0)} \\ &= F_{ab}(x,y) - \frac{i}{2}\rho_{ab}(x,y)\,\mathrm{sign}_{\mathcal{C}}(x^0-y^0)\,. \end{aligned} \tag{3.88}$$

From the evolution equation for G it is now simple to derive the corresponding equations for F and ρ. It is useful to decompose the functions $\mathbf{K}$, $\mathbf{I}$, etc. into their spectral and statistical components as well. As this is merely a rewriting of the previous section we only give the results here and refer to [122, 123] for details.
First, we consider the field equation (3.77) which now reads

$$-\left(\Box_x + m^2 + \frac{\lambda}{6N}\left[\phi^2(x) + F_{cc}(x,x)\right]\right)\phi_a(x) = \mathbf{K}^F_a(x) \tag{3.89}$$

with

$$\begin{aligned} \mathbf{K}^F_a(x,x) = &\frac{\lambda}{3N}F_{ab}(x,x)\phi_b(x) \\ &-\frac{\lambda}{3N}\int_0^{x^0} dy\,\left[\mathbf{I}_\rho(x,y)F_{ab}(x,y) + \mathbf{I}_F(x,y)\rho_{ab}(x,y)\right]\phi_b(y). \end{aligned} \tag{3.90}$$

The statistical and spectral components of the chain of bubble diagrams $\mathbf{I}(x,y)$ read

$$\begin{aligned} \mathbf{I}_F(x,y) = -\frac{\lambda}{3N}\Pi_F(x,y) + \frac{\lambda}{3N}\int_0^{x^0} dz\,\mathbf{I}_\rho(x,z)\Pi_F(z,y) \\ -\frac{\lambda}{3N}\int_0^{y^0} dz\,\mathbf{I}_F(x,z)\Pi_\rho(z,y), \\ \mathbf{I}_\rho(x,y) = -\frac{\lambda}{3N}\Pi_\rho(x,y) + \frac{\lambda}{3N}\int_{y^0}^{x^0} dz\,\mathbf{I}_\rho(x,z)\Pi_\rho(z,y)\,, \end{aligned} \tag{3.91}$$

with Π_F and Π_ρ given by

$$\begin{aligned} \Pi_F(x,y) &= -\frac{1}{2}\left[F_{ab}(x,y)F_{ab}(x,y) - \frac{1}{4}\rho_{ab}(x,y)\rho_{ab}(x,y)\right], \\ \Pi_\rho(x,y) &= -F_{ab}(x,y)\rho_{ab}(x,y)\,. \end{aligned} \tag{3.92}$$

The propagator equation (3.61) gives the following equations of motion for F and ρ

$$\left[\Box_x\delta_{ac}+M^2_{ac}(x)\right]F_{cb}(x,y)=-\int_0^{x^0}dz\,\Sigma^\rho_{ac}(x,z)F_{cb}(z,y)$$
$$+\int_0^{y^0}dz\,\Sigma^F_{ac}(x,z)\rho_{cb}(z,y)\,, \tag{3.93}$$
$$\left[\Box_x\delta_{ac}+M^2_{ac}(x)\right]\rho_{cb}(x,y)=-\int_{y^0}^{x^0}dz\,\Sigma^\rho_{ac}(x,z)\rho_{cb}(z,y)\,, \tag{3.94}$$

involving the non-local self energies

$$\begin{aligned}\Sigma^F_{ab}(x,y) &= -\frac{\lambda}{3N}\Big\{\mathbf{I}_F(x,y)\left[\phi_a(x)\phi_b(y)+F_{ab}(x,y)\right]-\frac{1}{4}\mathbf{I}_\rho(x,y)\rho_{ab}(x,y)\\ &\quad+\mathbf{P}_F(x,y)F_{ab}(x,y)-\frac{1}{4}\mathbf{P}_\rho(x,y)\rho_{ab}(x,y)\Big\},\end{aligned} \tag{3.95}$$
$$\begin{aligned}\Sigma^\rho_{ab}(x,y) &= -\frac{\lambda}{3N}\Big\{\mathbf{I}_\rho(x,y)\left[\phi_a(x)\phi_b(y)+F_{ab}(x,y)\right]+\mathbf{I}_F(x,y)\rho_{ab}(x,y)\\ &\quad+\mathbf{P}_\rho(x,y)F_{ab}(x,y)+\mathbf{P}_F(x,y)\rho_{ab}(x,y)\Big\}.\end{aligned} \tag{3.96}$$

The functions $\mathbf{P}_F$ and $\mathbf{P}_\rho$, finally, contain the nested integrals and explicitly read

$$\begin{aligned}\mathbf{P}_F(x,y) &= -\frac{\lambda}{3N}\Bigg\{\Delta_F(x,y)\\ &\quad-\int_0^{x^0}dz\,\left[\Delta_\rho(x,z)\mathbf{I}_F(z,y)+\mathbf{I}_\rho(x,z)\Delta_F(z,y)\right]\\ &\quad+\int_0^{y^0}dz\,\left[\Delta_F(x,z)\mathbf{I}_\rho(z,y)+\mathbf{I}_F(x,z)\Delta_\rho(z,y)\right]\\ &\quad-\int_0^{x^0}dz\int_0^{y^0}dv\,\mathbf{I}_\rho(x,z)\Delta_F(z,v)\mathbf{I}_\rho(v,y)\\ &\quad+\int_0^{x^0}dz\int_0^{z^0}dv\,\mathbf{I}_\rho(x,z)\Delta_\rho(z,v)\mathbf{I}_F(v,y)\\ &\quad+\int_0^{y^0}dz\int_{z^0}^{y^0}dv\,\mathbf{I}_F(x,z)\Delta_\rho(z,v)\mathbf{I}_\rho(v,y)\Bigg\},\end{aligned} \tag{3.97}$$

and

$$\begin{aligned}\mathbf{P}_\rho(x,y) &= -\frac{\lambda}{3N}\Bigg\{\Delta_\rho(x,y)\\ &\quad-\int_{y^0}^{x^0}dz\,\left[\Delta_\rho(x,z)\mathbf{I}_\rho(z,y)+\mathbf{I}_\rho(x,z)\Delta_\rho(z,y)\right]\\ &\quad+\int_{y^0}^{x^0}dz\int_{y^0}^{z^0}dv\,\mathbf{I}_\rho(x,z)\Delta_\rho(z,v)\mathbf{I}_\rho(v,y)\Bigg\},\end{aligned} \tag{3.98}$$

with $\Delta_F(x,y) = -\phi_a(x)F_{ab}(x,y)\phi_b(y)$ and $\Delta_\rho(x,y) = -\phi_a(x)\rho_{ab}(x,y)\phi_b(y)$.
In a later section we consider the above non-perturbative equations of motion for ϕ_a (3.89), F (3.93) and ρ (3.93) in the nonrelativistic case for N=2. These can be solved numerically to simulate BEC dynamics far from equilibrium.

3.3 Generalized GP dynamics from 2PI equations

In this section we provide a systematic non-perturbative approximation scheme for the nonequilibrium evolution of a Bose-Einstein condensate based on the 2PI effective action [124]. Our aim is to recover the ZNG theory from the NLO 2PI-1/N equations (3.77) and (3.84) as a nontrivial test of our approach. We need a two component scalar field φ_1, φ_2. One may worry if our ansatz is reasonable for N=2. In [125] the 1/N expansion is compared to exact results in the classical limit showing that it gives precise results already for moderate values of N.
It is convenient to work with the same field variables as used in the ZNG results (3.34) and (3.36). Thus we perform the redefinition

$$\begin{aligned} \Psi^\dagger &= \tfrac{1}{\sqrt{2}}\left(\varphi_1 - i\varphi_2\right) , \\ \Psi &= \tfrac{1}{\sqrt{2}}\left(\varphi_1 + i\varphi_2\right) , \end{aligned} \tag{3.99}$$

with $\Psi = \langle\Psi\rangle + \widetilde{\Psi} = \phi + \widetilde{\Psi}$, and $\langle\widetilde{\Psi}\rangle = 0$. Similarly, the iterative function $\mathbf{K}_a$, defined in (3.83), is changed to

$$\begin{aligned} \mathbf{K}(x,y) &= \frac{1}{\sqrt{2}}\left(\mathbf{K}_1(x,y) - i\mathbf{K}_2(x,y)\right) \\ &= \frac{\lambda}{6}\Big(\phi(x)\langle T\widetilde{\Psi}^\dagger(x)\widetilde{\Psi}(y)\rangle + \phi^\dagger(x)\langle T\widetilde{\Psi}(x)\widetilde{\Psi}(y)\rangle\Big) \\ &+ i\frac{\lambda}{6}\int_z \Pi(x,z)\mathbf{K}(z,y)\,. \end{aligned} \tag{3.100}$$

The function Π, defined in (3.82), is now given by

$$\Pi(x,y) = -\Big(\langle T\widetilde{\Psi}^\dagger(x)\widetilde{\Psi}^\dagger(y)\rangle\langle T\widetilde{\Psi}(x)\widetilde{\Psi}(y)\rangle + \langle T\widetilde{\Psi}^\dagger(x)\widetilde{\Psi}(y)\rangle\langle T\widetilde{\Psi}(x)\widetilde{\Psi}^\dagger(y)\rangle\Big)\,. \tag{3.101}$$

The 2PI field equation (3.77) reads in terms of the complex field

$$-\left(\Box_x + m^2 + \frac{\lambda}{6}\left[\phi^\dagger(x)\phi(x) + \langle\widetilde{\Psi}^\dagger(x)\widetilde{\Psi}(x)\rangle\right]\right)\phi(x) = \mathbf{K}(x,x)\,. \tag{3.102}$$

From the propagator equation (3.84) we shall need an equation for the time ordered two point function $\langle T\widetilde{\Psi}^\dagger(x)\widetilde{\Psi}(y)\rangle$. Using $G_{11} + iG_{12} - iG_{21} + G_{22} = 2\langle T\widetilde{\Psi}^\dagger\widetilde{\Psi}\rangle$ this equation is determined to

$$\begin{aligned} &-\left(\Box_x + m^2 + \frac{\lambda}{6}\left[\phi^\dagger(x)\phi(x) + \langle\widetilde{\Psi}^\dagger(x)\widetilde{\Psi}(x)\rangle\right]\right)\langle T\widetilde{\Psi}^\dagger(x)\widetilde{\Psi}(y)\rangle \\ &= i\delta_{\mathcal{C}}(x-y) + \phi^\dagger(x)\mathbf{K}(x,y) \\ &-i\int_z \mathbf{D}(x,z)\Big[\langle T\widetilde{\Psi}^\dagger(x)\widetilde{\Psi}^\dagger(z)\rangle\langle T\widetilde{\Psi}(z)\widetilde{\Psi}(y)\rangle + \langle T\widetilde{\Psi}^\dagger(x)\widetilde{\Psi}(z)\rangle\langle T\widetilde{\Psi}^\dagger(z)\widetilde{\Psi}(y)\rangle\Big]\,, \end{aligned} \tag{3.103}$$

where $\mathbf{D}(x,y)$, defined in equation (3.81), becomes

$$\begin{aligned}\mathbf{D}(x,y) &= i\frac{\lambda}{6}\delta_{\mathcal{C}}(x-y)+\frac{\lambda}{6}\Big(\mathbf{K}(y,x)\Phi^{\dagger}(x)+\mathbf{K}^{\dagger}(y,x)\Phi(x)\Big)\\ &+ i\frac{\lambda}{6}\int_z \Pi(x,z)\mathbf{D}(z,y). \end{aligned} \tag{3.104}$$

3.3.1 Aside on Weyl order divergencies

Here we briefly discuss a technical problem arising in the $x=y$ limit of the correlators $\langle T\widetilde{\Psi}^{\dagger}(x)\widetilde{\Psi}(y)\rangle$ and $\langle T\widetilde{\Psi}(x)\widetilde{\Psi}^{\dagger}(y)\rangle$. The complex field $\widetilde{\Psi}$ obeys the bosonic commutation relation (3.6). This makes appear in equation (3.102) a divergent term $\delta^3(\mathbf{0})$ as for $x^0=y^0$ one has

$$\begin{aligned}G_{cc}(\mathbf{x},\mathbf{x}) \overset{N=2}{=} G_{11}(\mathbf{x})+G_{22}(\mathbf{x}) &= \langle\phi_1(\mathbf{x})\phi_1(\mathbf{x})\rangle+\langle\phi_2(\mathbf{x})\phi_2(\mathbf{x})\rangle\\ &= \langle\widetilde{\Psi}(\mathbf{x})\widetilde{\Psi}^{\dagger}(\mathbf{x})\rangle+\langle\widetilde{\Psi}^{\dagger}(\mathbf{x})\widetilde{\Psi}(\mathbf{x})\rangle\\ &= 2\langle\widetilde{\Psi}^{\dagger}(\mathbf{x})\widetilde{\Psi}(\mathbf{x})\rangle+\delta^3(\mathbf{0})\,. \end{aligned} \tag{3.105}$$

This divergence comes from the Weyl ordering of the underlying Hamiltonian and disappears when taking an equivalent but normal ordered one [120, 126]. Physically, it corresponds to a shift in the energy zero so we can omit it in our analytical study.

3.3.2 Nonrelativistic limit

Now we need to take the nonrelativistic limit of the above equations (3.102) and (3.103). Following Zee [127] we therefore replace

$$\phi(x)\longrightarrow\frac{1}{\sqrt{m}}e^{-imx^0}\Phi(x)\,, \tag{3.106}$$

$$\widetilde{\Psi}(x)\longrightarrow\frac{1}{\sqrt{m}}e^{-imx^0}\widetilde{\psi}(x)\,, \tag{3.107}$$

where the nonrelativistic fields Φ and $\widetilde{\psi}$ are assumed to vary slowly in time. The dimensionful prefactors arise because of the different normalizations of relativistic and nonrelativistic fields. As an example, let us consider the free Klein-Gordon equation

$$\left(\Box_x+m^2\right)\phi(x)=0. \tag{3.108}$$

The above replacement, implying that terms $\sim\partial^2_{x^0}\Phi(x)$ can be neglected, indeed leads to the Schrödinger equation

$$-2\sqrt{m}e^{-imx^0}\left(i\partial_{x^0}+\frac{\Delta}{2m}\right)\Phi(x)=0. \tag{3.109}$$

In a similar way, applying (3.106) to the field equation (3.102) leads to

$$\left(i\partial_{x^0}+\frac{\Delta}{2m}-gn(x)\right)\Phi(x)=\widetilde{\mathbf{K}}(x,x)\,, \tag{3.110}$$

where we identified

$$
\begin{aligned}
g &= \frac{\lambda}{12m^2}\,, && (3.111)\\
n(x) &= n_c(x) + \widetilde{n}(x) \\
&= \Phi^\dagger(x)\Phi(x) + \langle\widetilde{\psi}^\dagger(x)\widetilde{\psi}(x)\rangle\,, && (3.112)
\end{aligned}
$$

and analogously for the anomalous noncondensate density $\widetilde{m}(x) = \langle\widetilde{\psi}(x)\widetilde{\psi}(x)\rangle$. The function $\widetilde{\mathbf{K}}$ in (3.110) is defined as

$$
\begin{aligned}
\widetilde{\mathbf{K}}(x,y) &= \frac{e^{-imy^0}}{2\sqrt{m}}\mathbf{K}(x,y) \\
&= g\left(\Phi(x)\langle\widetilde{\psi}^\dagger(x)\widetilde{\psi}(y)\rangle + \Phi^\dagger(x)\langle\widetilde{\psi}(x)\widetilde{\psi}(y)\rangle\right) \\
&+ 2ig\int_z \Pi(x,z)\widetilde{\mathbf{K}}(z,y)\,, && (3.113)
\end{aligned}
$$

where Π now contains the nonrelativistic fields. For the propagator equation (3.103) one obtains in the same way

$$
\begin{aligned}
&\left(-i\partial_{x^0} + \frac{\Delta}{2m} - gn(x)\right)\langle T\widetilde{\psi}^\dagger(x)\widetilde{\psi}(y)\rangle = \frac{i}{2}e^{-im(x^0-y^0)}\delta_{\mathcal{C}}(x-y) + \Phi^\dagger(x)\widetilde{\mathbf{K}}(x,y) \\
&-\frac{i}{2}\int_z \widetilde{\mathbf{D}}(x,z)\big[\langle T\widetilde{\psi}^\dagger(x)\widetilde{\psi}^\dagger(z)\rangle\langle T\widetilde{\psi}(z)\widetilde{\psi}(y)\rangle + \langle T\widetilde{\psi}^\dagger(x)\widetilde{\psi}(z)\rangle\langle T\widetilde{\psi}^\dagger(z)\widetilde{\psi}(y)\rangle\big], \qquad (3.114)
\end{aligned}
$$

with

$$
\begin{aligned}
\widetilde{\mathbf{D}}(x,y) &= \frac{\mathbf{D}(x,y)}{m^2} \\
&= 2ig\delta_{\mathcal{C}}(x-y) + 4g\Phi^\dagger(x)\widetilde{\mathbf{K}}(y,x) + 4g\Phi(x)\widetilde{\mathbf{K}}^\dagger(y,x) \\
&+ 2ig\int_z \Pi(x,z)\widetilde{\mathbf{D}}(z,y)\,. && (3.115)
\end{aligned}
$$

Note that the correct nonrelativistic replacement of the Klein-Gordon operator is here

$$
(\Box + m^2) \longrightarrow -2\sqrt{m}e^{+imx^0}(-i\partial_{x^0} + \frac{\Delta}{2m}), \qquad (3.116)
$$

as it acts on $\widetilde{\psi}^\dagger$.

3.3.3 Field evolution in the kinetic approximation

Now we are prepared to rederive the kinetic ZNG equation (3.34) for Φ in terms of the noncondensate distribution functions. This exercise involves several steps where the various approximations of the ZNG theory come into the game. For instance, ZNG neglect the anomalous density $\widetilde{m}(x)$ as well as the correlations $\langle\widetilde{\psi}(x)\widetilde{\psi}(y)\rangle$ and $\langle\widetilde{\psi}^\dagger(x)\widetilde{\psi}^\dagger(y)\rangle$. In addition, they assume that the coupling constant g is small. Indeed, equation (3.34) only includes terms up to g^2. Higher order terms in the 2PI field equation (3.110) are encoded in the iterative function $\widetilde{\mathbf{K}}(x,x)$. To second order this function then reads

$$\begin{aligned}
\widetilde{\mathbf{K}}(x,x) &= g\left(\Phi(x)\widetilde{n}(x)+\Phi^\dagger(x)\widetilde{m}(x)\right)+2ig\int_{\mathcal{C}}dz^0\int d^3z\Pi(x,z)\widetilde{\mathbf{K}}(z,x)\\
&\simeq g\Phi(x)\widetilde{n}(x)+2ig^2\int_{\mathcal{C}}dz^0\int d^3z\langle T\widetilde{\psi}^\dagger(x)\widetilde{\psi}(z)\rangle\langle T\widetilde{\psi}(x)\widetilde{\psi}^\dagger(z)\rangle\Phi(z)\langle\widetilde{\psi}^\dagger(z)\widetilde{\psi}(x)\rangle\\
&= g\Phi(x)\widetilde{n}(x)+2ig^2\int_{-\infty}^{x^0}dz^0\int d^3z\Big[\langle\widetilde{\psi}^\dagger(z)\widetilde{\psi}(x)\rangle\langle\widetilde{\psi}(z)\widetilde{\psi}^\dagger(x)\rangle\Phi(z)\langle\widetilde{\psi}^\dagger(z)\widetilde{\psi}(x)\rangle\\
&- \langle\widetilde{\psi}(x)\widetilde{\psi}^\dagger(z)\rangle\langle\widetilde{\psi}^\dagger(x)\widetilde{\psi}(z)\rangle\Phi(z)\langle\widetilde{\psi}(x)\widetilde{\psi}^\dagger(z)\rangle\Big]. \qquad (3.117)
\end{aligned}$$

We explicitly evaluated here the integration along the CTP. Next we apply a quasiparticle approximation. Following the discussion in section 3.1.3 this amounts to assume that the correlation length of the system is sufficiently small and one can write

$$\begin{aligned}
\langle\widetilde{\psi}^\dagger(y)\widetilde{\psi}(x)\rangle &= \int\frac{d^3p}{(2\pi)^3}e^{i\mathbf{ps}-i\omega s^0}f(\mathbf{p},X)\,,\\
\langle\widetilde{\psi}(x)\widetilde{\psi}^\dagger(y)\rangle &= \int\frac{d^3p}{(2\pi)^3}e^{i\mathbf{ps}-i\omega s^0}\left(1+f(\mathbf{p},X)\right)\,, \qquad (3.118)
\end{aligned}$$

where $s=x-y$ and $X=\frac{x+y}{2}$ are the relative and center of mass coordinates, respectively, while $p=(\omega,\mathbf{p})$ denotes the noncondensate quasiparticle four-momentum. The dependence of the correlation functions in (3.118) on the relative time $s^0=x^0-y^0$ is assumed to be determined by these quasiparticles. The Hartree-Fock energy is according to ZNG given by $\omega_p=\frac{\mathbf{p}^2}{2m}+2g[n_c(x)+\widetilde{n}(x)]$. Following [114] we suppose the condensates atoms local velocity $\mathbf{v}_c$ and energy ϵ_c to be slowly varying in space in time such that the expansion

$$\Phi(z)\simeq\Phi(x)e^{im\mathbf{v}_c(\mathbf{z}-\mathbf{x})-i\epsilon_c(z^0-x^0)} \qquad (3.119)$$

applies. Inserting the above approximations in (3.117) together with (3.110) gives

$$\begin{aligned}
&\left(i\partial_{x^0}+\frac{\Delta}{2m}-g[n_c(x)+2\widetilde{n}(x)]\right)\Phi(x)=2ig\Phi(x)\int_{-\infty}^{x^0}dz^0\int d^3z\\
&\times\int\prod_{i=1}^{3}\left(\frac{d^3p_i}{(2\pi)^3}\right)e^{i(m\mathbf{v}_c-\mathbf{p}_1-\mathbf{p}_2+\mathbf{p}_3)(\mathbf{z}-\mathbf{x})-i(\epsilon_c-\omega_1-\omega_2+\omega_3)(z^0-x^0)}\\
&\times\left[f_2\left(1+f_3\right)f_1-\left(1+f_2\right)f_3\left(1+f_1\right)\right], \qquad (3.120)
\end{aligned}$$

where f_i means $f(\mathbf{p}_i,X)$. One may approximate (again following [114]) the time integral in (3.120) by

$$\int_{-\infty}^{x^0}dz^0e^{i(\epsilon_c-\omega_1-\omega_2+\omega_3)(x^0-z^0)}f\left(\frac{x^0+z^0}{2}\right)\simeq f(x^0)\pi\delta(\epsilon_c-\omega_1-\omega_2+\omega_3). \qquad (3.121)$$

The space dependence of the distribution functions may be simplified using a gradient expansion around $\mathbf{x}$ giving $f(\mathbf{X})\simeq f(\mathbf{x})$. The $\mathbf{z}$-integral in (3.121) can then easily be performed and one finally obtains

$$\left(i\partial_{x^0}+\frac{\Delta}{2m}-g[n_c(x)+2\widetilde{n}(x)]\right)\Phi(x)=$$
$$\frac{ig^2\Phi(x)}{(2\pi)^5}\int d^3p_1d^3p_2d^3p_3\quad\delta^3(m\mathbf{v}_c-\mathbf{p}_1-\mathbf{p}_2+\mathbf{p}_3)\delta(\epsilon_c-\omega_1-\omega_2+\omega_3)$$
$$\times\left[f_2(1+f_3)f_1-(1+f_2)f_3(1+f_1)\right]. \tag{3.122}$$

This equation is in agreement with the result derived in [114], see equation (3.34).

3.3.4 Boltzmann equation for excited quasiparticles

We now derive a Boltzmann equation for the noncondensate distribution function. Starting from equation (3.114) we neglect again anomalous correlators and contributions in higher order than g^2, giving

$$\begin{aligned}&(-i\partial_{x^0}+\frac{\Delta}{2m}-2gn(x))\langle T\widetilde{\psi}^\dagger(x)\widetilde{\psi}(y)\rangle=\\&\frac{i}{2}\delta_{\mathcal{C}}(x-y)-2ig^2\int_{\mathcal{C}}dz^0\int d^3z\\&\times\left[\Phi^\dagger(x)\Phi(z)\langle T\widetilde{\psi}^\dagger(x)\widetilde{\psi}(z)\rangle\langle T\widetilde{\psi}(x)\widetilde{\psi}^\dagger(z)\rangle\langle T\widetilde{\psi}^\dagger(z)\widetilde{\psi}(y)\rangle\right.\\&+\Phi^\dagger(z)\Phi(x)\langle T\widetilde{\psi}(z)\widetilde{\psi}^\dagger(x)\rangle\langle T\widetilde{\psi}^\dagger(x)\widetilde{\psi}(z)\rangle\langle T\widetilde{\psi}^\dagger(z)\widetilde{\psi}(y)\rangle\\&+\Phi^\dagger(x)\Phi(z)\langle T\widetilde{\psi}^\dagger(z)\widetilde{\psi}(x)\rangle\langle T\widetilde{\psi}^\dagger(x)\widetilde{\psi}(z)\rangle\langle T\widetilde{\psi}^\dagger(z)\widetilde{\psi}(y)\rangle\\&\left.+\langle T\widetilde{\psi}^\dagger(x)\widetilde{\psi}(z)\rangle\langle T\widetilde{\psi}(x)\widetilde{\psi}^\dagger(z)\rangle\langle T\widetilde{\psi}^\dagger(x)\widetilde{\psi}(z)\rangle\langle T\widetilde{\psi}^\dagger(z)\widetilde{\psi}(y)\rangle\right].\end{aligned} \tag{3.123}$$

From the structure of the right hand side one can already guess the essential physics of the upcoming Boltzmann equation. The first three terms under the integral describe interactions between the condensed and excited parts, while the last term only involves noncondensate atoms. The next steps proceed along similar lines as discussed in section 3.3.3. Therefore, we limit ourselves to a brief description of the left hand side of (3.124). A Vlasov-type form comes in reach by

- constructing a second equation from the complex conjugate of (3.124) with interchanged x and y,
- chosing without loss of generality $x^0>y^0$ for both equations,
- sum these equations such that $\partial_X=\partial_x+\partial_y$ appears.

These manipulations lead to

$$\left(-i\left[\partial_{x^0}+\partial_{y^0}\right]+\frac{1}{2m}\left[\Delta_{\mathbf{x}}-\Delta_{\mathbf{y}}\right]-2g\left[n(x)-n(y)\right]\right)\langle T\widetilde{\psi}^\dagger(x)\widetilde{\psi}(y)\rangle=... \tag{3.124}$$

where the somewhat lenghty right hand side is omitted for a better readability. The last approximation we need is a gradient expansion, which for the terms in (3.124) gives

$$\Delta_{\mathbf{x}}-\Delta_{\mathbf{y}}\ \simeq\ 2\partial_{\mathbf{X}}\partial_{\mathbf{s}}\,, \tag{3.125}$$
$$n_x-n_y\ \simeq\ s\cdot\partial_X n(X)|_{s=0}\,. \tag{3.126}$$

At the end, we set $s^0 = 0$ in order to be left with only one time variable $X^0 = T$. Performing the Wigner transform (3.118) one finally obtains

$$\left[\partial_T + \frac{1}{m}\mathbf{p}\cdot\partial_{\mathbf{x}} - 2g(\partial_{\mathbf{x}} n(X))\cdot\partial_{\mathbf{p}}\right] f(\mathbf{p},\mathbf{x},T) = C_{12} + C_{22}. \tag{3.127}$$

The right hand side of the above equation consists of two collision integrals describing two body collisions between noncondensate atoms (C_{22}) and collisions involving one condensate atom (C_{12}). They explicitly read

$$\begin{aligned} C_{22} = \frac{2g^2}{(2\pi)^5}\int d^3p_1 d^3p_2 d^3p_3 \delta^3(\mathbf{p}_1+\mathbf{p}_2-\mathbf{p}_3-\mathbf{p})\delta(\omega_1+\omega_2-\omega_3-\omega) \\ \times\left[f_1 f_2(1+f_3)(1+f) - f f_3(1+f_2)(1+f_1)\right], \end{aligned} \tag{3.128}$$

$$\begin{aligned} C_{12} = \frac{4g^2 n_c(X)}{(2\pi)^2}\int d^3p_1 d^3p_2 \delta^3(m\mathbf{v}_c+\mathbf{p}_1-\mathbf{p}_2-\mathbf{p})\delta(\epsilon_c+\omega_1-\omega_2-\omega) \\ \times\left[f_1(1+f_2)(1+f) - f f_2(1+f_1)\right] \\ + \frac{2g^2 n_c(X)}{(2\pi)^2}\int d^3p_1 d^3p_2 \delta^3(m\mathbf{v}_c-\mathbf{p}_1-\mathbf{p}_2+\mathbf{p})\delta(\epsilon_c-\omega_1-\omega_2+\omega) \\ \times\left[f_1 f_2(1+f) - f(1+f_2)(1+f_1)\right]. \end{aligned} \tag{3.129}$$

This result is in agreement with the one derived by Griffin, Nikuni and Zaremba [114] and by Stoof [119].

In summary, the approach followed in this section provides a systematic approximation scheme for the nonequilibrium evolution of a Bose-Einstein condensate. Starting from the nonperturbative equations (3.110, 3.114) for scalar fields including scattering and memory effects it gives as approximation a practicable system of kinetic equations (3.122, 3.127) at order g^2 describing the dynamical properties of condensate formation. A full solution of the coupled 2PI equations (3.110, 3.114) requires extensive numerical work which is presented below.

3.4 Numerical study of BEC dynamics far from equilibrium

As we emphasized before, it is convenient in numerical studies to use spectral and statistical functions. One may thus write equations (3.110, 3.114) in terms of the nonrelativistic 2-component field ϕ_a as well as F and ρ or, equivalently, perform the nonrelativistic limit of (3.89), (3.93) and (3.93). The resulting equations have first been written down by Berges et al. in [126] starting from a nonrelativistic Hamiltonian. For a local interaction they obtain

$$\Big[-i\sigma_{2,ij}\partial_{x_0} - \delta_{ij}\frac{1}{2}g\phi_k(x)\phi_k(x) - M_{ij}(x;\phi=0,F)\Big]\phi_j(x) = \int_0^{x_0} dy\,\Sigma^{\rho}_{ij}(x,y;\phi=0;G)\,\phi_j(y)\,, \quad (3.130)$$

$$\Big[-i\sigma_{2,ik}\partial_{x_0} - M_{ik}(x;\phi,F)\Big]F_{kj}(x,y) = \int_0^{x_0} dz\,\Sigma^{\rho}_{ik}(x,z;\phi,G)F_{kj}(z,y) - \int_0^{y_0} dz\,\Sigma^{F}_{ik}(x,z;\phi,G)\rho_{kj}(z,y)\,, \quad (3.131)$$

$$\Big[-i\sigma_{2,ik}\partial_{x_0} - M_{ik}(x;\phi,F)\Big]\rho_{kj}(x,y) = \int_{y_0}^{x_0} dz\,\Sigma^{\rho}_{ik}(x,z;\phi,G)\rho_{kj}(z,y)\,, \quad (3.132)$$

where $\int_t^{t'} dx = \int_t^{t'} dx_0 \int d^3\mathbf{x}$ and

$$M_{ij}(x;\phi,F) = \delta_{ij}\Big[-\frac{\Delta}{2m} + \frac{1}{2}g\Big(\phi_k(x)\phi_k(x) + F_{kk}(x,x)\Big)\Big] + g\Big(\phi_i(x)\phi_j(x) + F_{ij}(x,x)\Big)\,. \quad (3.133)$$

The involved Pauli matrix reads explicitly

$$\sigma_2 = \begin{pmatrix} 0 & -i \\ i & 0 \end{pmatrix}. \quad (3.134)$$

These equations are very general and without some simplifying assumptions a numerical study would require large computer resources. Berges et al. limit their computation to one spatial dimension [126].
We want to investigate these equations in three dimensions and assume spatial homogeneity and isotropy. As a consequence, only the absolute value of a momentum $|\mathbf{p}| = p$ matters. This means that we will not be able to describe realistic experimental situations as one would then need to include a confining potential. We emphasize that spatially inhomogeneous fields pose no complication in principle but are computationally more expensive.
Most importantly, we decide to set the field $\phi = 0$. At first sight this seems as we would not be able to capture the condensed part of the system. But the condensate consists by definition of the modes in the lowest energy state, i.e. the $p = 0$ modes. In this language the condensate density in momentum space is written like

$$n_c(t) = \frac{1}{2}\left(F_{11}(t,t,p=0) + F_{22}(t,t,p=0)\right). \quad (3.135)$$

Clearly, this formalism requires a special treatment of the zero modes which we describe below.
Applying these simplifications to the above equations (3.131, 3.132) and performing a spatial Fourier transform leads to

$$
\begin{aligned}
\left(-i\sigma_2\partial_t - \Delta(t)\right)^{ik} F^{kj}(t,t',p) &= \int_0^t dt'' \Sigma_\rho^{ik}(t,t'',p) F^{kj}(t'',t',p) \\
&- \int_0^{t'} dt'' \Sigma_F^{ik}(t,t'',p)\rho^{kj}(t'',t',p)\,, \qquad (3.136)\\
\left(-i\sigma_2\partial_t - \Delta(t)\right)^{ik} \rho^{kj}(t,t',p) &= \int_{t'}^t dt'' \Sigma_\rho^{ik}(t,t'',p)\rho^{kj}(t'',t',p), \qquad (3.137)
\end{aligned}
$$

with

$$
\Delta(t)_{ij} = \delta_{ij}\left[\frac{p^2}{2m} + \frac{g}{2}\int_{\mathbf{q}} F_{aa}(t,t,q)\right] + g\int_{\mathbf{q}} F_{ij}(t,t,q). \qquad (3.138)
$$

The equations of motion involve the self energies

$$
\begin{aligned}
\Sigma_F^{ij}(t,t',p) &= -g\int_{\mathbf{q}}\Big[\mathbf{I}_F(t,t',q)F^{ij}(t,t',|\mathbf{p}-\mathbf{q}|) \\
&\qquad -\frac{1}{4}\mathbf{I}_\rho(t,t',q)\rho^{ij}(t,t',|\mathbf{p}-\mathbf{q}|)\Big]\,, \qquad (3.139)\\
\Sigma_\rho^{ij}(t,t',p) &= -g\int_{\mathbf{q}}\Big[\mathbf{I}_F(t,t',q)\rho^{ij}(t,t',|\mathbf{p}-\mathbf{q}|) \\
&\qquad +\mathbf{I}_\rho(t,t',q)F^{ij}(t,t',|\mathbf{p}-\mathbf{q}|)\Big], \qquad (3.140)
\end{aligned}
$$

with

$$
\begin{aligned}
\mathbf{I}_F(t,t',p) &= \Pi_F(t,t',p) - \int_0^t dt'' \mathbf{I}_\rho(t,t'',p)\Pi_F(t'',t',p) \\
&+ \int_0^{t'} dt'' \mathbf{I}_F(t,t'',p)\Pi_\rho(t'',t',p)\,, \qquad (3.141)\\
\mathbf{I}_\rho(t,t',p) &= \Pi_\rho(t,t',p) - \int_{t'}^t dt'' \mathbf{I}_\rho(t,t'',p)\Pi_\rho(t'',t',p)\,, \qquad (3.142)
\end{aligned}
$$

and

$$
\begin{aligned}
\Pi_F(t,t',p) &= \frac{1}{2}g\int_{\mathbf{q}}\Big[F^{ij}(t,t',q)F^{ij}(t,t',|\mathbf{p}-\mathbf{q}|) \\
&\qquad -\frac{1}{4}\rho^{ij}(t,t',q)\rho^{ij}(t,t',|\mathbf{p}-\mathbf{q}|)\Big]\,, \qquad (3.143)\\
\Pi_\rho(t,t',p) &= g\int_{\mathbf{q}} F^{ij}(t,t',q)\rho^{ij}(t,t',|\mathbf{p}-\mathbf{q}|)\,. \qquad (3.144)
\end{aligned}
$$

Note that differently to equations (3.91, 3.92) we decided here to include the coupling in the Π's rather than in the $\mathbf{I}$'s.
We now explicitly extract the zero-modes. This requires writing of factors $\frac{1}{V}$ (where V is the spatial volume) to take into account the infinitesimal measure of a single mode. Note that

the statistical propagators at equal times give the number density of atoms in a particular momentum state

$$n_p(t) = \frac{1}{2}\left(F_{11}(t,t,p) + F_{22}(t,t,p) - 1\right). \tag{3.145}$$

Here, the -1 cuts the Weyl order divergence that we already referred to in section 3.3.1 in order to prevent the intermediate computation of large numbers.
As particle numbers grow potentially large, the same is true for the statistical propagators with equal time arguments while the corresponding spectral propagators are determined by the equal time commutation relation $[\varphi_1(p), \varphi_2(p)] = i$ and take the values

$$\begin{aligned} \rho_{11}(t,t,p) &= 0\,, \qquad \rho_{12}(t,t,p) = -1\,, \\ \rho_{21}(t,t,p) &= 1\,, \qquad \rho_{22}(t,t,p) = 0\,. \end{aligned}$$

We therefore introduce scaled statistical variables $F^0_{ij} = \frac{1}{V}F_{ij}(p=0)$, $\Pi^0_F = \frac{1}{V}\Pi_F(p=0)$ and $\Sigma^0_{Fij} = \frac{1}{V}\Sigma_{Fij}(p=0)$ to absorb the $\frac{1}{V}$ factors. In the infinite volume limit our equations finally read

$$\begin{aligned} \Sigma_{Fij}(t,t',p\neq 0) &= -g(\mathbf{I}^0_F(t,t')F_{ij}(t,t',p) + \mathbf{I}_F(t,t',p)F^0_{ij}(t,t')) \\ &- g\int_{\mathbf{q}\neq\mathbf{0}}\Big[\mathbf{I}_F(t,t',q)F_{ij}(t,t',|\mathbf{p}-\mathbf{q}|) \\ &\qquad -\frac{1}{4}\mathbf{I}_\rho(t,t',q)\rho_{ij}(t,t',|\mathbf{p}-\mathbf{q}|)\Big]\,, \qquad (3.146) \\ \Sigma^0_{Fij}(t,t') &= -g\mathbf{I}^0_F(t,t')F^0_{ij}(t,t')\,, \qquad (3.147) \\ \Sigma_{\rho ij}(t,t',p\neq 0) &= -g(\mathbf{I}^0_F(t,t')\rho_{ij}(t,t',p) + \mathbf{I}_\rho(t,t',p)F^0_{ij}(t,t')) \\ &- g\int_{\mathbf{q}\neq\mathbf{0}}\Big[\mathbf{I}_F(t,t',q)\rho_{ij}(t,t',|\mathbf{p}-\mathbf{q}|) \\ &\qquad +\mathbf{I}_\rho(t,t',q)F_{ij}(t,t',|\mathbf{p}-\mathbf{q}|)\Big]\,, \qquad (3.148) \\ \Sigma^0_{\rho ij}(t,t') &= -g(\mathbf{I}^0_F(t,t')\rho^0_{ij}(t,t') + \mathbf{I}^0_\rho(t,t')F^0_{ij}(t,t')) \\ &- g\int_{\mathbf{q}\neq\mathbf{0}}\Big[\mathbf{I}_F(t,t',q)\rho_{ij}(t,t',q) \\ &\qquad +\mathbf{I}_\rho(t,t',q)F_{ij}(t,t',q)\Big]\,, \qquad (3.149) \end{aligned}$$

and

$$\begin{aligned}
\Pi_F(t,t',p\neq 0) &= gF^0_{ij}(t,t')F_{ij}(t,t',p) \\
&+ \frac{1}{2}g\int_{\mathbf{q}\neq\mathbf{0}}\Big[F_{ij}(t,t',q)F_{ij}(t,t',|\mathbf{p}-\mathbf{q}|) \\
&\qquad -\frac{1}{4}\rho_{ij}(t,t',q)\rho_{ij}(t,t',|\mathbf{p}-\mathbf{q}|)\Big]\,, \qquad (3.150)\\
\Pi^0_F(t,t') &= \frac{1}{2}gF^0_{ij}(t,t')F^0_{ij}(t,t')\,, \qquad (3.151)\\
\Pi_\rho(t,t',p\neq 0) &= gF^0_{ij}(t,t')\rho_{ij}(t,t',p) \\
&+ g\int_{\mathbf{q}\neq\mathbf{0}}F_{ij}(t,t',q)\rho_{ij}(t,t',|\mathbf{p}-\mathbf{q}|)\,, \qquad (3.152)\\
\Pi^0_\rho(t,t') &= gF^0_{ij}(t,t')\rho^0_{ij}(t,t') \\
&+ g\int_{\mathbf{q}\neq\mathbf{0}}F_{ij}(t,t',q)\rho_{ij}(t,t',q)\,, \qquad (3.153)
\end{aligned}$$

while the equations for F, ρ, $\mathbf{I}_F$ and $\mathbf{I}_\rho$ remain unchanged. For the sake of a better orientation, we give in figure 3.14 an overview of the involved functions and their respective relations.

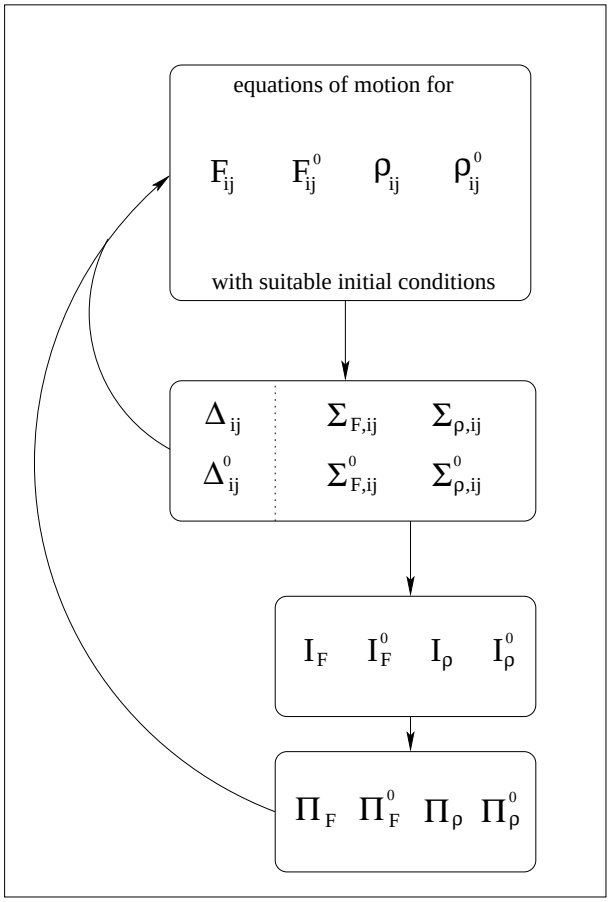

Figure 3.14: Overview of involved functions.

3.4.1 Conservation laws

In order to test the reliability of our code we need some analytical results which we then reproduce numerically. These are in our case the conservation of the particle number $n(t)$ and energy density $\epsilon(t)$, respectively. First, $n(t)$ is given by

$$n(t) = \int_{\mathbf{p}} \left(F_{11}(t,t,p) + F_{22}(t,p) - 1\right). \tag{3.154}$$

As it is a useful exercise to clarify the interplay of the various functions and equations, we show explicitly the conservation of $n(t)$.

$$\begin{aligned}
\partial_t n(t) &= \int_{\mathbf{p}} \partial_t F_{11}(t,t,p) + \partial_t F_{22}(t,t,p) \\
&\overset{3.136}{=} \int_{\mathbf{p}} \Bigg(\Delta^{21}(t) F^{11}(t,t,p) + \Delta^{22}(t) F^{21}(t,t,p) \\
&\quad - \Delta^{11}(t) F^{12}(t,t,p) - \Delta^{12}(t) F^{22}(t,t,p) \\
&\quad + \int_0^t dt'' \left[\Sigma_\rho{}^{21}(t,t'',p) F^{11}(t,t'',p) + \Sigma_\rho{}^{22} F^{12} - \Sigma_\rho{}^{11} F^{21} - \Sigma_\rho{}^{12} F^{22} \right] \\
&\quad + \int_0^t dt'' \left[\Sigma_F{}^{21}(t,t'',p) \rho^{11}(t,t'',p) + \Sigma_F{}^{22} \rho^{12} - \Sigma_F{}^{11} \rho^{21} - \Sigma_F{}^{12} \rho^{22} \right] \Bigg) \\
&\overset{3.138-3.140}{=} g \int_{\mathbf{p},\mathbf{q}} \Bigg(\Big[F_{21}(t,t,q) \Big\{ \left(F_{11}(t,t,p) - F_{22}(t,t,p)\right) \Big\} \\
&\qquad + \Big\{ F_{22}(t,t,q) - F_{11}(t,t,q) \Big\} F_{12}(t,t,p) \Big] \\
&\quad + \int_0^t dt'' \Big[\Big\{ \mathbf{I}_F(t,t'',q) \rho_{21}(t,t'',|\mathbf{p}-\mathbf{q}|) \\
&\qquad + \mathbf{I}_\rho(t,t'',q) F_{21}(t,t'',|\mathbf{p}-\mathbf{q}|) \Big\} F_{11}(t,t'',p) + \left(\mathbf{I}_F \rho_{22} + \mathbf{I}_\rho F_{22}\right) F_{12} \\
&\qquad - \left(\mathbf{I}_F \rho_{11} + \mathbf{I}_\rho F_{11}\right) F_{21} - \left(\mathbf{I}_F \rho_{12} + \mathbf{I}_\rho F_{12}\right) F_{22} + \left(\mathbf{I}_F F_{21} - \mathbf{I}_\rho \rho_{21}\right) \rho_{11} \\
&\qquad + \left(\mathbf{I}_F F_{22} - \mathbf{I}_\rho \rho_{22}\right) \rho_{12} - \left(\mathbf{I}_F F_{11} - \mathbf{I}_\rho \rho_{11}\right) \rho_{21} - \left(\mathbf{I}_F F_{12} - \mathbf{I}_\rho \rho_{12}\right) \rho_{22} \Big] \Bigg) \\
&= 0.
\end{aligned} \tag{3.155}$$

This result is valid to all orders in g, as no truncation of $\mathbf{I}_F$ or $\mathbf{I}_\rho$ needs to be performed. Extraction of zero-modes and subsequent introduction of scaled statistical variables does not change the result, as one may easily check.

The energy density $\epsilon(t)$ is given by

$$\begin{aligned}\epsilon(t) &= \int_{\mathbf{p}} \frac{p^2}{2m}\left(F_{11}(t,t,p)+F_{22}(t,t,p)-1\right)\\ &+ \frac{g}{8}\int_{\mathbf{p},\mathbf{q}} F_{aa}(t,t,q)F_{bb}(t,t,|\mathbf{p}-\mathbf{q}|)\\ &+ \frac{1}{2}\int_{\mathbf{p}} \mathbf{I}_F(t,t,p). \end{aligned} \tag{3.156}$$

This quantity is also conserved, as is shown e.g. in [128].

3.4.2 Numerical implementation

The nonlinear integro-differential equations (3.136) and (3.137), together with the self energies obtained from the $1/N$ expansion, describe the time evolution of our system. Although these equations are in general too complicated to be solved analytically without additional approximations, they can be very efficiently implemented and solved on a computer. A detailed account on the numerical implementation of relativistic 2PI equations can be found in [86]. We mainly follow this presentation.

First, it is useful to note that all involved equations are explicit in time, i.e. all quantities at some later time t_l can be obtained by integration over the explicitly known functions for times $t < t_l$. This means that a numerical study only requires a set of initial conditions for the statistical propagators F_{11}, F_{12}, F_{21} and F_{22} for all momentum modes. The respective initial conditions for the spectral propagators are completely fixed by the equal time commutation relations.

In our numerical study we apply a time discretization $t = na_t$, $t' = ma_t$ with stepsize a_t such that $F(t,t') \mapsto F(n,m)$. The time derivatives and integrals are replaced by

$$\partial_t F(t,t') \;\mapsto\; \frac{1}{2a_t}\Big(F(n+1,m)+F(n-1,m)\Big), \tag{3.157}$$

$$\int_0^t dt F(t,t') \;\mapsto\; a_t \sum_{l=0}^{n-1} F(l,m)\,, \tag{3.158}$$

where we have suppressed the momentum labels in the notation. The above simple discretization already leads to stable numerics for small enough stepsize a_t.

As for the continuum the propagators obey the symmetry properties $F(n,m) = F(m,n)$ and $\rho(n,m) = -\rho(m,n)$. Consequently, only half of the matrix components have to be computed. The same (anti)symmetry applies to the (spectral) statistical components of the self energy Σ and the chain of bubbles $\mathbf{I}$. One can exploit these features in order to save memory space. Therefore, we code our equations such that any function $A(n,m)$ appears with time arguments $n \geq m$.

To give an example, the 21-component of (3.136) reads in the discretized form

- $m = 0$

$$\begin{aligned} F_{11}(n+1,0) &= F_{11}(n-1,0) \\ &+ 2a_t\left(\Delta_{21}(n)F_{11}(n,0) + \Delta_{22}(n)F_{21}(n,0)\right) \\ &+ 2a_t^2\sum_{l=0}^{n-1}\left(\Sigma^\rho_{21}(n,l)F_{11}(l,0) + \Sigma^\rho_{22}(n,l)F_{21}(l,0)\right), \end{aligned}$$

- $1 \leq m \leq n-1$

$$\begin{aligned} F_{11}(n+1,m) &= F_{11}(n-1,m) \\ &+ 2a_t\left(\Delta_{21}(n)F_{11}(n,m) + \Delta_{22}(n)F_{21}(n,m)\right) \\ &+ 2a_t^2\sum_{l=0}^{m-1}\left(\Sigma^\rho_{21}(n,l)F_{11}(m,l) + \Sigma^\rho_{22}(n,l)F_{12}(m,l)\right) \\ &+ 2a_t^2\sum_{l=m}^{n-1}\left(\Sigma^\rho_{21}(n,l)F_{11}(l,m) + \Sigma^\rho_{22}(n,l)F_{21}(l,m)\right) \\ &+ 2a_t^2\sum_{l=0}^{m-1}\left(\Sigma^F_{21}(n,l)\rho_{11}(m,l) + \Sigma^F_{22}(n,l)\rho_{12}(m,l)\right), \end{aligned}$$

- $m \geq n$

$$\begin{aligned} F_{11}(n+1,m) &= F_{11}(m,n-1) \\ &+ 2a_t\left(\Delta_{21}(n)F_{11}(m,n) + \Delta_{22}(n)F_{12}(m,n)\right) \\ &+ 2a_t^2\sum_{l=0}^{n-1}\left(\Sigma^\rho_{21}(n,l)F_{11}(m,l) + \Sigma^\rho_{22}(n,l)F_{12}(m,l)\right) \\ &+ 2a_t^2\sum_{l=0}^{m-1}\left(\Sigma^F_{21}(n,l)\rho_{11}(m,l) + \Sigma^F_{22}(n,l)\rho_{12}(m,l)\right). \end{aligned}$$

Finally, we have to deal with the momentum integrations, especially the convolutions of momentum integrals in (3.146), (3.148), (3.150) and (3.152). They are computed in the usual way by fast Fourier transformations making use of the relation

$$\begin{aligned} C(\mathbf{p}) &= \int_{\mathbf{q}} A(\mathbf{q})B(\mathbf{p}-\mathbf{q}) \\ &= \int_{\mathbf{z}} \exp(-i\mathbf{p}\mathbf{z})A(\mathbf{z})B(\mathbf{z}). \end{aligned} \tag{3.159}$$

So instead of computing a three dimensional integral we subsequently Fourier fransform three functions $A(\mathbf{q})$, $B(\mathbf{q})$ and $A(\mathbf{z}) \cdot B(\mathbf{z})$. This is a crucial advantage as the computing time grows only like $3 \cdot \log(N)$ inspite of N^3, where N is the number of momentum steps.

3.4.3 Results

We present the results of our numerical study concentrating on one exemplatory run. As we emphasized before, our goal is not to implement all the features of a realistic experimental situation but rather to concentrate on the nonequilibrium evolution of a simple BEC model. Condensate growth can be successfully described by the ZNG kinetic equations [116] which we showed to be a limiting case of our approach. As the excited atoms and their interaction with the condensate are described by Boltzmann equations the ZNG theory is limited to near equilibrium situations.

In [130, 131] Barci et al. present a nonequilibrium field theory description of Bose gases. In this scenario the system is initially in an equilibrated state well above the critical temperature T_c. Then it is coupled to a thermal bath with a much lower temperature $T \ll T_c$. For $T \simeq T_c$ this description breaks down as the dynamics between the condensed and excited atoms are treated as a two-level problem. The authors also manage to simulate condensate growth, but the relevant time scales differ significantly from ZNG (we will comment on this point below).

As it stands, none of the above approaches is able to deal with the inverse process (which we refer to as condensate melting) as both nonequilibrium dynamics and large energy densities (to obtain large temperatures) are involved.
Nevertheless, condensate melting plays naturally an important role in BEC experiments. After a BEC has been created, the trap is suddenly turned off and the gas expands freely about 10-20 ms before the velocity distribution is measured [102]. Thus, a certain fraction of the condensate melts away before an image is taken.
So we are interested in the time evolution of an initially pure condensate with a large energy density. The latter is most efficiently implemented by chosing a large value for the coupling constant g, which is possible due to the nonperturbative nature of our equations.

We set the mass $m = 1$ for simplicity and thus work, for the time being, in arbitrary units. Below, we compute physical values from our results, taking ^{87}Rb as an example. The relevant parameters are

- time step $a_t = 0.001$,
- number of timesteps $N_t = 250$,
- momentum step $a_p = \frac{1}{32}$,
- number of modes $N_p = 32$,
- interaction strength $g = 1$.

So the value of the momentum variable p ranges from 0 to $N_p \cdot a_p = \Lambda = 1$.

Note that $g = 1$ in our code does not necessarily correspond to strong coupling in a physical application. It is dimensionful and thus depends on the input of physical quantities, namely the scattering length a and atomic mass. Below we will see that g rather serves as a turning knob to tune the diluteness parameter na^3.

As initial conditions we chose

- $F_{11}(p=0) = F_{22}(p=0) = n_{\text{ini}}(p=0)$,
- $F_{11}(p\neq 0) = F_{22}(p\neq 0) = n_{\text{ini}}(p\neq 0) + 0.5$,
- $F_{12} = F_{21} = 0$ for all modes.

Here we defined the initial particle ditribution

$$n_{\text{ini}}(p) = A \cdot \exp\left(\frac{p-\bar{p}}{2\sigma^2}\right),$$

with the amplitude $A = 50$, the average momentum $\bar{p} = 0.3$ and the width $\sigma = 0.7$. Again, the initial values of the spectral functions are completely determined by the commutation relations.

We will see shortly that these initial values lead, as we desired, to an almost pure initial condensate that rapidly melts away due to a large energy density.

Condensate melting

First, we need to check if the numerical code preserves the conservation laws of our system which we have discussed above analytically. In figures 3.15 and 3.16 the time evolution of the particle number and energy density are respectively plotted. A good conservation of both quantities is observed, showing the reliability of our code.

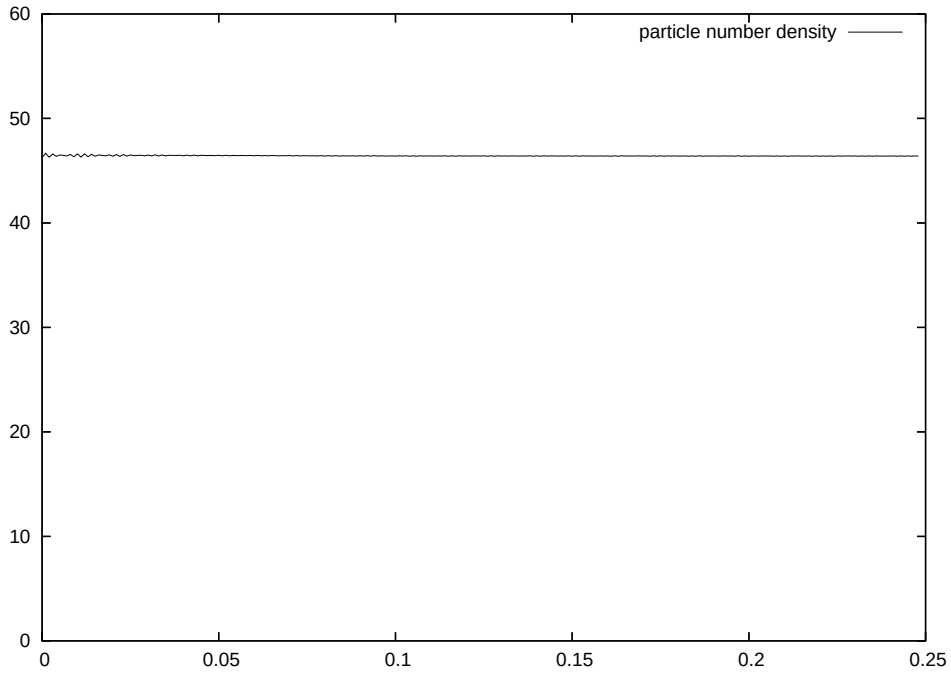

Figure 3.15: Particle number density as a function of time.

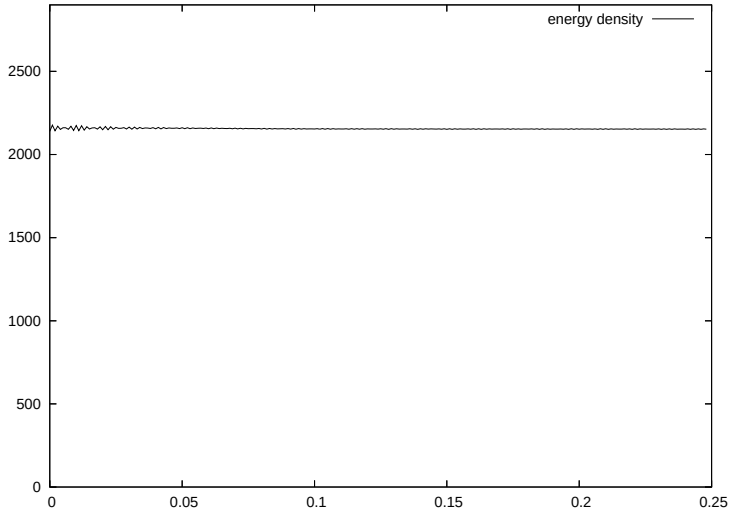

Figure 3.16: Energy density as a function of time.

Nevertheless, some tiny deviations from a straight line are still visible. In figure 3.17 we take a closer look on these uncertainties. One observes typical oscillations resulting from the discretization of the underlying equations. In addition, mainly in the time interval $0.05 - 0.1$ a small dent shows up. Below we will see that in this interval the condensed part of the system decreases from the large initial value to nearly 0. So this uncertainty is due to our special treatment of the zero modes which also explains why the oscillation amplitude is bigger at the beginning. After all, the magnitude of numerical errors never surmounts 1% of the absolute value of the particle number density, which is a satisfactory result.

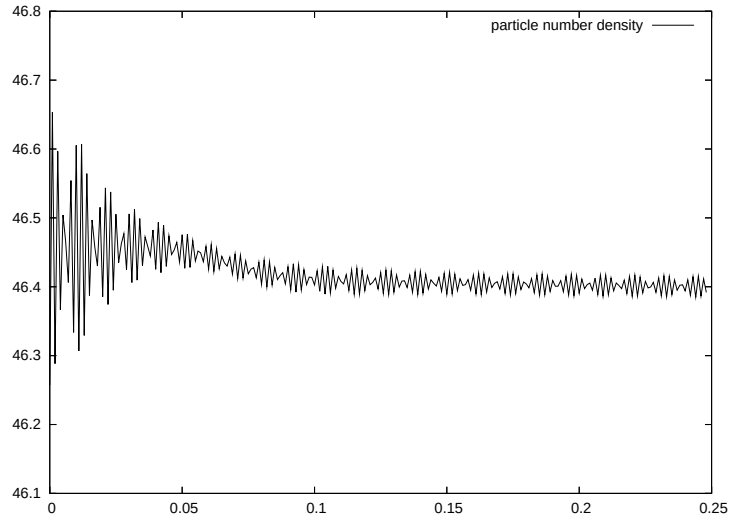

Figure 3.17: Numerical uncertainties in the particle number density.

Now we turn to the time evolution of the condensed part of our system (see fig. 3.18). Initially, we have an almost pure condensate. As our coupling constant is nonperturbatively large, the energy density is large, as well. Thus we expect a rapid decrease of the zero modes which is confirmed in our simulation. After about half the simulation time in figure 3.18, they fall from the initial maximum value to strictly zero and do not recover until the end of the simulation. This behaviour is also confirmed in the zero mode contribution to the energy density, see figure 3.19.

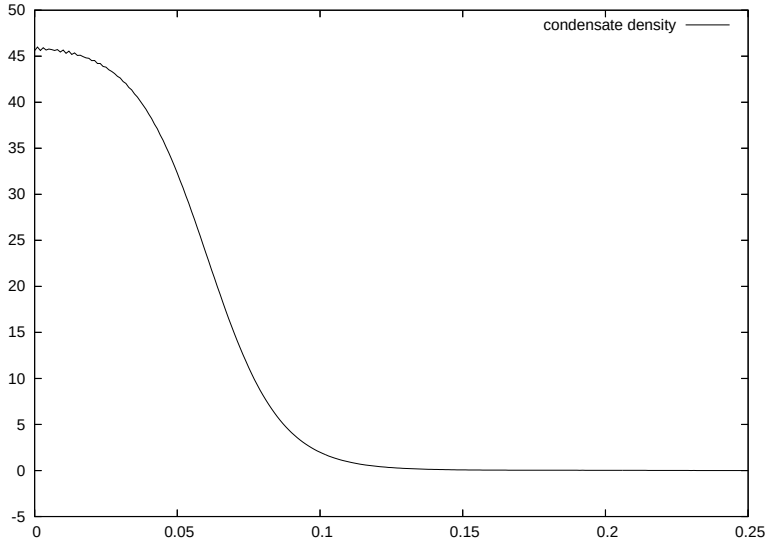

Figure 3.18: Condensate density as a function of time.

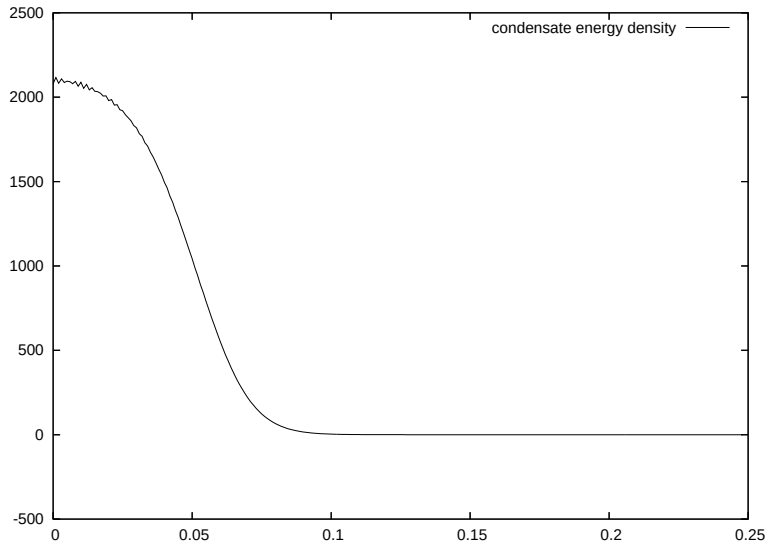

Figure 3.19: Zero mode contribution to the energy density.

Damping of nonequal time correlations

It is insightful to have a look at the nonequal time correlations in the system. As some examples, we show in figures 3.20 to 3.23 the evolution in the second time variable of F_{11}, F_{12}, ρ_{11} and ρ_{12} when the first time variable is kept zero. In each plot we show three curves corresponding to the momentum modes $p = 0$, $p = 15$ and $p = 30$, respectively.

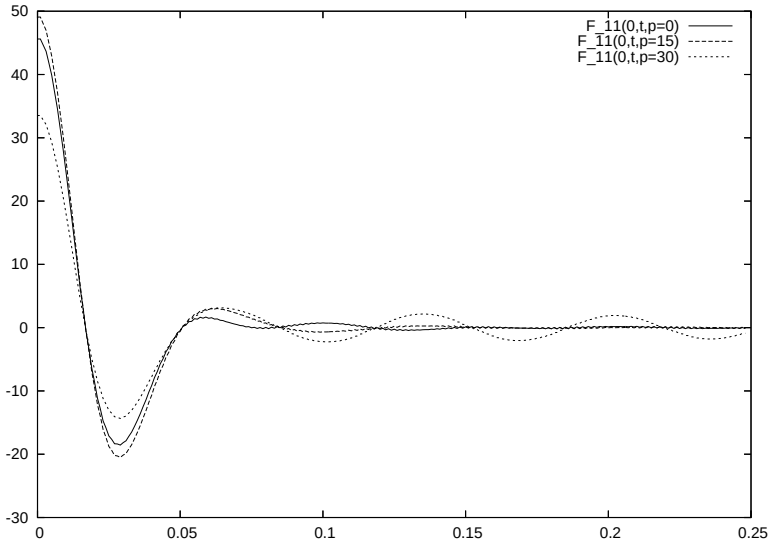

Figure 3.20: Evolution of the unequal time correlator $F_{11}(0,t)$ for low ($p = 0$), medium ($p = 15$) and large ($p = 30$) momentum states.

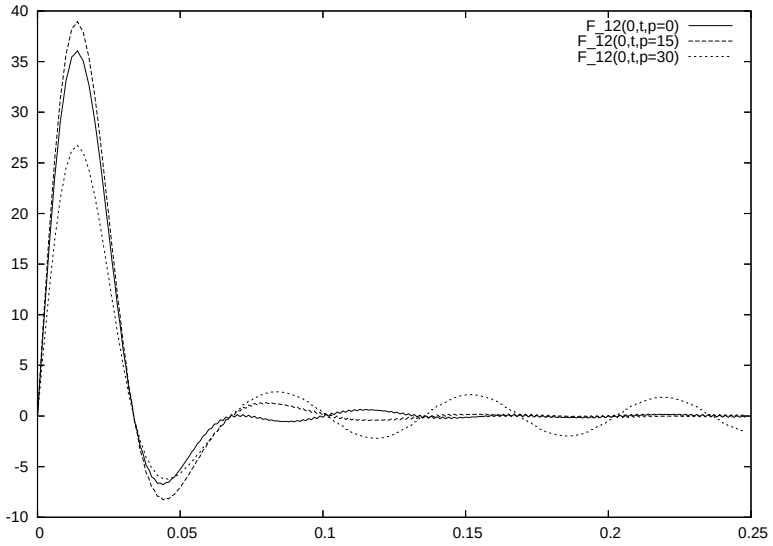

Figure 3.21: Evolution of $F_{12}(0,t)$ for $p = 0, 15, 30$.

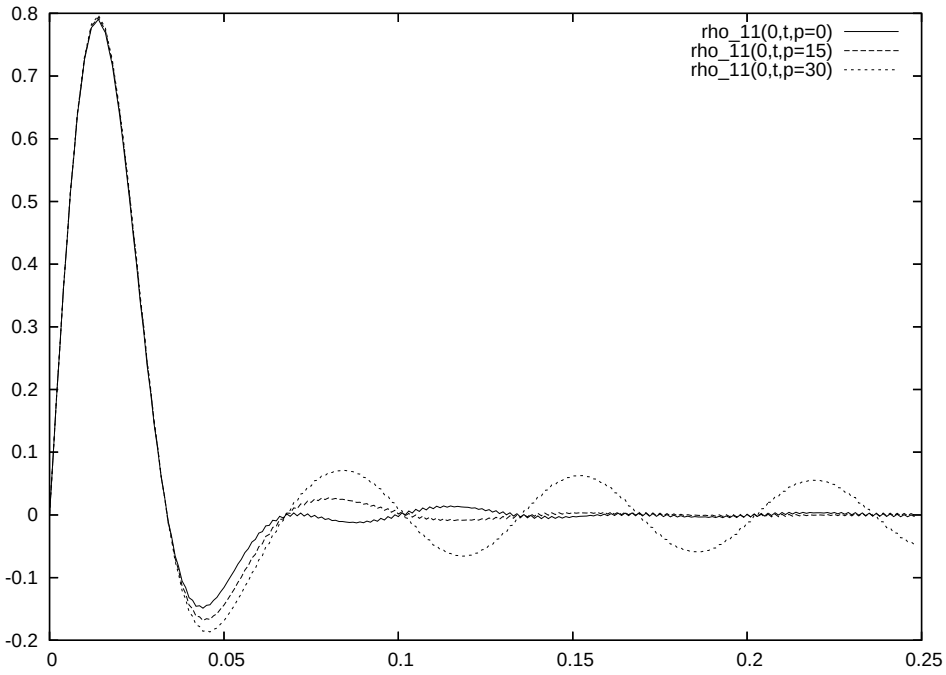

Figure 3.22: Evolution of $\rho_{11}(0,t)$ for $p = 0, 15, 30$.

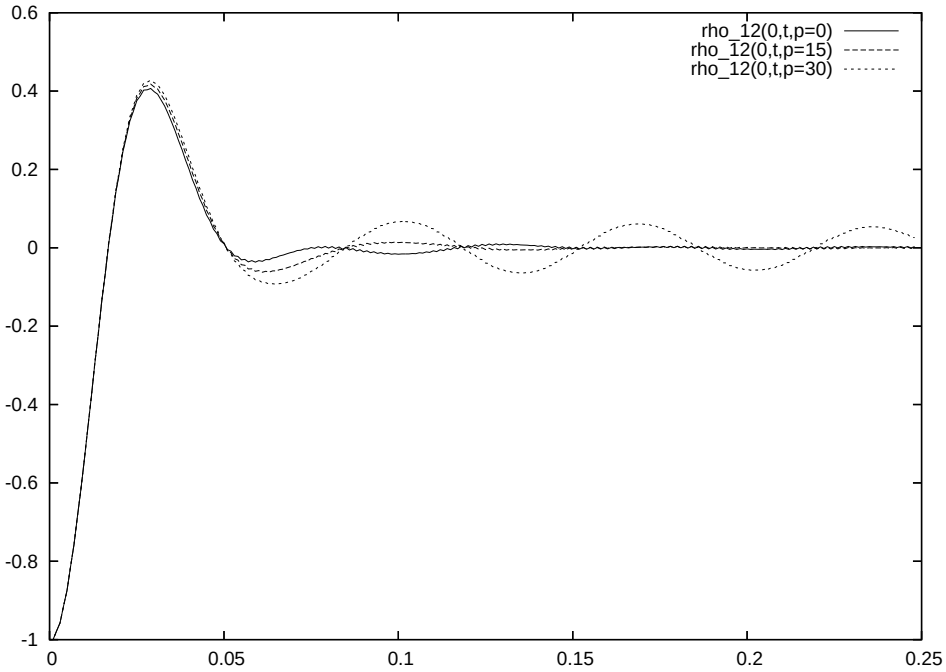

Figure 3.23: Evolution of $\rho_{12}(0,t)$ for $p = 0, 15, 30$.

The unequal time correlations of the zero mode are quickly damped to zero, while the highest modes still show a clear oscillation at the end of the simulation. Thus, the system did not yet forget all information about the initial conditions and is still out of equilibrium. Consequently, one cannot attribute a temperature to it (and the concept of an effective temperature does not reveal much information about the final one, either, see the discussion on this point in [126]).

Dependence of time scales on the interaction strength

In order to see how the results depend on the coupling constant we performed some additional runs with different values for g and all other parameters unchanged. As expected, we find that for smaller interaction strengths (and thus smaller energy densities) the time scale on which the zero modes evolve grows, as can be seen in figure 3.24. In this region the dependence is nearly proportional, meaning that a decrease of g by some factor leads to an increase in the melting time by the same factor.

When looking at the unequal time correlations this relation becomes more evident. In figure 3.25 we show the time evolution of $F_{11}(0, t, p = 0)$ for various interactions ranging from $g = 1$ to $g = 0.15$. The qualitative behaviour is always the same, e.g. the minimum value is about -19 for all curves. But the time when this value is reached differs e.g. by a factor 2 for the $g = 0.3$ and $g = 0.15$ plots.

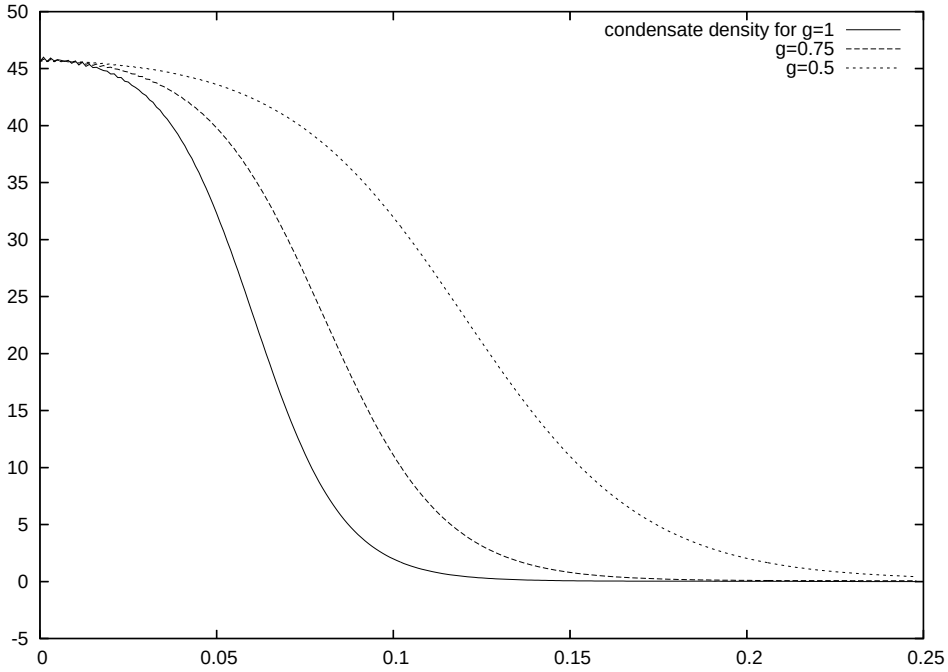

Figure 3.24: Condensate melting for different values of the interaction strength.

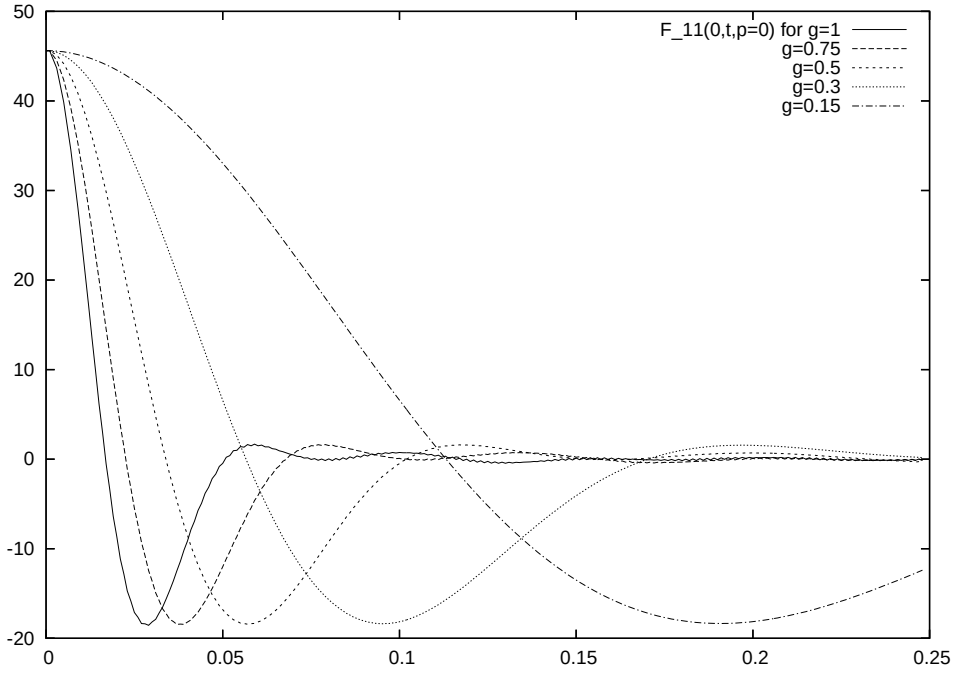

Figure 3.25: Damping of unequal time correlators for different values of the interaction strength.

Physical example: ^{87}Rb

So far, we presented our results in the general context of arbitrary units. As an application, we now take the specific values of ^{87}Rb atoms (scattering length $a = 58 \cdot 10^{-10} m$, atomic mass $m_a = 1.4 \cdot 10^{-25} kg$) to compare our data with related work.

It is convenient to introduce the dimensionless variable

$$\gamma = \frac{m_a g \Lambda}{2\pi^2 \hbar^3} \,. \tag{3.160}$$

The scattering length a, introduced in (3.8), can then be written like

$$\begin{aligned} a &= \frac{m_a g}{4\pi\hbar^2} \\ &= \frac{\pi\gamma\hbar}{2\Lambda} \,. \end{aligned} \tag{3.161}$$

From this relation one quickly translates the unit length in our code into meters, resulting in

$$1 \cong 7 \cdot 10^{-8} m \,.$$

Similarly, one translates the momentum, energy and time units by using the physical value of m_a. For our observables n and ϵ the numerical results then correspond to

$$n \simeq 1 \cdot 10^{23} \frac{1}{m^3},$$
$$\epsilon \simeq 1 \cdot 10^{-3} \frac{J}{m^3}.$$

The particle number density is large compared to typical experimental densities of pure condensates which are around $n \simeq \frac{10^{19}-10^{20}}{m^3}$ [102]. However, it roughly coincides with an experiment on condensate growth in a gas of $4 \cdot 10^6$ ^{87}Rb atoms performed in Munich [132] and is thus a realistic value.
In addition, the condition $na^3 \simeq 0.02 \ll 1$ is still valid and the approximation of a local two-body interaction holds.

As we emphasized above, it is not possible to extract a temperature from our data as the system is not fully equilibrated. To estimate the expected order of magnitude one may use the ideal gas as a reasonable approximation to our weakly coupled system. For a uniform ideal Bose gas one has [88, 92]

$$\frac{\epsilon}{nk_BT_c} = \frac{3\zeta(5/2)}{2\zeta(3/2)} \cdot \left(\frac{T}{T_c}\right)^{5/2}, \tag{3.162}$$

where the transition temperature for ^{87}Rb is from (3.2) determined to $T_c \simeq 6 \cdot 10^{-5}K$. With the measured energy density we obtain $T \simeq 3 \cdot T_c \simeq 2 \cdot 10^{-4}K$. This value seems very reasonable as it is ultracold, yet well above the critical temperature (which is of course needed to ensure a complete melting of the condensate).

Finally, the time interval covered by our simulation corresponds for ^{87}Rb to $\triangle t \simeq 2 \cdot 10^{-6}s$ which gives a time scale of one μs for condensate melting. As a comparison, from figure 3.5 one sees that condensate growth in the ZNG theory is completed after some ms. Our simulation, however, is expected to give quite different values as a consequence of homogeneity. Recall that ZNG implement a confining potential in their equations and thus work in a nonuniform system.
On the other hand, Barci et al. [130, 131] work with a homogeneous ^{87}Rb gas. Their diluteness parameter $na^3 \simeq 0.01$ is two times smaller than ours, what a priori might be quite relevant for the time scales. To obtain the same value we would need to change the unit length in our system by a factor $2^{1/3}$. According to equation (3.161) this corresponds to a change of g in our code from 1 to $2^{-1/3} = 0.8$. From figures 3.24 and 3.25 we know that time scales are then stretched by the inverse factor $2^{1/3} = 1.26$, what does not lead to dramatic changes in this case. Consequently, the formation time obtained by Barci et al. ($t \simeq 1 \cdot 10^{-6}s$) nicely coincides with our scale for condensate melting.

3.5 Summary and outlook

We started this chapter with a short review of the standard theoretical tools to describe Bose condensed systems. The main results of the ZNG approach were presented and some shortcomings like the limitation to weakly coupled gases near equilibrium were discussed. We then switched to the 2PI effective action as a powerful method to investigate far from equilibrium phenomena. We concentrated on the $1/N$-expansion which provided us with nonperturbative

equations of motion.

In the nonrelativistic case we showed how these can be reduced to kinetic equations which are known in the literature to describe Bose condensed systems at finite temperature. As the full nonrelativistic equations are well suited for numerical investigation, we were able to present a three dimensional dynamical study of a Bose condensed gas far from equilibrium. We prepared our system in an almost completely condensed yet highly energetic state and observe the expected fast condensate melting. Applied to a gas of ^{87}Rb atoms our numerical results give reasonable values for all physical quantities.

When one includes features like the trapping potential in our model, future simulations of condensate melting could be compared to experimental data. As our approach is nonperturbative, a further extension to nonlocal interactions may provide insight into the physics of strongly coupled quantum gases near a Feshbach resonance.

Bibliography

[1] M. Cheng *et al.*, arXiv:hep-lat/0608013.

[2] M. H. Thoma, arXiv:hep-ph/0010164.

[3] L. Boltzmann, Wien. Ber.,**66**, 275 (1872).

[4] A. K. Das, World Sci. (1997).

[5] A. K. Das, arXiv:hep-ph/0004125.

[6] M. Le Bellac Cambridge Univ. Press (1996).

[7] J. I. Kapusta and P. V. Landshoff, J. Phys. G **15** (1989) 267.

[8] J. S. Schwinger, J. Math. Phys. **2** (1961) 407.

[9] L. V. Keldysh, Zh. Eksp. Teor. Fiz. **47** (1964) 1515 [Sov. Phys. JETP **20** (1965) 1018].

[10] P. M. Bakshi and K. T. Mahanthappa, J. Math. Phys. **4** (1963) 1.

[11] P. M. Bakshi and . T. Mahanthappa, J. Math. Phys. **4** (1963) 12.

[12] S. Mrowczynski, Phys. Rev. D **56** (1997) 2265.

[13] M. E. Carrington and S. Mrowczynski, Phys. Rev. D **71** (2005) 065007.

[14] L. P. Kadanoff and G. Baym, Benjamin, N.Y. (1962).

[15] J. P. Blaizot and E. Iancu, Phys. Rept. **359** (2002) 355.

[16] S. Mrowczynski and P. Danielewicz, Nucl. Phys. B **342** (1990) 345.

[17] S. Mrowczynski and U. W. Heinz, Annals Phys. **229** (1994) 1.

[18] S. Mrowczynski, Phys. Part. Nucl. **30** (1999) 419.

[19] E. Calzetta and B. L. Hu, Phys. Rev. D **37** (1988) 2878.

[20] P. Arnold, D. T. Son and L. G. Yaffe, Phys. Rev. D **59** (1999) 105020.

[21] M. M. Muller, J. Phys. Conf. Ser. **35**, 390 (2006).

[22] J. Berges and S. Borsanyi, Phys. Rev. D **74** (2006) 045022.

[23] M. Gell-Mann, Phys. Lett. **8**, 214 (1964).

[24] G. Zweig, CERN TH **401** 412 (1964).

[25] H. Fritzsch and M. Gell-Mann, Proc. XVI Int. Conf. on High Energy Physics, Chicago-Batavia, 1972.

[26] H. Fritzsch, M. Gell-Mann, H. Leutwyler, Phys. Lett. B **47**, 365 (1973).

[27] D. E. Kharzeev and J. Raufeisen, arXiv:nucl-th/0206073.

[28] M. H. Seymour, arXiv:hep-ph/0505192.

[29] G. Altarelli, arXiv:hep-ph/0204179.

[30] T. Muta, World Sci. Lect. Notes Phys. **57**, 1 (1998).

[31] K. Symanzik, Commun. Math. Phys. **18** (1970) 227.

[32] S. Bethke, arXiv:hep-ex/0606035.

[33] H. D. Politzer, Phys. Rev. Lett. **30** (1973) 1346.

[34] D. J. Gross and F. Wilczek, Phys. Rev. Lett. **30** (1973) 1343.

[35] W. E. Caswell, Phys. Rev. Lett. **33** (1974) 244.

[36] D. R. T. Jones, Nucl. Phys. B **75** (1974) 531.

[37] E. Egorian and O. V. Tarasov, Teor. Mat. Fiz. **41** (1979) 26

[38] T. van Ritbergen, J. A. M. Vermaseren and S. A. Larin, Phys. Lett. B **400**, 379 (1997).

[39] S. Hands, Contemp. Phys. **42** (2001) 209.

[40] F. Karsch, E. Laermann and A. Peikert, Phys. Lett. B **478** (2000) 447.

[41] L. D. McLerran and R. Venugopalan, Phys. Rev. D **49** (1994) 2233.

[42] R. Baier, A. H. Mueller, D. Schiff and D. T. Son, Phys. Lett. B **502** (2001) 51

[43] L. V. Gribov, E. M. Levin and M. G. Ryskin, Phys. Rept. **100** (1983) 1.

[44] J. P. Blaizot and A. H. Mueller, Nucl. Phys. B **289** (1987) 847.

[45] L. D. McLerran and R. Venugopalan, Phys. Rev. D **50** (1994) 2225.

[46] A. Krasnitz, Y. Nara and R. Venugopalan, Phys. Rev. Lett. **87** (2001) 192302.

[47] T.S. Biró, B. Müller, X.-N. Wang, Phys. Lett. B **283** (1992) 171.

[48] J. Bjoraker and R. Venugopalan, Phys. Rev. C **63**, 024609 (2001).

[49] G. C. Nayak, A. Dumitru, L. D. McLerran and W. Greiner, Nucl. Phys. A **687**, 457 (2001).

[50] J.F. Gunion, G. Bertsch, Phys. Rev. D **25** (1982) 746.

[51] J.D. Bjorken, Phys. Rev. D **27** (1983) 140.

[52] A. H. Mueller, Nucl. Phys. A **715** (2003) 20.

[53] T. Stockamp, J. Phys. G **32**, 39 (2006).

[54] A. H. Mueller and D. T. Son, Phys. Lett. B **582** (2004) 279.

[55] G. Aarts and J. Smit, Nucl. Phys. B **511** (1998) 451.

[56] S. Jeon, Phys. Rev. C **72** (2005) 014907.

[57] R. Cutler and D. W. Sivers, Phys. Rev. D **17** (1978) 196.

[58] R. Baier, Y. Mehtar-Tani and D. Schiff, Nucl. Phys. A **764** (2006) 515.

[59] M. Gyulassy and L. McLerran, Nucl. Phys. A **750**, 30 (2005).

[60] J. L. Nagle, arXiv:nucl-th/0608070.

[61] U. W. Heinz, AIP Conf. Proc. **739** (2005) 163.

[62] D. Kharzeev and K. Tuchin, Nucl. Phys. A **753** (2005) 316.

[63] Y. V. Kovchegov, Nucl. Phys. A **764** (2006) 476.

[64] Y. V. Kovchegov, Nucl. Phys. A **762** (2005) 298.

[65] J. Berges, S. Borsanyi and C. Wetterich, arXiv:hep-ph/0505182.

[66] S. Mrowczynski, Phys. Lett. B **393** (1997) 26.

[67] P. Arnold, G. D. Moore and L. G. Yaffe, JHEP **0301**, 030 (2003).

[68] P. Romatschke and M. Strickland, Phys. Rev. D **68** (2003) 036004.

[69] A. Rebhan, P. Romatschke and M. Strickland, Phys. Rev. Lett. **94** (2005) 102303.

[70] A. H. Mueller, A. I. Shoshi and S. M. H. Wong, Eur. Phys. J. A **29**, 49 (2006).

[71] P. Arnold and J. Lenaghan, Phys. Rev. D **70** (2004) 114007.

[72] P. Arnold, J. Lenaghan, G. D. Moore and L. G. Yaffe, Phys. Rev. Lett. **94** (2005) 072302.

[73] A. Einstein, Preussische Akademie der Wissenshaften **1**, 3 (1925).

[74] M.H. Anderson, J.R. Ensher, M.R. Matthews, C.E. Wieman and E.A. Cornell, Science **269**, 198 (1995).

[75] K.B. Davis, M.-O. Mewes, M.R. Andrews, N.J. van Druten, D.S. Durfee, D.M. Kurn and W. Ketterle, Phys. Rev. Lett. **75**, 3969 (1995).

[76] C.C. Bradley, C.A. Sackett, J.J. Tollett and R.G. Hulet, Phys. Rev. Lett. **75** 1687 (1995).

[77] J. Berges and J. Cox, Phys. Lett. B **517** (2001) 369.

[78] J. Berges, S. Borsanyi and J. Serreau, Nucl. Phys. B **660**, 51 (2003).

[79] J. Berges and J. Serreau, Phys. Rev. Lett. **91**, 111601 (2003).

[80] J. Berges, S. Borsanyi, U. Reinosa and J. Serreau, Phys. Rev. D **71**, 105004 (2005).

[81] A. Arrizabalaga, J. Smit and A. Tranberg, JHEP **0410**, 017 (2004).

[82] G. Aarts and J. M. Martinez Resco, Phys. Rev. D **68**, 085009 (2003).

[83] J. Berges and J. Serreau, arXiv:hep-ph/0302210.

[84] J. Berges and J. Serreau, arXiv:hep-ph/0410330.

[85] J. Berges and S. Borsanyi, arXiv:hep-ph/0610015.

[86] J. Berges, AIP Conf. Proc. **739**, 3 (2005).

[87] S.N. Bose, Z. Phys. **26**, 178 (1924).

[88] K. Huang, John Wiley, N.Y. (1987).

[89] Ensher, J.R., D.S. Jin, M.R. Matthews, C.E. Wieman, and E.A. Cornell, Phys. Rev. Lett. **77**, 4984 (1996).

[90] A. Griffin, arXiv:cond-mat/9911419.

[91] F. London, Nature **141**, 643 (1938).

[92] F. Dalfovo, S. Giorgini, L.P. Pitaevskii and S. Stringari, Rev. Mod. Phys. **71**, 463 (1999).

[93] A. Griffin, *in* Proceedings of the 13th Physics Summer S chool: Bose-Einstein Condensation, eds. C.M. Savage and M. Das (World Scientific, 2000).

[94] L.D. Landau, J. Phys. U.S.S.R. **5**, 71 (1941).

[95] S. T. Beliaev, Sov. Phys. JETP **7**, 289 (1958).

[96] N. N. Bogoliubov, J. Phys. U.S.S.R. **11**, 23 (1947).

[97] J. Gavoret and P. Nozières, Ann. Phys. (N. Y.) **28**, 349 (1964).

[98] P.C. Hohenberg and P.C. Martin, Ann. Phys. (N. Y.) **34**, 291 (1965).

[99] Jens O. Andersen, Rev. Mod. Phys. **76**, 599 (2004).

[100] H. T. C. Stoof, arXiv:cond-mat/9910441.

[101] A. J. Leggett, Rev. Mod. Phys. **73**, 307 (2001).

[102] M. Greiner, C. A. Regal and D. S. Jin, arXiv:cond-mat/0502539.

[103] Q. Chen, J. Stajic, s. Tan and K. Levin, Physics Reports **412**, 1 (2005).

[104] C. A. Regal and D. S. Jin, arXiv:cond-mat/0302246.

[105] E. P. Gross, Nuovo Cimento **20**, 454 (1961).

[106] L. P. Pitaevskii, Sov. Phys. JETP **13**, 451 (1961).

[107] L. Pitaevskii and S. Stringari, arXiv:cond-mat/9905409.

[108] A. Griffin, Phys. Rev. B **53**, 9341 (1996).

[109] M. Imamović-Tomasović and A. Griffin, Phys. Rev. A **60**, 494 (1999).

[110] S. Giorgini, Phys. Rev. A **57**, 2949 (1998).

[111] Hua Shi and A. Griffin, Physics Reports **304**, 1 (1998).

[112] A. Minguzzi and M.P. Tosi, J. Phys. Cond. Mat. **9**, 10211 (1997).

[113] D.A.W. Hutchinson, E. Zaremba and A. Griffin, Phys. Rev. Lett. **78**, 1842 (1997).

[114] E. Zaremba, T. Nikuni, and A. Griffin, Journ. Low Temp. Phys. **116**, 277 (1999).

[115] B. Jackson and E. Zaremba, arXiv:cond-mat/0106652.

[116] B. Jackson and E. Zaremba, arXiv:cond-mat/0205421.

[117] J. E. Williams and A. Griffin, arXiv:cond-mat/0003481.

[118] T. Nikuni and A. Griffin and E. Zaremba, arXiv:cond-mat/9911336.

[119] H.T.C. Stoof, Journ. Low Temp. Phys. **114**, 11 (1999).

[120] M. E. Peskin and D. V. Schroeder, Addison-Wesley (1995)

[121] J. M. Cornwall, R. Jackiw and E. Tomboulis, Phys. Rev. D **10**, 2428 (1974).

[122] J. Berges, Nucl. Phys. A **699**, 847 (2002).

[123] G. Aarts, D. Ahrensmeier, R. Baier, J. Berges and J. Serreau, Phys. Rev. D **66** (2002) 045008.

[124] R. Baier and T. Stockamp, arXiv:hep-ph/0412310.

[125] G. Aarts and J. Berges, Phys. Rev. Lett. **88** (2002) 041603.

[126] T. Gasenzer, J. Berges, M. G. Schmidt and M. Seco, Phys. Rev. A **72** (2005) 063604.

[127] A. Zee, Princeton Univ. Pr. (2003)

[128] A. Arrizabalaga, J. Smit and A. Tranberg, Phys. Rev. D **72** (2005) 025014

[129] J. Serreau and T. Stockamp, in preparation.

[130] D. G. Barci, E. S. Fraga and R. O. Ramos, Phys. Rev. Lett. **85**, 479 (2000).

[131] D. G. Barci, E. S. Fraga, M. Gleiser and R. O. Ramos, Physica A **317**, 535 (2003).

[132] M. Kohl, M. J. Davis, C. W. Gardiner, T. W. Hansch and T. Esslinger, arXiv:cond-mat/0106642.

Acknowledgments

It is a pleasure to thank all those people who helped me so much during the last three years.

- I am deeply indebted to my advisor Rolf Baier for his patient and experienced guidance. Vielen Dank! Many thanks to Julien Serreau for his friendly help and encouragement in our numerical project. Merci beaucoup!
- I also thank Dietrich Bödeker for being so kind to referee my thesis.
- I immensly benefited from the international graduate school „Quantum fields and strongly interacting matter“. Many thanks to all the people involved in this great project, notably the coordinators Dominique Schiff and Edwin Laermann.
- A very special thanks to our amazing team of secretaries, Gudrun Eickmeyer and Susi von Reder.
- Thanks to all my colleagues and friends on E6/D6. It was great to share this time with you!
- Last not least, I would like to thank my mom Christa and my sister Judith for all their love, care and understanding.

Selbstständigkeitserklärung

Hiermit erkläre ich, die vorliegende Arbeit selbstständig verfasst und nur die angegebene Literatur verwendet zu haben.

Bielefeld, 22.Dezember 2006

Tim Stockamp